Collisional interactions and the transition between lava dome sector collapse and pyroclastic density currents at Tutupaca volcano (Southern Peru)

Karine Bernard, Benjamin van Wyk de Vries, Pablo Samaniego, Patricio Valderrama, Jersy Mariño

▶ **To cite this version:**

Karine Bernard, Benjamin van Wyk de Vries, Pablo Samaniego, Patricio Valderrama, Jersy Mariño. Collisional interactions and the transition between lava dome sector collapse and pyroclastic density currents at Tutupaca volcano (Southern Peru). Journal of Volcanology and Geothermal Research, 2022, 431, ⟨10.1016/j.jvolgeores.2022.107668⟩. ⟨insu-03825079⟩

HAL Id: insu-03825079

https://insu.hal.science/insu-03825079v1

Submitted on 9 Nov 2023

HAL is a multi-disciplinary open access archive for the deposit and dissemination of scientific research documents, whether they are published or not. The documents may come from teaching and research institutions in France or abroad, or from public or private research centers.

L'archive ouverte pluridisciplinaire **HAL**, est destinée au dépôt et à la diffusion de documents scientifiques de niveau recherche, publiés ou non, émanant des établissements d'enseignement et de recherche français ou étrangers, des laboratoires publics ou privés.

Distributed under a Creative Commons CC BY 4.0 - Attribution - International License

Journal of Volcanology and Geothermal Research

Collisional interactions and the transition between lava dome sector collapse and pyroclastic density currents at Tutupaca volcano (Southern Peru).

--Manuscript Draft--

Manuscript Number:	VOLGEO-D-21-00343R3
Article Type:	Research Paper
Keywords:	volcanic debris-avalanche deposit, local kinematics, block clusters, striations, sedimentology.
Corresponding Author:	Karine Bernard, Professor AUBIERE, FRANCE
First Author:	Karine Bernard, Professor
Order of Authors:	Karine Bernard, Professor
	Benjamin van Wyk de Vries
	Pablo Samaniego
	Patricio Valderrama
	Jersy Mariño
Abstract:	We describe sedimentological variations of the block-rich debris avalanche deposits and associated pyroclastic density current deposits emplaced around AD 1802 from Tutupaca volcano in southern Peru. We use these exceptionally well-preserved features to document the collisional shearing contact between the avalanche and coeval pyroclastic density currents. Furthermore, w e show how the first stages of the edifice collapse and syn-cataclastic emplacement process affect the block-size distributions. With field observations, we describe imbricated block clusters, jigsaw cracks and striations related to elongated ridge structures on the deposit surface. Sedimentological and statistical methods (Fourier Shape analysis and Shape Preferred Orientation measured on 208 blocks and 566 mesoscale structures) help us to characterize the cataclastic gradient and establish the collisional relationships between different units. We determine that the proximal impacted deposits and block lithofacies from ridges may be related to distal block units around ~ 10 km run-out distance. Different block clusters indicate a kinematic transition between avalanche units to pyroclastic density currents. Block shape parameters help to differentiate rounded blocks resulting from matrix abrasion with a nd striated blocks from ridges related to proximal imbricated block cl usters. From the statistical dataset, a few equations have been developed indicating a common cataclastic origin with a co-genetic evolution of block lithofacies during sequential syn -cataclastic emplacement . The dome collapse is associated with a specific granular flow regime between avalanche and pyroclastic density currents with secondary reworking. Cyclic impact waves contribute to block cluster growth. Clusters are disaggregated during shock propagation. T he inherited shapes of the block lithofacies with a/b = 1.2-2 and ellipse = 0.2-2.5 indicate the reworking by impact waves. A multidirectional switch to mass spreading in the median zone between 2 and 6 km may be considered with secondary flow and segregation waves. A basal frictional regime with striations is differentiated from collisional cataclastic flow, generating polymodal grooves during peak velocity at the flow front. Impact forces around ~ 15.7 X 10 10 N are implied by suggested clast velocities around 8.86 m.s -1 and the transitional regime between avalanche units and pyroclastic density currents between 15.5 and 39.6 m.s -1 . An extensional disaggregation with the fractal dimensions (D) of the surrounded matrix between 0.6 and 2.8 characterizes the granular transport. A collisional shearing contact probably operated between avalanche units and pyroclastic density currents, which contribute to co-genetic evolution of block clusters from median to frontal distal zones . In the distal zone, abraded block clusters and tilted blocks are related to frontal reworking by impact wave. The cataclastic gradient of avalanche units is correlated with the pyroclastic flow

Powered by Editorial Manager® and ProduXion Manager® from Aries Systems Corporation

	regime. Semi-quantitative analysis of block clusters provides information about syn - emplacement processes during sequential impact waves related to volcanic debris-avalanche units and pyroclastic density currents.
Suggested Reviewers:	Lucia Capra lcapra@geociencias.unam.mx Debris avalanche
	Jean-Luc Schneider l.schneider@epoc.u-bordeaux1.fr debris avalanche
	Marcus Bursik mib@buffalo.edu Striations and PDC
	Greg Valentine gav4@buffalo.edu Volcanic deposits
Opposed Reviewers:	
Response to Reviewers:	

Powered by Editorial Manager® and ProduXion Manager® from Aries Systems Corporation

Clermont-Ferrand, August 22, 2022

Journal of Volcanology and Geothermal Research

Editor-in-Chief, Dr. Jose Luis Macias

Dear Sir,

We would like to re-submit the revised manuscript entitled: '*Collisional interactions and the transition between lava dome sector collapse and pyroclastic density currents at Tutupaca volcano (Southern Peru).*" to the Journal of Volcanology and Geothermal Research. We acknowledge your editorial comments as well as the reviewers for their useful remarks. The rebuttal letter describes how we abode by all requested changes, which appear in blue in the revised paper. This revised manuscript contains 26 pages, 5 tables, 10 figures and 2 Supplemental files. The research project presented in this manuscript has been conducted by a group of five researchers from the Laboratory Magmas and Volcans at the University Clermont Auvergne in French and the Institut de la Recherche pour le Développement (IRD) and supported by LMV and IRD.

The revision takes account of the suggestions about the definitions and the figure of the shape parameters (Feret diameter, roughness...) for the debris avalanche, which are described separately in Table 3. To facilitate the reading of this study, we provide the original data in Supplementary files 1 and 2 to calculate the fractal dimension, the mean values and standard errors of the shape parameters. The negative values of fractal dimension have been removed and the standard errors ($<10^{-3}$) related to photographic shot geometries have been considered. Figures and statistical parameters with no clear correlations (with $R^2 \leq 0.5$) that we attributed to the shape variations of block lithofacies and striations based on textural parameters have been removed (Figs. 9B-10B) according to reviewers 1 and 2.

We hope that our revised manuscript meets the high standard of the Journal of Volcanology and Geothermal Research, and we look forward to hearing from the Editorial Board. Thank you very much for your consideration on this matter.

Yours sincerely,

Karine Bernard and co-authors

Please address all correspondence to the first and corresponding Author:
Laboratoire Magmas et Volcans LMV UMR6524 CNRS, OPGC and IRD UR 163,
Université Clermont-Auvergne, 6 avenue Blaise Pascal, Campus les Cézeaux, 63178 Aubière, France.
Phone: +33 (0)4 73 34 67 74; E-mail: kbernard@opgc.univ-bpclermont.fr
Co-authors: Benjamin van Wyk de Vries, also at LMV and UCA, Pablo Samaniego, also at LMV and IRD, Patricio Valderrama at Departemento de Ingenieria, Pontificia Univesidad Catòlica del Perú, Jersy Mariño at INGEMMET.

Revised Manuscript with Changes Marked
Click here to view linked References

1. Introduction

Volcanic debris-avalanche deposits are often associated with pyroclastic density currents and lahar deposits (*i.e.* Mount Saint Helens in the USA, Glicken, 1986), suggesting interactions during flow propagation. The stratigraphic relationships between the associated *syn*-eruptive volcanic deposits are described, implying differential kinematic between the mass flow such as striations and grooves on clast faces related to dome-collapse generating avalanche deposits interstratified between pyroclastic units (Mono Craters, CA, Dennen et al., 2014); matrix transformations into lahar deposits (Misti in Peru, Bernard et al., 2017). Block lithofacies are rarely used to characterize the differential movements inside the mass flow during *syn*-eruptive collapse. A basal frictional regime with striations is differentiated from an upper collisional cataclastic flow for block lithofacies (*e.g.* Parinacota and Ollagüe in Chile, Clavero et al., 2002; Clavero et al., 2004; El Zaguan, Mexico, Caballero and Capra, 2011).

Lava dome extrusion produced block lithofacies may be mixed with matrix-rich debris-avalanche deposits (Mount Saint Helens, Glicken 1986; Parinacota in Chile, Clavero et al., 2002; Tutupaca in Peru, Samaniego et al., 2015; Valderrama et al., 2016). Different avalanche structures are identified with such block lithofacies: (1) torevas that are large blocks (L >100 m), which occur in the proximal zones and could constitute up to ~30% of the debris avalanche deposits (Socompa in Chile, Davies et al., 2010). (2) Type A hummocks that are large cataclased blocks (H <80 m, w <300 m, L <400 m, Mount Saint Helens, Voight et al., 1981; Glicken, 1998; Jocotitlán in Central Mexico, Siebe et al., 1992; Parinacota and Taapaca in Chile, Clavero et al., 2002; Clavero et al., 2004) with steep slopes. (3) Longitudinal or transverse ridges (H = 10-30 m, Shea and van Wyk de Vries, 2008; Dufresne and Davies, 2009; Andrade and van Wyk de Vries, 2010), that are attributed to deflection of the mass flow (Valderrama et al., 2018). The alignment of blocks or isolated blocks between 0.01 and 1000 m can be observed in some debris avalanche deposits (Socompa, van Wyk de Vries et al., 2001; Shea and van Wyk de Vries, 2008). The frontal lobes thrust the large blocks in distal zones (Jocotitlán, Siebe et al., 1992) showing fluidization with matrix transformations into lahars (Perrier in French Massif Central, Bernard and van Wyk de Vries, 2017). Different mesoscale structures have been described related to specific kinematic context such as gravitational flank collapse with an initial dilation of jigsaw-fit textures (Mount Saint Helens, Glicken, 1986), abrasion and striations along fault planes (Mehl and Schmincke, 1999), collisional textures during transport (El Zaguán in Mexico, Caballero and Capra, 2011), and impact waves with pseudotachylite and gouge along avalanche fault zones (Pichu Pichu in Peru, Legros et al., 2000; Mont Dore in French Massif Central, Bernard and van Wyk de Vries, 2017).

Syn-eruptive collapses of a volcanic edifice and volcano-sedimentary processes have been well documented at Las Derrumbadas Volcano, Mexico (Guilbaud et al., 2022), Panum Crater, (Mono Crater, CA, Dennen et al., 2014) and Tutupaca volcano in southern Peru (Samaniego et al., 2015; Valderrama et al., 2016; Mariño et al. 2021). This volcano hosts probably the well-preserved and displayed lava dome related debris avalanche

and pyroclastic density current features that are young and little altered by the climate or human interference. Two volcanic avalanche units exposed in the northeastern part of the Tutupaca collapsed edifice are interstratified with the pyroclastic density current deposits (Samaniego et al., 2015). Block-rich ridge structures have been attributed to granular segregation and differential block velocities in the flowing mass, suggesting the interactions between debris-avalanche units and the associated PDC deposits.

In this study, we show how semi-quantitative sedimentological analysis of the block lithofacies and mesoscale structures associated to these exceptionally well-preserved volcanic deposits provide information about *syn*-emplacement processes during a collapsing dome generating pyroclastic density currents. To facilitate the reading of this study, we provide a list of the acronyms in Table 1.

2. Collisional interactions between volcanic-debris avalanche and pyroclastic density currents: a State-of-the-Art

The volcanic debris avalanche deposits are commonly associated with PDC. Mount Saint Helens in the USA (Crandell et al., 1984; Glicken, 1986), Bezymianni in Kamchatka (Siebert et al., 1987), Soufrière in Guadeloupe (Boudon et al., 1984) show several sequences of lava dome collapses associated with decompression to the co-magmatic deposits in *syn*-eruptive sequences. The hot volcanic debris-avalanche deposits, gravitational mass spreading (v = 50-70 m.s^{-1}) of the collapsed edifice, interacted with the blast-generated the PDC, transport of the fluidized mixture of clasts and gas ($v \geq$100 m.s^{-1}, Soufrière, Boudon et al., 1984; Mount Saint Helens 1980, Glicken, 1986; Bezyamanni 1956, Saint Augustine, Siebert et al., 1987). The PDCs are interstratified between the debris avalanche units, related to cyclic volcanoclastic sedimentation. Cyclic phases can be differentiated: precursor stages with seismes and localized collapses with hydrothermal alteration, large collapse of alterated lava-dome edifice with explosion and the blast-generated the PDC including an open conduit, and different post-collapse eruption. Volcanic lateral blast is associated to the successive shock waves during collapse, with ballistic clasts and sliding blocks generating internal shock structures. Transformations of the debris-avalanche deposits into lahars (v = 30-40 m.s^{-1}) by dewatering have been observed during initiation of pyroclastic flow such as Mount Saint Helens (Glicken, 1986).

Deposit structures have been formed by interactions between the moving avalanche and the superposed PDC, implicating a strong frictional contact. We observed aggregation of lava block clusters (Taranaki, Zernack et al., 2009) with brechification and curviplanar surfaces related to blocky morphology interactions, pyroclastic slump blocks with progressive disaggregation of blocks, fingering segregation related to ridge structures (Tutupaca, Samaniego et al., 2015; Valderrama et al., 2016), striations and flow bands (Lastaria in Chile, Naranjo and Francis, 1987) with distal digitations related to weak pyroclastic material.

Different generations of striations have been described related to sliding mode transport during interactions

between no-cohesive avalanche lithofacies and PDC: striations of the bedrock in scar (Mount Saint Helens, Glicken, 1986); grooves and striations at the base and the underlying substratum; and parallel grooves and furrow at the base and the upper part of faulted megablocks (Gran Canaria, Spain, Mehl and Schmincke, 1999). We differentiate an upper collisional regime with impact marks at the surface of block lithofacies (Parinacota and Ollague in Chile, Clavero et al., 2002; Clavero et al., 2004). Impact marks and linear trends appear concentrated on one side of blocks, showing conchoidal fractures related to collisional interactions between the blocks.

We examine how block lithofacies of volcanic debris avalanche deposits interact with PDC to generate block clusters and grooves with striations related ridges structures. We show how semi-quantitative sedimentological analysis of the block lithofacies and mesoscale structures provide information about *syn*-emplacement processes such as the force *F* of impact of clasts onto block surfaces and the clast velocity for making impact marks (Clavero et al., 2002).

3. Analytical methods

From the field observations on the debris-avalanche units, we have described the textural variations of the block lithofacies assemblages and assessed their relationships to avalanche fault zones. A semi-quantitative sedimentological analysis was conducted to characterize block distributions (Table 2). From these data, we were able to differentiate the block lithofacies in each zone associated with cataclastic gradient between the avalanche units and pyroclastic density current deposits (Samaniego et al., 2015; Valderrama et al., 2016). To facilitate the reading of this study, we provide a list of the acronyms in Table 1.

3.1. Field observations and outcrop analysis

The lithology of different outcrops were identified from proximal to distal zones to characterize the discontinuous block-rich lithofacies, related to interactions between volcanic avalanche and pyroclastic density current deposits. From field observations and Google Earth imagery, the block-rich avalanche units were described and mapped according to stratigraphic and geomorphological context and avalanche structures (Samaniego et al., 2015; Valderrama et al., 2016).

Quantitative morphological data such as area (*S*), thickness (*T*) and volume ($V = ST$; Table 1) on the surface avalanche deposits are calculated from the mapped surfaces and georeferenced Google Earth images (Samaniego et al., 2015; Valderrama et al., 2016). These morphological data are compared to other avalanche deposits worldwide such as those emplaced around Mount Saint Helens and Mount Shasta in the USA (Crandell et al., 1984; Glicken, 1986), Bezymianni in Kamchatka (Siebert et al., 1987), Parinacota in Chile (Clavero et al., 2002), Soufrière in Guadeloupe (Boudon et al., 1984) and Mont Dore in French Massif

Central (Bernard and van Wyk de Vries, 2017). From these examples, we correlate the morphological data with the structural units of avalanche deposits, implying interactions between lava dome sector collapse and pyroclastic density currents. The contacts between the block lithofacies and matrix textures of volcanic debris-avalanche deposits with interstratified PDC were analyzed. Lithostratigraphic sections were established and correlated with textural variations.

The use of the Shape Preferred Orientation 2003 software (Fig. 1A, SPO, Launeau and Robin, 2005) provided a semi-quantitative description of block avalanche units, allowing us to estimate imbrication of 508 blocks and block axial distributions with the inertia and intercepts method. Image analysis of the block lithofacies and mesoscale structures provide relative information because photographs can be affected by perspective. Two-dimensional shape parameters of blocks, such as the *a/b* ratio (the largest axis / minor axis) and sectional ellipse values from system of linear equations (see Launeau and Robin, 2005 for mathematical definitions), have been calculated, to characterize block fabric related to *syn*-emplacement structures (Bernard, 2015; Bernard and van Wyk de Vries, 2017; Bernard et al., 2019), together with striations and grooves in blocks. Ellipse/*a/b* values contribute to establish textural classes of avalanche fault zones (~2.14 for the plane collapse, 1.75 to 2 for the crushing, *a* <1.7 for the thermal effect of fragmentation, Bernard et al., 2019). Mesostructures such as fractures and striations from 2 mm to 20 cm were also analyzed.

3.2. Sedimentary analysis

From SPO analysis (Launeau and Robin, 2005) of the blocks, the fractal distributions were used to compare transport and cataclastic process acting on each avalanche unit. Each cumulative frequency is plotted *versus* clast long-axis on double-logarithmic graphs. Fractal dimensions *h* and *D* of size distributions were estimated from the power regressions (Table 4; see Supplemental File 1; Suzuki-Kamata et al., 2009). The cumulative curves of the clast-size distributions *vs. a/b* (Fig. 8) were compared to distinguish the block avalanche units from proximal to distal zones. The calculated block-size distributions estimated from 41 outcrop photographs with the inertia and intercepts methods using the SPO analysis (from metric-size blocks to clasts >10 cm; Fig. 8B; Launeau and Robin, 2005). The longest axis of 404 block outlines were measured and counted per image area from the photographs. The normalized frequency histograms (Launeau and Robin, 2005) were produced by grouping the longest axis of blocks (cm) into 100-cm bins (number of size intervals) and normalizing the number of occurrences in each bin to the total number of measurements from automatic image analysis. The sectional effects have been considered (Launeau and Robin, 2005). These data contribute to differentiate the effect of cataclasis between each fraction correlated with different structural units from proximal to distal zones. The subdued blocks and clasts below 10 cm are not considered related to resolution limits.

The shape analysis using the ImageJ Plugin “Gold morph” has been applied to 404 blocks and 635 striations

of the avalanche units to compute minor and major axis length, Feret's diameter defined as the longest distance between two parallel tangential lines, perimeter and convex perimeter, radii of the smallest inscribed and largest circumscribed circles (Fig. 1B; Table 3; Crawford and Mortensen, 2009). From these data, we calculate the *a/b* ratio, the roundness defined as the ratio of the perimeter to convex perimeter, and the Riley's circularity, the square root of the ratio of the diameter of the largest inscribed circle to the diameter of the smallest circumscribed circle of the volcanic clast (Table 3, Blott and Pye, 2008; Bernard, 2015). The values of Riley's circularity are less than 1 for the non-spherical volcanic clasts (Table 5).

To characterize the two-dimensional shape of mesoscale structures, we took 5.9 megapixel photographs of abraded flat surfaces of two blocks with a digital camera. A digital camera (6.2-18.6 mm lens, 35-105 mm focal length) image at a camera distance of <20 cm had a standard error for mean distortion around ~10^{-3}. All the striations observed in the median zone have been quantified by using high-resolution images (3648 X 2736 pixels) of two block faces. Abraded flat surfaces of the two megablocks on these scales contribute to preserve geometries of these grooves and striations with circular depressions (~1-5 cm depth, 2-3 mm wide). These are enough to generate semi-quantitative analysis using the ImageJ Plugin “Gold morph” and SPO (566 mesoscale structures, Launeau and Robin, 2005; Blott and Pye, 2008; Crawford and Mortensen, 2009). The roundness, the Riley's circularity, the *a/b* ratio, ellipse, fractal *D*-values of each mesoscale structure have been calculated. The calculated standard errors characterize the shape variations between the blocks rather than the measurements' uncertainty. Moreover, the calculated standard errors for image analysis are between 0.03 and 0.3 for *a/b* ratio and around ± 0.9 for ellipse values (Launeau and Robin, 2005; Table 5).

Several statistical regressions (Eqs. 1-21 in Figs. 2 and 8-10) have been established to characterize the evolution of block shape and striations related to cataclastic processes between the volcanic debris-avalanche units and pyroclastic density current deposits. Figure 9 shows the evolution of the roundness with Feret's diameter for block lithofacies and striations. Figure 10 shows the evolution of the roundness with Feret's diameter for block clusters. The intersecting points between few regressions indicate similar values of shape parameters related to the inherited clast shape for lava blocks and co-genetic relationships between block lithofacies.

Statistical and shape parameters were compared with those from other avalanche units in the Andean Central Volcanic Zone such as the Pichu Pichu debris avalanche deposit, and the matrix of the ridges from the Tutupaca volcanic debris-avalanche deposits (Bernard, 2015; Valderrama et al., 2016; Bernard et al., 2019).

The impact of clasts onto block surfaces (Clavero et al., 2002) can be approximated as $r = 0.5a^2/h$ with r, radius of spherical portion of clasts; a, radius of hemispherical damage zone, and h, distance that penetrated into the block. The force F of impact is given by Clavero et al. (2002):

$$F = \Pi a^2 \rho_0$$

where ρ_0 is the hardness of the material. The clast velocity for making impact marks can be estimated by using $V = (0.5\ \Pi\rho_0/Mr)^{1/2}a^2$ with M, the mass of the rock (Clavero et al., 2002). The avalanche velocity in the

middle zone is considered by using $v = (2gH)^{1/2}$.

A combination of several semi-quantitative methods has been used to determine (Table 1): (1) the links between the different block-rich units related to the debris avalanche and the associated pyroclastic density currents; (2) the quantitative sedimentary comparisons of the block lithofacies to define the conditions generating these deposits; (3) the in-motion controls and the dynamic cataclasis during the differential sedimentary emplacement between the volcanic debris-avalanche units and the pyroclastic density current deposits.

4. Geological and geomorphological context of the study area

4.1. Tutupaca volcanic complex and the geomorphological context

The Tutupaca volcanic complex (~5815 m on above sea level, Fig. 3) is composed by three edifices: an eroded basal edifice (Lower to Middle Pleistocene, Marino et al., 2021) with strong hydrothermal alteration; the Western Tutupaca peak, which was eroded by the late Pleistocene glaciers, and the Holocene Eastern peak composed of seven coalescing lava domes (Holocene, domes I to VII, Fig. 3B, Samaniego et al., 2015; Valderrama et al., 2016; Marino et al., 2021), constructed on the older hydrothermally-altered basal edifice. The activity of the recent domes is historic (about 218±14 calBP), and little altered by the arid, stable, cold climate, or by human activity, apart from a few small tracks and limited mining exploration excavations. The area is mostly wild, and in its natural state. The lava domes of the Eastern Tutupaca peak are cut by a horseshoe-shaped amphitheater open to the northeast, with an orthogonal direction to the N140° regional faults. From this, debris avalanche and pyroclastic density current deposits extend, are preserved with very little modification from their initial state (there is some limited frost shattering, and ice related solifluxion).

Geomorphological parameters on the surface avalanche deposits associated with PDC are calculated and compared to other avalanche deposits worldwide such as those emplaced around Mount Saint Helens and Mount Shasta in the USA (Crandell et al., 1984; Glicken, 1986), Bezymianni in Kamchatka (Siebert et al., 1987), Soufrière in Guadeloupe (Boudon et al., 1984). Impact marks of Parinacota debris avalanche in Chile (Clavero et al., 2002) and pseudotachylite impact in French Massif Central (Bernard and van Wyk de Vries, 2017) are considered. A relationship between area (A) and volume (V) is calculated for the Tutupaca units with $A = 28.07\ V^{1.01}$ (Eq. 1 in Fig. 2). These are compared to the power regressions of other volcanic debris-avalanche deposits (Eqs. 2-4 in Fig. 2, Glicken, 1986; Clavero et al., 2002; Legros, 2002; Bernard and van Wyk de Vries, 2017). We differentiate an intersecting point A with area around ~140 and 180 km^2 and volume between 5 and 7 km^3.

4.2. The Paipatja debris-avalanche deposits

Samaniego et al. (2015) described the Paipatja debris avalanche, exposed in the northeastern part of the Tutupaca volcano between the amphitheater and the Paipatja plain (L = 6-8 km, S = 12-13 km^2, T = 25-40 m, Samaniego et al., 2015; Valderrama et al., 2016). Stratigraphic and textural variations are correlated to the syn-emplacement structures. The hydrothermally rich debris avalanche deposit (HA-DAD, L = 6-8 km, V< 1 km^3; H/L = 0.17-0.23, Samaniego et al., 2015), that involved large quantities of the basal edifice, is characterized by torevas (H = 20-40 m, L = 1.5 km), long lateral levees (L = 1.5 km) and hummocky-structures (L = 200-800 m, H = 20-40 m) up to 4-6 km from the scar (Samaniego et al., 2015; Valderrama et al., 2016).

Block ridge structures and levees are observed between 2 and 6 km from the amphitheater (Valderrama et al., 2016). In the median zone, elongated and sub-parallel ridge structures (w = 5-10 m, H = 2-5 m, L = 150-400 m, Fig. 3A), regularly spaced, are related to interstratified pyroclastic density current deposits between two avalanche units, implying a *syn*-collapse explosive eruption at Tutupaca volcano (Samaniego et al., 2015). The hydrothermally rich debris avalanche deposit is covered by Paipatja pyroclastic density current deposits (P-PDC, ~218 aBP, sections B to E in Fig. 3A).

A dome-rich debris-avalanche deposit (DR-DAD of Samaniego et al., 2015) overlain the P-PDC unit in the median zone (section B in Fig. 3). Cross-sections within the ridge structures reveal the dipping and undulating contacts between the P-PDC units and the DR-DAD (section B in Fig. 3A). The P-PDC, on the upper part of HA-DAD, appears thickest between the ridge structures and around the largest blocks (Valderrama et al., 2016). We have observed dome fragments (from centimeters to several meters in size), such as metric-size dacitic blocks and prismatically jointed blocks showing inherited jigsaw-cracks, cataclastic and shearing structures. The abraded and sub-rounded blocks are subdued in the underlying avalanche deposit and PDC.

The Tutupaca volcanic debris-avalanche deposits show different units with specific granular assemblages (30% of HA-DAD and 70% of DR-DAD, Valderrama et al., 2016). Dense blocks (3-20 cm in diameter) and bombs from the P-PDC unit (20-40%) have highly similar chemical content (~65-68 wt.% SiO_2, Samaniego et al., 2015), similar to the brecciated lava domes. A progressive decrease in block-size is observed with distance. Large blocks (~0.5-1 m in diameter) are occasional. The few distal blocks (>1 m in length) surrounded by P-PDC unit are associated to the underlying avalanche deposit.

4.3. The syn-emplacement block lithofacies

Using the Google Earth imagery, we differentiate different block lithofacies from proximal to distal zones. The eastern flank collapse of the Tutupaca volcano shows at the summit two brecciated zones related to lava dome collapse (domes V to VII in Fig. 3B, Fig. 4A). We observe along the East crest (1 in Fig. 4A) angular

dome fragments adjacent to the PDC (in red in Figs. 3A and 4A) without preferential orientation, and on the west side (2 in Fig. 4A) an impacted and crushed zone showing imbricated block clusters with tabular planar surfaces. The long axis of 56 blocks are tilted N112E. In the median zone, block ridge structures show an isolated polyhedral block (white arrow in Fig. 4B), which exhibits planar surfaces with angular edges. We observe in downstream sigmoid fish of clasts, which appears disaggregated and truncated in N40E, related to the interactions between avalanche and the blast-generated the PDC (Fig. 4B). The isolated distal blocks (>1 m in length, Fig. 4C) surrounded by P-PDC unit are transverse with extensional lateral spreading (N176E, Fig. 4C).

The textural and sedimentological variations of the block avalanche lithofacies (HA-DAD and DR-DAD) are described with associated volcanic deposits to correlate *syn*-emplacement process between volcanic debris-avalanche units and pyroclastic density current deposits.

5. Results

The SPO analysis of the block lithofacies contribute to a semi-quantitative description of block deposits. The comparison of each block lithofacies with cumulative curves and fractal distributions helps to distinguish the deposits. The analysis of the block shapes has enabled us to identify the inherited structures and the relationships between the proximal and distal block clusters.

5.1. Block lithofacies

In the Paipatja DAD, we have observed block clusters and block avalanche lithofacies with a specific distribution on and between blocks. From proximal to distal zones, the block characteristics were quantified using the software ImageJ and SPO analysis (>400 blocks, Launeau and Robin, 2005). We characterized the localized mesoscale structures observed on few blocks associated with the ridged structures.

5.1.1. Block clusters lithofacies of DR-DAD

Imbricated block clusters are localized under the collapse scar (A in Figs. 3A and 4A). The dacitic dome fragments (from centimeters to several meters in size) present similar chemical characteristics (64.5-65.9 wt. % SiO_2, Samaniego et al., 2015). We observed impacted blocks with planar fractures and undulated borders (Fig. 5A), and tilted blocks in imbricated piles. Inherited clasts are observed with jigsaw-fractured breccias showing polymodal distribution of the clasts and ellipse/*a/b* = 5.1 (Fig. 5B). Block-rich ridge structures of the Paipatja DAD (B in Fig. 3A) contain abraded and sub-rounded blocks, which are also found in the underlying avalanche deposit and P-PDC (ellipse/*a/b* = 2.3-2.6 in Fig. 5C). There are also impacted blocks (Fig. 5D)

showing polymodal distribution of the clasts. In the Paipatja plain, abraded and sub-rounded blocks are found isolated at the front of P-PDC (Fig. 3). Along the lateral levee, in the proximal zone, we have observed large blocks with sigmoidal jigsaw-breccias (Fig. 5E) and a bimodal clast distribution. Angular lava blocks (~1 m in length) are impacted between aligned and subdued blocks (Fig. 5F), which exhibit planar surface with conchoidal fractures or abraded surface with striations. We differentiate block clusters and ridged avalanche units (ellipse/*a/b* = 2.3-2.5, DR-DAD, Fig. 5G) from imbricated block clusters (ellipse/*a/b* = 1.74) and subdued and tilted blocks in the distal zone (ellipse/*a/b* ~2.12, PDC, Fig. 5H).

5.1.2. Block avalanche lithofacies

Some transverse blocks appear isolated or aligned in N30° (DR-DAD, Figs. 3B and 6A), parallel to the elongated depressions. We observed sub-rounded faces with striations in upstream and planar faces with conchoidal fractures in downstream. Along the lateral levee, we described quenched and cracked surfaces in the upper part with jigsaw-fit texture and imbricated subangular clasts along basal contact of blocks (Fig. 6B). A large polyhedral block (~3 m high and ~5 m length, HA-DAD, Fig. 6C) on the ridge crest presents an oriented abrasion: sub-rounded face in the front and planar face in the downstream. In the PDC deposits, a bimodal distribution of the surrounded clasts is quantified. The sub-rounded lava block displays two distinct surfaces: a quenched and cracked surface in the upper part and an altered vitreous phase in the lower part. A distal sub-rounded block, surrounded by the P-PDC deposits, appears isolated (Fig. 6D) with bimodal distribution of the surrounded clasts related to the PDC deposits. Subdued blocks exhibit abraded surfaces with striations.

5.1.3. Grooves and striations

At 5.5 km from the collapse scar, a few blocks associated with the ridge structures (Fig. 7A; Valderrama et al., 2016) exhibit grooves and striations with roughly circular depressions on the upstream, abraded face. These localized mesoscale structures are often irregular and grouped in the lower part of the abraded and striated surfaces. The largest striations (>3 cm wide) are parallel to each other (at 3.19°, Fig. 7) and observed in the upper part of the block face. There are small striations perpendicular to the grooves (Fig. 7B). Grooves or furrows 1-5 cm depth ranged from roughly circular (<5 cm in diameter) to elliptic (~8-15 cm for longest axis) in shape. Fractal *D* values, calculated from exponent *h* of power regressions (100 striations, Table 4; Suzuki-Kamata et al., 2009), are 1.09 in the 8.4-46.4 cm mark-size range.

The macroscopic characteristics of grooves and striations with circular depressions were used for the shape analysis with the software ImageJ and SPO analysis (566 mesoscale structures, Launeau and Robin, 2005). Grooves and striations show polymodal distributions, with ellipse/*a/b* around ~5.1-5.9 (Fig. 7A-B). In the lower part of the block face, basal striations (~2-3 mm wide) with perpendicular diaclasis are differentiated. Fractal *D* values, calculated from exponent *h* of power regressions (90 striations, Table 4, Suzuki-Kamata et

al., 2009), are 0.67 in the 5.2-20.96 cm mark-size range.

5.2. Sedimentary characteristics of block lithofacies

Sedimentary characteristics of block lithofacies were compared with fractal *D* values to distinguish textures in the block avalanche units (HA-DAD, DR-DAD) and PDC deposits from proximal to distal zones. Block lithofacies of HA-DAD are hydrothermalized and cataclased with jigsaw-cracks. These are angular to subangular in PDC (20-30% of HA-DAD, Samaniego et al., 2015). We differentiate imbricated blocks with jigsaw structures in zones A and C (Fig. 3A), the abraded and subdued blocks observed in ridges structures and the distal zone (F in Fig. 3A), and the dacitic block lithofacies in zones D and E. The cumulative curves of block-size distributions *vs. a/b* are compared to distinguish block lithofacies in different zones, which are characterized by five logarithmic regressions (Eqs. 5-9 with R^2 >0.9 in Fig. 8A). These are compared to the logarithmic regressions of the impact breccias in French Massif Central (Eq. 12 in Fig. 8A; Mont Dore, Bernard and van Wyk de Vries, 2017). The intersecting points *a* to *d* with *a/b* between 2.5 and 4.7 imply a co-evolution between the grooves and striations (Eqs. 10-11 with R^2 >0.9 in Fig. 8A) and the ridged debris-avalanche unit (Eq. 6), in accordance with the field observations. We differentiated the hydrothermalized matrix (HA-DAD) from the breccia matrix (DR-DAD) showing sandy-gravel lithofacies of the red matrix with few angular clasts (< cm, Bernard, 2015; Valderrama et al., 2016).

The effect of cataclasis is shown by a decrease in the content of the smallest fractions (<100 cm, Fig. 8B) of block lithofacies (<18%), an increase in the striation ratio (25 to 45%), together with a concomitant high ratio in amount of block clusters (~20 to 40%). The variations of these data are correlated with different structural units from proximal to distal zones. The basal striations appear differentiated (Table 4). A specific clast-size fractal distribution is calculated in the range between 6.7 and 539 cm. The mean fractal *D* value, calculated from exponent *h* of power regressions, is around ~1.28 in the 11.4-40.3 cm clast-size range (Table 4; see Supplemental File 1; Suzuki-Kamata et al., 2009). The distal block lithofacies present the highest *D* values around ~1.83 compared to the proximal ridged deposits around ~1.64. These are differentiated from the surrounded matrix between 0.64 and 2.84 in the 0.0016-6.4 clast-size range. The mean fractal *D* value of striations is around ~0.62 in a range from 5.9 to 44.6 cm.

5.3. Block shape parameters

Shape analysis using the software ImageJ and SPO analysis (404 blocks from the HA-DAD and DR-DAD, 635 striations; Launeau and Robin, 2005; Blott and Pye, 2008; Crawford and Mortensen, 2009) has been applied to compare shape parameters of blocks from proximal to distal zones, together with striations and

grooves in blocks. This comparison is intended to characterize the cataclastic evolution with co-genetic relationships between volcanic debris-avalanche units and P-PDC, including the inherited clast shape for lava blocks. The mean values of *a/b* ratio and ellipse (~1.7±0.03 and 3.5±0.15, Table 5) are different from the clasts observed in the matrix of ridged units (DR-DAD, ~1.69±0.05 and 2.72±0.09, 1891 clasts from SPO analysis, Bernard, 2015). The calculated standard errors indicate the measurement errors and the sum of internal variability between the block shape parameters. These values imply distinct evolution between the avalanche block lithofacies and PDC.

5.3.1. Avalanche block lithofacies

We distinguish an inherited clast shape for lava blocks with *a/b* = 0.9 and ellipse = -3.5 implying textural relationships between the block lithofacies of HA-DAD and DR-DAD. Three regressions characterize the roundness *vs.* maximum Feret's diameter (Eqs. 13-17 in Fig. 9) for the block lithofacies. Two regressions (Eqs. 14-15 in Fig. 9) characterize the block lithofacies observed in the proximal and median zones. These values are compared to the breccias forming the ridged avalanche matrix (HA-DAD and DR-DAD) and the distal lobe of the Pichu Pichu debris-avalanche deposit (Eqs. 14-15 and 17 in Fig. 9; Bernard, 2015).

5.3.2. Distal block lithofacies

Three points of intersection indicate similar values of roundness for different zones of cataclasis (*a-c* in Fig. 9A). We distinguish an inherited clast shape with roundness around ~0.9 (*a*, Fig. 9), indicating textural relationships between the tilted distal blocks (PDC) and the blocks from the ridges, close to those of the sheared lava breccias in the distal lobe of the Pichu Pichu debris-avalanche deposit. The intersecting points *b* and *c* with roundness between 1.05 and 1.08 imply a co-evolution between the impacted blocks (Eq. 14) observed in the proximal and distal zones and the sheared sigmoid along the lateral levee (Eq. 15 in Fig. 9).

5.3.3. Grooves and striations

The values of *a/b* = 3.2 and ellipse = 15 are correlated to a co-genetic evolution between the grooves and striations, the blocks from ridges and the distal, impacted blocks (PDC). The mean values increase for roundness from 1 to 1.7 and ellipse/*a/b* from 0.2 to 2.7 (Table 5), while the values of Riley's circularity decrease. A regression characterizes the roundness *vs.* maximum Feret's diameter (Eq. 13 in Fig. 9) for the striations. The intersecting point *c* (Eqs. 13-14 in Fig. 9) with Feret's diameter <0.05 m and roundness around ~1.05 characterizes the inherited clast shape of the proximal block lithofacies generating striations and impact marks in the ridged debris-avalanche unit. We observed decreasing values of Riley's circularity related to Feret's diameter (Table 5).

5.4. Block clusters and shape variations

More than six cluster structures have been described with the shape analysis using the software ImageJ and SPO analysis from 312 blocks in the unconsolidated avalanche matrix from the HA-DAD (Fig. 10). Lava block clusters (~30-70 vol.%) from 40 cm to 5 m in diameter are impacted and thrust in unconsolidated avalanche matrix. The *a/b* ratio related to ellipse values show increasing values for the impacted jigsaw-clusters; and for the tilted block in the distal zone. Similar characteristics appear for the striated blocks from the ridges and the distal clusters. Similar ellipse values are calculated between proximal jigsaw breccias and the tilted and impacted blocks in the distal zone (ellipse = 0.7); between distal clusters (ellipse = 1-1.8) or between tilted blocks in the distal zone (ellipse = 2.7). *Syn*-cataclastic emplacement of block clusters with a co-genetic evolution of shape parameters may be envisaged.

The roundness is high (>1) for the block clusters, close to those of the experimental crushed stones (Janoo, 1998). Four regressions characterize the roundness *vs.* Feret's diameter (Eqs. 18-21 in Fig. 10) between 0.05 and 1 m. The increasing macro-roundness reflects the effects of clast crushing due to the collisional transport and cataclastic sorting between the proximal and distal zones. We have highlighted a power regression for the imbricated block clusters in the proximal zone with roundness >1 (Eq. 18 in Fig. 10). Two categories of regressions are identified for the impacted and tilted block clusters in the distal zone with roundness between 0.9 and 1.08 (Eqs. 19-20 in Fig. 10). Three points of intersection (*a-c* in Fig. 10) indicate similar values of block roundness for cluster structures characterized by different regressions: between impacted and tilted blocks in distal zone (*a* = 1.05, Eqs. 19-20); between distal clusters and the striated blocks from the ridges (*b* ~1, Eqs. 18-20) or proximal breccias with jigsaw features. We distinguish an inherited block shape for lava blocks with roundness around ~0.9 and Feret's diameter = 0.05 m (*c* in Fig. 10), implying textural relationships between these block clusters and sheared contact of the Pichu Pichu volcanic debris-avalanche deposit.

The Riley's circularity of block clusters shows decreasing values from the proximal to distal zones (Table 5, see Supplemental File 2) related to Feret's diameter, implying textural relationships between the block clusters with the run-out distance.

6. Discussion

From field observations, we used complementary methods to describe surface and internal structures of the Paipatja volcanic debris-avalanche deposits of the Tutupaca volcano and the associated pyroclastic density currents. The quantitative sedimentary analysis contributes to correlate the block clusters, the block avalanche lithofacies and mesoscale structures with different stages of cataclastic flow regime between the DR-DAD and the associated pyroclastic density currents from proximal to distal zones. Quantitative

morphological and sedimentological parameters are correlated and compared to other avalanche deposits worldwide, showing that the brecciation have recorded the collisional interactions between lava dome sector collapse and pyroclastic density currents.

6.1. Classification of volcanic debris-avalanche deposits

The volcanic debris avalanche deposits are commonly associated with PDC. The area and volume of the volcanic debris avalanche deposits associated with PDC are compared to Bezymianny eruptive sequence (Siebert et al., 1987) showing lava dome collapses with hydrothermally alteration interacted with the blast-generated the PDC (Fig. 2): Mount Saint Helens in the USA (Glicken, 1986), Bezymianni in Kamchatka (Siebert et al., 1987), Soufrière in Guadeloupe (Boudon et al., 1984). A relationship between the area (*A*) and volume (*V*) for the Tutupaca units is compared to the power regressions of other volcanic debris-avalanche deposits such as Mount Shasta and Mount Saint Helens in the USA (Fig. 2, Glicken, 1986; Siebert et al., 1987; Legros, 2002). The fault breccias have recorded the propagation of impact waves. The Tutupaca volcanic debris-avalanche deposits with *H/L* around ~0.15-0.2 (12-13 km^2, <1 km^3, *L* = 6-8 km, Samaniego et al., 2015; Valderrama et al., 2016) show different units characterized by granular segregation and fingering instabilities (Figs. 3-4, Valderrama et al., 2018). A power regression (Eq. 2 in Fig. 2) characterizes the Tutupaca units compared to the proximal scar of the Mount Saint Helens deposits showing striations of the bedrock and the impacted distal zone in French Massif Central. This co-evolution of geomorphological parameters may be related to digitate shape of the avalanche deposits (Samaniego et al., 2015). The largest volcanic avalanche deposits (Mount Shasta, Legros, 2002) appears different from other volcanic debris-avalanche deposits in accordance with field observations, on ridge structures, striations, and block clusters. The geomorphological parameters of the largest avalanche units tend toward similar values (Eqs. 1-4 in Fig. 2). We differentiate the intersecting point A (Fig. 2) with an area around ~140 and 180 km^2 and volume between 5 and 7 km^3, implying a convergent evolution between the largest structural units with run-out distance of over 22 km (Mount Saint Helens in the USA and Parinacota in Chili, Fig. 2; Siebert and Roverato, 2020) and the high velocity of volcanic debris avalanche associated with the blast lateral collapse and fluidization.

For the Tutupaca volcanic debris-avalanche deposits, the mean values of *a/b* ratio and ellipse, around ~1.7 and ~3.5 respectively (Table 5) are between the Rio Chili, tilted block-rich debris-avalanche deposits in Peru and the lateral levee from the Mont Dore in French Massif Central (Bernard, 2015; Bernard et al., 2017). The mean ellipse/*a/b* values around 1.88 characterize the crushing effects (Table 5, Bernard et al., 2019). We differentiate the thermal effect of fragmentation in proximal zone with ellipse/*a/b* between 0.23 and 1.7 and the transfer of the plane collapse in the median zone showing ridge structures (ellipse/*a/b* = 2.04-2.78). For the Tutupaca example, we have a dome collapse with a cataclastic gradient and a granular segregation during

a lateral spreading over ~1 km (Fig. 3). These statistical comparisons with other volcanic debris-avalanche units contribute to establish a geomorphological classification of the volcanic debris-avalanche deposits related to kinematic process. Secondary reworking of the Paipatja volcanic debris-avalanche deposits with impact waves and fingering instabilities during flow propagation of the pyroclastic density current must be considered. Successive collapses of the volcanic edifice contribute to the discontinuous units of the debris-avalanche deposits.

6.2. Granular flow regime between the debris avalanche and pyroclastic density currents

Field observations show a reverse grading of the lithofacies assemblage (Socompa, van Wyk de Vries et al., 2001; Davies et al., 2010): the HA-DAD is overlain by the DR-DAD interstratified with pyroclastic density current deposits (Samaniego et al., 2015). A similar block-size distribution of the avalanche deposits and the regressions (Eqs. 5-12 in Fig. 8) indicate a similar cataclastic origin with a co-genetic evolution of block lithofacies linked with a sequential *syn*-cataclastic emplacement (Samaniego et al., 2015; Valderrama et al., 2016).

The comparison of each block size-fractions with cumulative curves and histograms (Figs. 8-10) help to identify the block lithofacies from proximal impact and cataclastic gradient with granular segregation in flowing mass (Valderrama et al., 2016). Sedimentary parameters show a co-genetic brecciation of block lithofacies (Eqs. 5-12, Fig. 8), which are compared to the impact breccia in French Massif Central. The lava dome brecciations have recorded the propagation of impact waves. The roundness *vs*. Feret's diameter suggests a co-genetic evolution between the proximal clusters, the abraded and striated blocks in the ridges and the distal block clusters (Eqs. 19-22 in Fig. 10A) due to differentiated breakage during collisional transport.

6.2.1. Cyclic impact waves and block clusters

The dome collapse with explosion is associated with a specific granular flow regime between avalanche and pyroclastic density currents with secondary reworking. The succession of slide blocks is associated to frontal propagation of cyclic impact wave in an extensional context during primary shear propagation generating a clastic matrix (PDC, Mount Saint Helens, Glicken, 1986). Inherited jigsaw-fit textures have recorded the initial dilation of the collapsed edifice (Mount Saint Helens, Glicken, 1986). The inherited shapes of the block lithofacies (a/b = 1.2-2, ellipse = 0.2-2.5) indicate the reworking by impact waves. Imbricated block clusters with jigsaw-fit texture and planar fractures are impacted under the collapse scar (A in Figs. 3A and 4A). Proximal imbricated block clusters may be generated during impact waves (Cox et al., 2019). Cyclic impact waves and initial dilation contribute to block cluster growth with jigsaw-fit texture during the first stage of avalanche emplacement. Clusters are disaggregated during shock propagation (Fig. 4A). The rock

fragmentation during the proximal impact wave increases the roundness (>1, Fig. 10; Szabo et al., 2015). The propagation of the impact wave with granular oscillatory stress (Bernard and van Wyk de Vries, 2017; Cox et al., 2019) may contribute to produce the imbricated block clusters. Waves during cyclic impact may be considered to cause block cluster growth.

Blocks are split into clusters of smaller aggregates during transport (Palmer et al., 1991). Stick-slip oscillations (Sandnes et al., 2011) and an oscillatory relative speed may be considered during impact waves and dilation, which change the apparent coefficient of friction in the proximal zone. The isolated sub-rounded blocks and impacted blocks (D ~1.64-2.83 and ellipse/a/b =1.7-1.8, Tables 4 and 5) may be related to cluster disaggregation (Fig. 8B) during shock propagation generating the polymodal clast distributions with a thinner clastic matrix related to polymodal striations of the blocks from the ridges (ellipse/a/b =1.7-1.8, Eqs. 9-12, Fig. 8, Table 5). The cataclastic finer fractions increase the particle-to-particle interactions during flow propagation (Dennen et al., 2014) generating grooves and striations on the abraded surface of the impacted blocks. Textural relationships appear between proximal blocks and the striated blocks from the ridges (Table 5) with decreasing values of Riley's circularity.

6.2.2. An upper collisional regime

Differentiated velocities related to transitional regime must be considered between the matrix-rich facies and the block facies ($v_1 < v_2$; Glicken, 1998; Caballero and Capra, 2011). Formation of the elongated ridges is attributed to granular segregation and differential block velocities in the flowing mass (Dufresne and Davies, 2009). The bimodal clast distributions in the medial zone (ellipse/a/b ~1.7) differentiate the transverse blocks, the elongated ridges and lateral levee with sigmoidal jigsaw-breccias (Fig. 6B-D). The DR-DAD lithofacies contribute to decreasing run-out velocity with localized secondary flow (Socompa, Kelfoun et al., 2008; Mont Dore in French Massif Central, Bernard and van Wyk de Vries, 2017) and segregation waves to the flow front (Gray, 2013).

A multidirectional switch of mass spreading may be considered, with segregation waves to the flow front (Glicken, 1998). Transverse orientations of blocks in the medial zone implicate a quick stop attributed to a compressive context. The lack of propagation of the proximal conditions contribute to plug flow and granular segregation, generating lateral levees and ridges in the upper collisional flow regime for the median zone (Shea and van Wyk de Vries, 2008; Valderrama et al., 2016). Along lateral levee, rafted blocks with sigmoidal jigsaw-breccias are related to transport by traction in shearing context, generating secondary fractures.

We differentiate the parent dome volcanic processes from the breakage due to collisional transport, which increases the roundness from 1 to 1.7, related to the frontal reworking by impact wave (Table 5). An upper collisional regime for block lithofacies generating impact marks is differentiated from basal frictional regime with striations (*e.g.* Parinacota and Ollagüe in Chile, Clavero et al., 2002, Clavero et al., 2004; El Zaguan, Mexico, Caballero and Capra, 2011). Collisional abrasion may be associated with the dispersive pressure

generated by the subsequent pyroclastic density current. Shock and brecciation of blocks limit the mixture of lithofacies (*e.g.* Pichu Pichu in Peru, Legros et al., 2000; El Zaguan, Mexico, Caballero and Capra, 2011). Stick-slip motion at the front of lobe and high-speed of blocks may also be considered (Bartali et al., 2015). Each of the block avalanche deposits and striations present a specific regression for the roundness *vs.* Feret's diameter diagram (Eqs. 13-17 with R^2 >0.5 in Fig. 9), implying a differentiated evolution of the breakage during collisional transport and granular segregation. Inherited clast shapes with roundness between 0.9 and 1.2 are related to a same cataclastic origin. The impact of clasts onto block surfaces ($r = 0.5a^2/h$, Clavero et al., 2002) can be approximated with a <5 cm radius of hemispherical damage zone, and h ~1-5 cm distance that penetrated into the block. Calculated r values between 2.5 and 12.5 cm is in accordance with the surrounded clasts. The impact force F has a value of about 15.7 X 10^{10} N by using $F = \Pi a^2 \rho_0$ with a typical ρ_0 value around ~2.10^9 Pa (Clavero et al., 2002). The clast velocity for making impact marks can be estimated around ~8.86 m.s^{-1} by using $V = (0.5\ \Pi\rho_0/Mr)^{1/2}a^2$ with M ~10^3 kg, a <5 cm and r values between 2.5 and 12.5 cm (Clavero et al., 2002), in accordance with impact marks analysis on clast faces of Panum block lithofacies (Mono Craters, CA, Dennen et al., 2014). The avalanche velocity in the middle zone (around ~3 and 6 km from source, Clavero et al., 2002) is considered between 15.5 and 39.6 m.s^{-1} by using $v = (2gH)^{1/2}$. Localized striations and grooves can be attributed to the peak velocity at the flow front. The inherited shapes of the lava blocks and the co-genetic evolution between the blocks from the ridges and striations may be associated to secondary fracturing with partial decompression during run-out propagation (Bernard et al., 2019).

The dome collapse is associated with a specific granular flow regime between avalanche and pyroclastic density currents: cyclic impact waves with disaggregation during shock propagation, and secondary flow with segregation waves. Basal frictional regime with striations is differentiated from higher collisional and cataclastic flow regime generating clast breakage and impact marks (*e.g.* Parinacota and Ollagüe in Chile, Clavero et al., 2002, Clavero et al., 2004; El Zaguan, Mexico, Caballero and Capra, 2011).

6.3. The frontal reworking

Logarithmic regressions of the abraded and sub-rounded block lithofacies in the median and distal zones (d ~1.64-1.83; ellipse/a/b ~2.7, Eqs. 7-11 in Fig. 8A) are close to those of the impact breccias along avalanche fault zone in French Massif Central (Eq. 12 in Fig. 8A, Bernard and van Wyk de Vries, 2017). The Riley's circularity (Table 5, see Supplemental File 2) shows that the polyhedral blocks with conchoidal fractures and striations of the ridge structures differentiated from sub-rounded blocks in the distal zone. These may be associated to an oriented abrasion and thermal shock generating tilted blocks with cracked surface. The clast breakage with striations due to collisional transport decreases the Riley's circularity (Table 5). These block lithofacies may be associated to crushing impact with frictional temperature during oscillatory stress

(Bernard and van Wyk de Vries, 2017) related to decompression in rotational shearing, and matrix segregation.

The inherited shapes of the blocks (*a/b* = 1.2-2; ellipse = 0.2-2.5; Riley's circularity ~0.6 in Table 5; Eq. 14 and *a* ~0.9 in Fig. 9) implied the reworking by impact wave (Cox et al., 2019) and similar processes of abrasion between the imbricated block clusters in the proximal zone, the striated blocks from ridges and the tilted distal blocks. These are close to those of the sheared lava breccias observed along the Pichu Pichu debris-avalanche deposit. Flow traction may contribute to block piles (Cox et al., 2019) up to a point where flows are not competent. Fractal *D*-values of the surrounded matrix between 0.6 and 2.8 are associated to an extensional disaggregation and granular transport (Table 4, Blekinsop and Fernandes, 2000). A *syn*-cataclastic emplacement of the blocks with a co-genetic evolution is differentiated between the proximal and median zones and between the striated blocks from ridges and the distal, impacted blocks.

7. Conclusions

Field observations together with quantitative sedimentological analyses help to characterize textural variations of the Paipatja avalanche deposits and the associated pyroclastic density current deposits from Tutupaca volcano in southern Peru. A typical lithofacies assemblage with a reverse grading shows jigsaw breccias, impacted block clusters and striations associated with the interaction between the debris avalanche and the subsequent pyroclastic density currents.

Cyclic impact waves and initial dilation of the Tutupaca lava dome have contributed to produce jigsaw breccias and imbricated block clusters during the first stage of avalanche emplacement. Cluster disaggregation during shock propagation contribute to an upper collisional regime, generating isolated blocks with striations. Transverse blocks, lateral levee and ridges are associated to a switch of mass spreading with granular segregation. The frontal reworking by impact wave with extensional disaggregation contributes to generate impacted block clusters in distal zone. From the statistical dataset, a few regressions have been established indicating the same cataclastic origin with a co-genetic evolution of block lithofacies.

Sequential events of *syn*-emplacement processes during impact waves have been established related to volcanic debris-avalanche units and pyroclastic density current deposits. These observations help to constrain the collisional shearing contact between avalanche units and associated pyroclastic density currents, and help to explain the block cluster growth and the block disaggregation correlated to sequential *syn*-emplacement processes of debris avalanche units with associated pyroclastic deposits.

The deposits at Tutupaca are exceptional for their freshness and clarity, and lack of disturbance. This area is an important record of lava dome collapse and debris avalanche and pyroclastic flow interaction.

Acknowledgments

The fieldwork in Peru trip has been funded by the “Institut de la Recherche pour le Développement” support (O. Roche and P. Samaniego, IRD) for Tutupaca volcano. The geoheritage context is provided through the UNESCO International Geosciences Program project 692, Geoheritage for Resilience.

References

Andrade, S.D., van Wyk de Vries, B., 2010. Structural analysis of the early stages of catastrophic strato-volcano flank-collapse using analogue models. Bull. Volcanol. 72, 771-789.

Bartali, R., Sarocchi, D., Nahmad-Molinari, Y., 2015. Stick-slip motion and high speed ejecta in granular avalanches detected through a multi-sensors flume. Eng. Geol. 195, 248-257.

Bernard, K., 2015. Quelques aspects sédimentaires des avalanches de débris volcaniques. Ph.D. Thesis, Univ. Clermont-Auvergne, France (Unpub., in French). Available at: <NNT : 2015CLF22624>.<tel-01330779>.

Bernard, K., van Wyk de Vries, B., 2017. Volcanic avalanche fault zone with pseudotachylite and gouge in French Massif Central. J. Volcanol. Geotherm. Res. 347, 112-135.

Bernard, K., Thouret, J-C., van Wyk de Vries, B., 2017. Emplacement and transformations of volcanic debris avalanches - A case study at El Misti volcano, Peru. J. Volcanol. Geotherm. Res. 340, 68-91.

Bernard, K., van Wyk de Vries, B., Thouret, J-C., 2019. Fault textures in volcanic debris-avalanche deposits and transformations into lahars: The Pichu Pichu thrust lobes in south Peru compared to worldwide avalanche deposits. J. Volcanol. Geotherm. Res. 371, 116-136.

Blekinsop, T.G., Fernandes, T.R.C., 2000. Fractal characterization of particle size distributions in chromitites from the Great Dyke, Zimbabwe. Pure Appl. Geophys. 157, 505-521.

Blott, S.J., Pye, K., 2008. Particle shape: a review and new methods of characterization and classification. Sedimentology 55, 31–63.

Boudon, G., Semet, M.P., Vincent, P.M., 1984. Flank-failure-directed blast eruption at Soufrière, Guadeloupe, French West Indies: A 3000-yr-old Mt. St. Helens? Geology 12, 350-353.

Caballero, L., Capra, L., 2011. Textural analysis of particles from El Zaguán debris avalanche deposit, Nevado de Toluca volcano, Mexico: Evidence of flow behavior during emplacement. J. Volcanol. Geotherm. Res. 200, 75-82.

Clavero, J.E., Sparks, R.S.J., Huppert, H.E., 2002. Geological constraints on the emplacement mechanism of the Parinacota avalanche, northern Chile. Bull. Volcanol. 64, 40–54.

Clavero, J.E., Polanco, E., Godoy, E., Aguilar, G., Sparks, R.S.J., van Wyk de Vries, B., Perez de Arce, C., Matthews, S., 2004. Substrata influence in the transport and emplacement mechanism of the Ollagüe debris avalanche (northern Chile). Acta Vulc. 16, 59–76.

Cox, R., O'Boyle, L., Cytrynbaum, J., 2019. Imbricated coastal boulder deposits are formed by storm

waves, and can preserve a long-term storminess record. Sci. Rep. 9, 10784.

Crandell, D.R., Miller, C.D., Glicken, H.X., Christiansen, R.L., Newhall, C.G., 1984. Catastrophic debris avalanche from ancestral Mount Shasta volcano, California. Geology 12, 143-146.

Crawford, E., Mortensen, K., 2009. An Image J plugin for the rapid morphological characterization of separated particle sand an initial application to placergold analysis. Comput. Geosci. 35, 347–359.

Davies, T.R., McSaveney, M.M., Kelfoun, K., 2010. Runout of the Socompa volcanic debris avalanche, Chile: a mechanical explanation for low basal shear resistance. Bull. Volcanol. 72, 933-944.

Dennen, R.L., Bursik, M.I., Roche, O., 2014. Dome collapse mechanisms and block-and-ash flow emplacement dynamics inferred from deposit and impact mark analysis, Mono Craters, CA. J. Volcanol. Geotherm. Res. 276, 1-9.

Dufresne, A., Davies, T., 2009. Longitudinal ridges in mass movement deposits. Geomorphology 105, 171-181.DOI:10.1016/j.geomorph.2008.09.009.

Glicken, H., 1986. Rockslide-debris avalanche of May 18, 1980, Mount Saint Helens Volcano, Washington. Ph.D. Thesis, Univ. Calif. Santa Barbara, p. 303.

Glicken, H., 1998. Rockslide-debris avalanche of May 18, 1980, Mount St. Helens Volcano, Washington Bull. Geol. Surv. Jpn. 49, 55-106.

Gray, J.M.N.T., 2013. A hierarchy of particle-size segregation models: from polydisperse mixture to depth-averaged theories. AIP Conf. Proc., 1542, 66-73.

Guilbaud, M-N., Chedeville, C., Molina-Guadarrama, A-N., Siebe, C., 2022. Volcano-sedimentary processes at Las Derrumbadas rhyolitic twin domes, Serdan-Oriental Basin, Eastern Trans-mexican Volcanic Belt. Geol. Soc. Spec. Publ., 520, 31.

Janoo, V., 1998. Quantification of Shape, Angularity, and Surface Texture of Base Course Materials. U.S. Army Corps of Engineers, Cold Regions Research & Engineering Laboratory, Hanover NH, pp. 1-22 (Special Report).

Kelfoun, K., Druitt, T., van Wyk de Vries, B., Guilbaud, M-N., 2008. Topographic reflection of the Socompa debris avalanche, Chile. Bull. Volcanol. 70, 1169-1187.

Launeau, P., Robin, Y.F., 2005. Determination of fabric and strain ellipsoids from measured sectional ellipses - Implementation and applications. J. Struct. Geol. 27, 2223-2233.

Legros, J.F., Cantagrel, J.M., Devouard, B., 2000. Pseudotachylite (Frictionite) at the base of the Arequipa Volcanic landslide (Peru): Implications for emplacement mechanisms. J. Geol. 108, 601-611.

Legros, J.F., 2002. The mobility of long-runout landslides. Eng. Geol. 63, 301–331.

Mariño, J., Samaniego, P., Manrique, N., Valderrama, P., Roche, O., van Wyk de Vries, B., Guillou, H., Zerathe, S., Arias, C., Liorzou, C., 2021. The Tutupaca volcanic complex (Southern Peru): Eruptive chronology and successive destabilization of a dacitic dome complex. J. S. Am. Earth

Sci., 109, 103-227.

Mehl, K.W., Schmincke, H.U., 1999. Structure and emplacement of the Pliocene Roque Nublo debris avalanche deposit, Gran Canaria, Spain. J. Volcanol. Geotherm. Res. 94, 105-134.

Naranjo, J.A., Francis, P., 1987. High velocity debris avalanche at Lastaria volcano in the north Chilean Andes. Bull. Volcanol. 49, 509-514.

Palmer, B.A., Alloway, B.V., Neall, V.E., 1991. Volcanic-debris avalanche deposits in New Zealand: lithofacies organization in unconfined, wet-avalanche flows. In: Fisher, R.V., Smith G.A; (Eds.), Sedimentation in volcanic setting. SEPM Spec. Pub. vol. 45, pp. 89-98.

Samaniego, P., Valderrama, P., Mariño, J., van Wyk de Vries, B., Roche, O., Manrique, N., Chedeville, C., Fidel, L., Malnati, J., 2015. The historical (218 ± 14 aAP) explosive eruption of Tutupaca volcano (Southern Peru). Bull. Volcanol. 77, 51.

Sandnes, B., Flekkoy, E.G., Knudsen, H.A., Maloy, K.J., See, H., 2011. Patterns and flow in frictional fluid dynamic. Nat. Commun. 2, 288.

Shea, T., van Wyk de Vries, B., 2008. Structural analysis and analogue modeling of the kinematics and dynamics of rockslide avalanches. Geosphere 4, 657–686.

Siebe, C., Komorowski, J-C., Sheridan, M-F., 1992. Morphology and emplacement collapse of an unusual debris avalanche deposit at Jocotitlán Volcano, Central Mexico. Bull. Volcanol. 54, 573-589.

Siebert, L., Roverato, M., 2020. A Historical Perspective on Lateral Collapse and Volcanic Debris Avalanche. In: Roverato, M., Dufresne, A., Procter, J., (Eds.), Volcanic Debris Avalanches from Collapse to Hazards. Springer, pp. 11-50.

Siebert, L., Glicken, H., Ui, T., 1987. Volcanic hazards from Bezymianny- and Bandai-type eruptions. Bull. Volcanol. 49, 435-459.

Suzuki-Kamata, K., Kusano, T., Yamasaki, K., 2009. Fractal analysis of the fracture strength of lava dome material based on the grain size distribution of block-and-ash flow deposits at Unze volcano, Japan. Sedim. Geol. 220, 162-168.

Szabo, I., Domokos, G., Grotzinger, J.P., Douglas, J.J., 2015. Reconstructing the transport history of pebbles on Mars. Nat. Commun. 6: 8366.

Valderrama, P., 2016. Origin and dynamics of volcanic debris avalanches: surface structure analysis of Tutupaca volcano (Peru). Earth Sciences. Univ. Blaise Pascal-Clermont-Ferrand II.

Valderrama, P., Roche, O., Samaniego, P., van Wyk de Vries, B., Bernard, K., Marino J., 2016. Dynamic implications of ridges on a debris avalanche deposit at Tutupaca volcano (southern Peru). Bull. Volcanol. 78, 14.

Valderrama, P., Roche, O., Samaniego, P., Van Wyk de Vries, B., Araujo, G., 2018. Granular fingering as a mechanism for ridge formation in debris avalanche deposits: laboratory experiments and implications for Tutupaca volcano, Peru. J. Volcanol. Geotherm. Res. 349, 409-418.

Van Wyk de Vries, B., Self, S., Francis, P.W., Keszthelyi, L., 2001. A gravitational spreading origin for the Socompa debris avalanche. J. Volcanol. Geotherm. Res. 105, 225-247.

Voight, B., Glicken, H., Janda, R.J., Douglass, P.M., 1981. Catastrophic rockslide-avalanche of May 18. In: Lipman, P. W., Mullineaux, D.R. (Eds.), The 1980 eruptions of Mount St. Helens, Washington. U.S. Geol. Surv. Prof. Pap. vol. 1250, pp. 347-371.

Zernack, A., Procter, J., Cronin S., 2009. Sedimentary signatures of cyclic growth and destruction of stratovolcanoes: a case study from Mt Taranaki, New Zealand. Sediment. Geol. 220, 288-305.

Figures and Tables

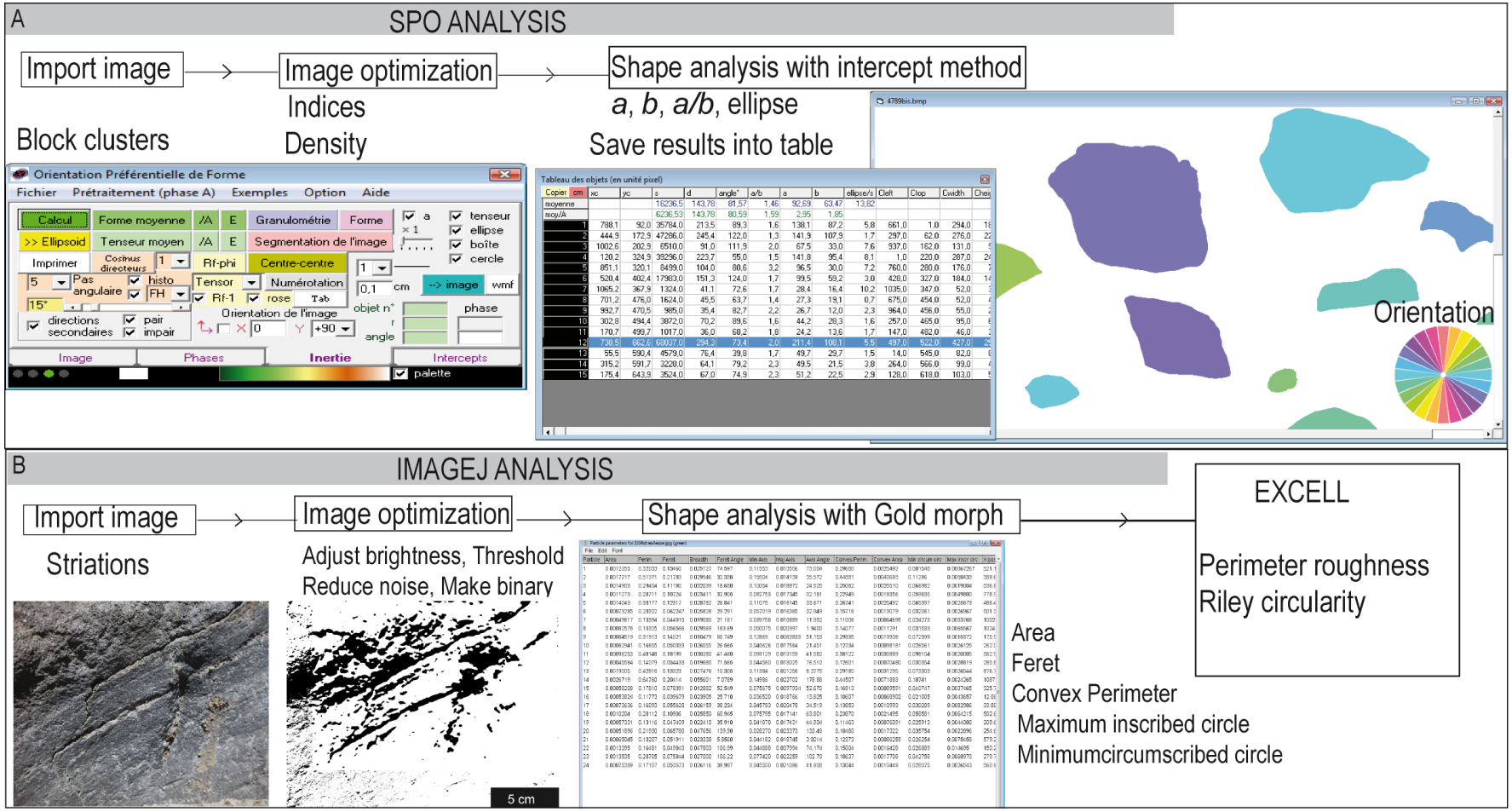

Revised Fig. 1. The flow chart for image analysis. A. The SPO analysis (Launeau and Robin, 2005) of block clusters with the inertia and intercepts method; B. The shape analysis of striations using the ImageJ Plugin "Gold morph" (Crawford and Mortensen, 2009).

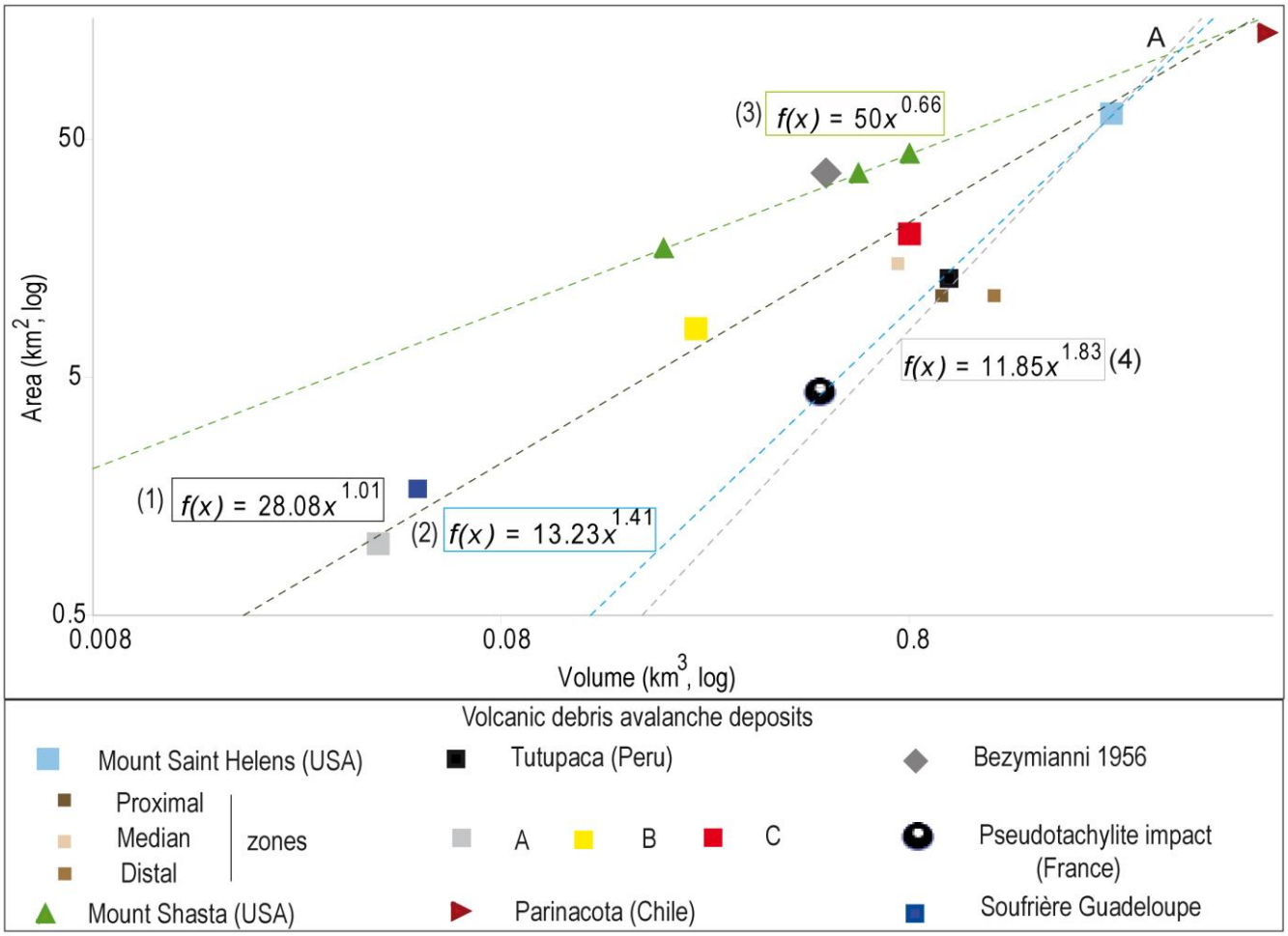

Fig. 2. Area (km^2) *vs.* volume (km^3) of volcanic debris avalanche deposits on double log graph: Mount Shasta and Mount Saint Helens in the USA (Glicken, 1986; Siebert et al., 1987); Bezymianni in Kamchatka (Siebert et al., 1987); Parinacota in Chile (Clavero et al., 2002; Legros, 2002); Tutupaca in Peru (Samaniego et al., 2015; Valderrama et al., 2016); Soufrière in Guadeloupe (Boudon et al., 1984) and Mont Dore in French Massif Central (Bernard and van Wyk de Vries, 2017). A. The proximal zone; B. The ridged unit; C. The distal zone.

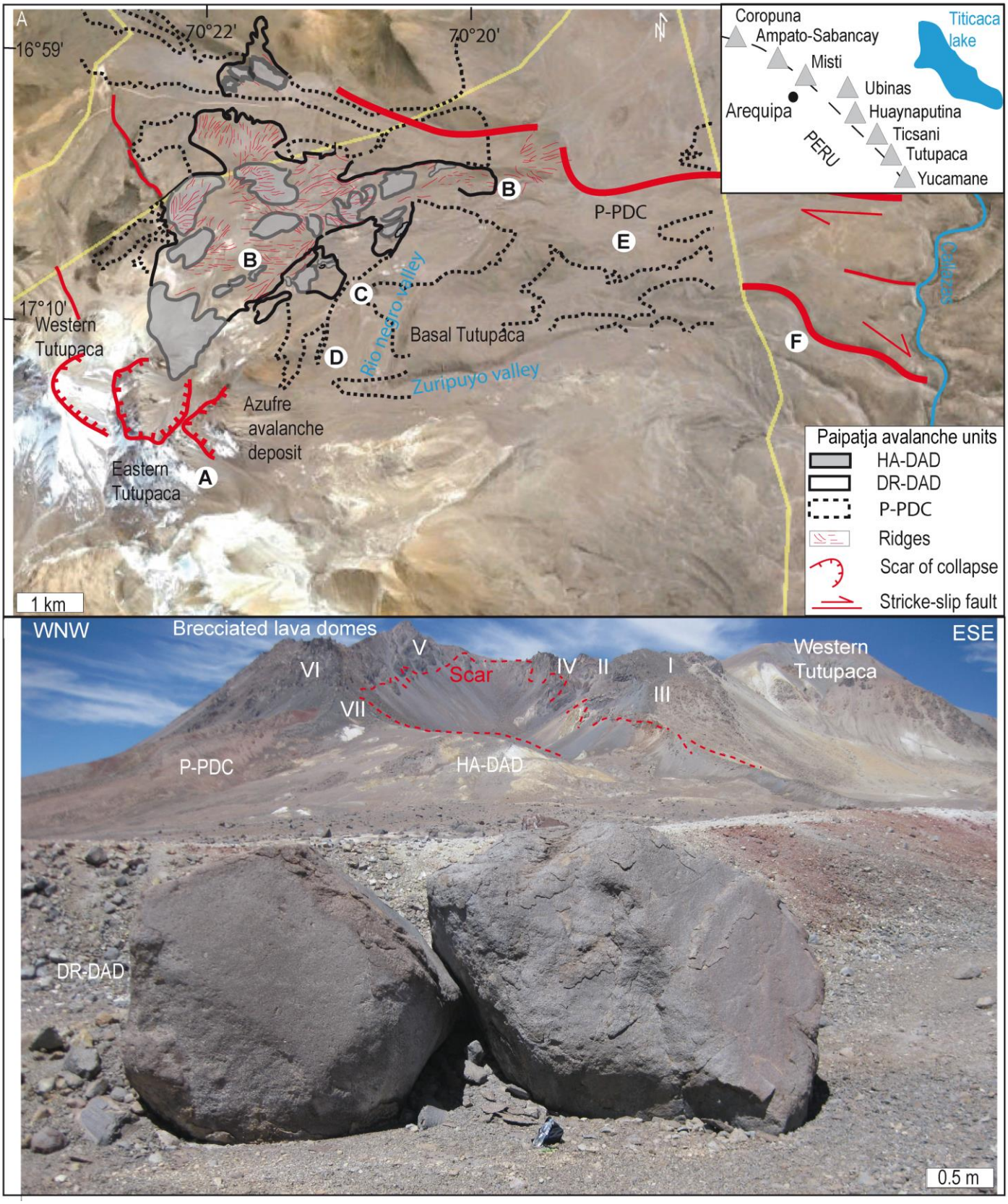

Revised Fig. 3. Geological setting of the Paipatja avalanche deposits exposed in the northeastern part of Tutupaca volcanic complex (Southern Peru, modified from Samaniego et al., 2015; Valderrama et al., 2016). A. Landforms of the avalanche deposits and structures at the North East of the brecciated lava domes from Google Earth with stratigraphic sections. We differentiate the hydrothermal rich avalanche deposit (HA-

DAD, L = 6-8 km, V <1 km^3; H/L = 0.23-0.17, Samaniego et al., 2015); a dome rich debris-avalanche deposit (DR-DAD); the Paipatja pyroclastic density current deposits (P-PDC, ~218 ± 14 aBP). The right-top inset shows the location of Pleistocene volcanoes in the Andean Central Volcanic Zone. The white points indicate the outcrop locations of the clusters and the block lithofacies. A. Under the erosional amphitheater of collapse scar in proximal zone; B. Transverse alignment of blocks and ridge structures; C. Extensional fault zone with abrasion and jigsaw-fractured lithofacies; D. Shear zone along lateral levee; E. Impact and lava bombs; F. Buried blocks and abrasion. B. Panoramic view of the northeast of Tutupaca volcano, showing the horseshoe-shape amphitheater and lava domes (I to VI) and DR-DAD with transverse alignment of blocks. Most of the domes are constructed on the older hydrothermally altered basal edifice (Samaniego et al., 2015; Valderrama et al., 2016).

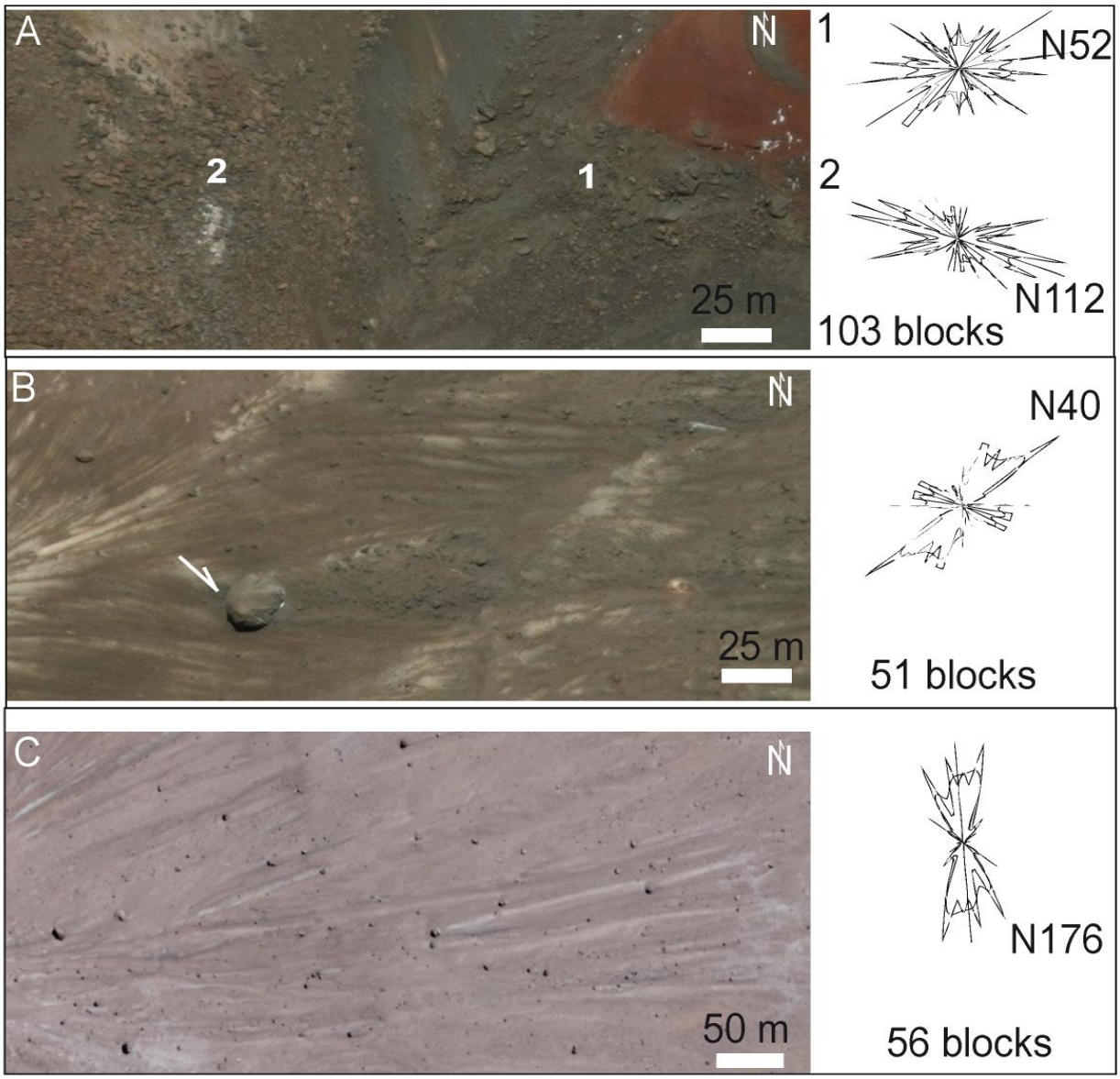

Fig. 4. The syn-emplacement block lithofacies and block orientations (SPO, Launeau and Robin, 2005) from proximal to distal zones using georeferenced Google Earth imagery. A. Proximal brecciated zones under the scar between domes V to VII: 1. An impacted and crushed zone showing imbricated block clusters without preferential orientation; 2. A tilted zone with N112E angular dome fragments adjacent to the PDC in red; B. Isolated polyhedral block (white arrow) of ridge structures in the median zone showing in downstream N40E disaggregated clasts; C. The transverse and isolated blocks (>1 m in length, N176E) surrounded by P-PDC unit in distal zone.

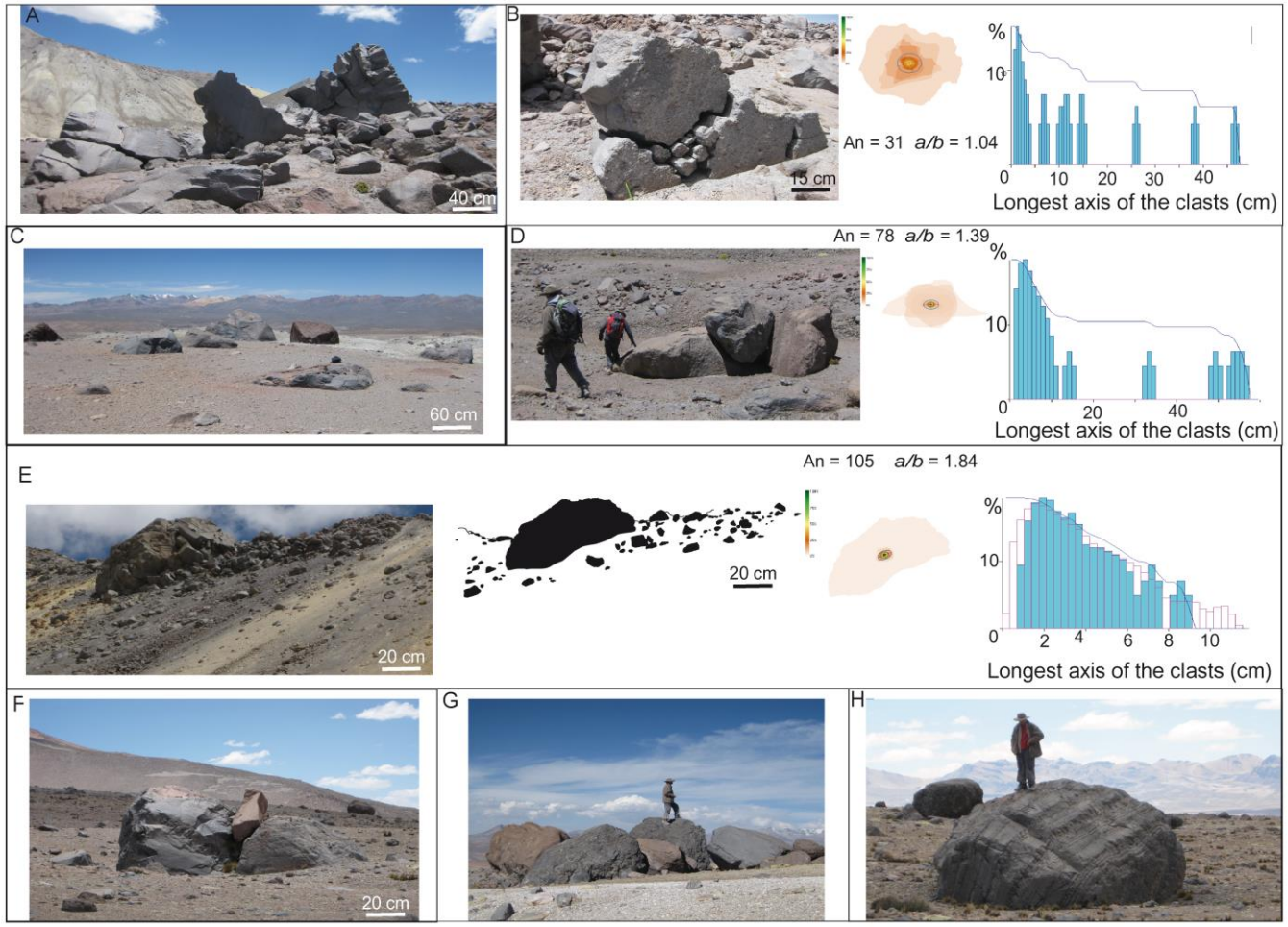

Fig. 5. Block clusters of DR-DAD from SPO analysis (Launeau and Robin, 2005). A. Vertical impact of blocks with abraded surface and undulated fractured borders under the erosional amphitheater of collapse scar; B. Impacted jigsaw-clusters with polymodal clast distribution; C. Subdued blocks in transverse ridges; D. Impacted blocks in distal zone with polymodal distribution of the clasts; E. Block along lateral levee with sigmoidal jigsaw-breccias showing a bimodal clast distribution; F. Angular and impacted block between aligned and subdued blocks; G. Block cluster in distal zone; H. Subdued and tilted blocks.

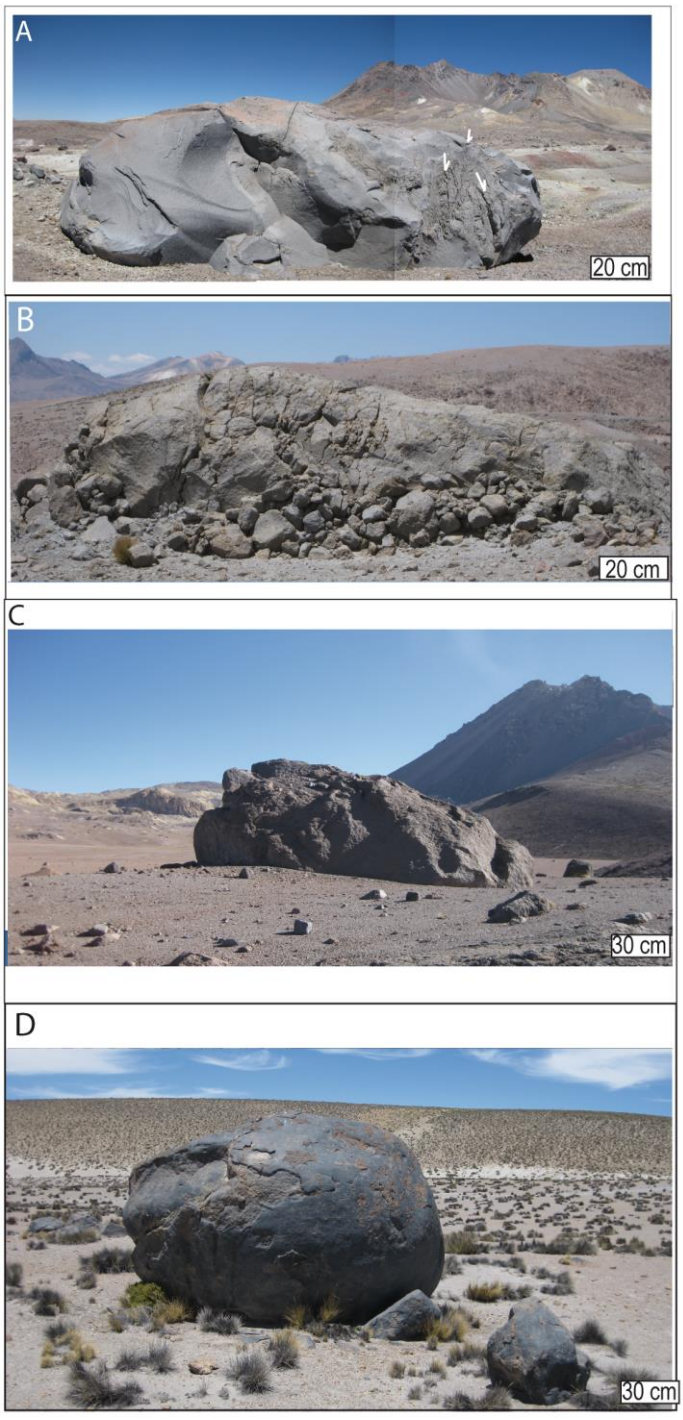

Fig. 6. Textural gradient of block lithofacies of the Paipatja avalanche deposits. A. Transverse blocks with an oriented abrasion: *white arrows* show striations on upstream sub-rounded faces and planar faces with conchoidal fractures in downstream; B. Large polyhedral block (~3 m high and ~5 m length) with an oriented abrasion, quenched and cracked surface in upper part and sub-rounded lava in altered vitreous phase in lower part; C. Transversal alignment of abraded blocks with bimodal clast distribution from SPO analysis (Launeau and Robin, 2005) related to pyroclastic density current deposits; D. Polymodal clast distribution (SPO analysis, Launeau and Robin, 2005) of pyroclastic density current deposits around a distal sub-rounded block.

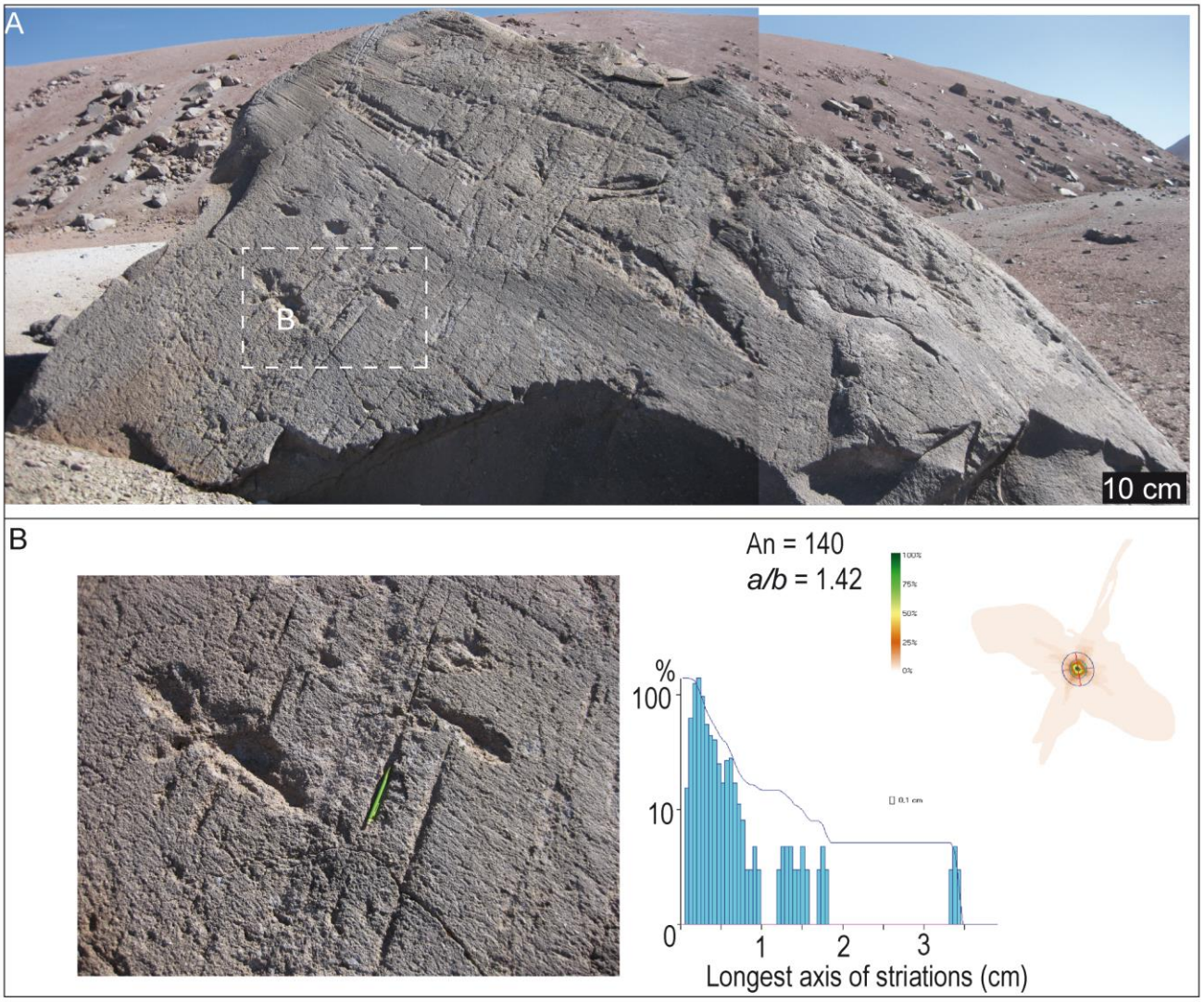

Fig. 7. Striations and grooves of ridged blocks from SPO analysis (635 striations, Launeau and Robin, 2005). A. Subdued block (~2 m high and 1.6 m length) with abraded planar surfaces, grooves and striations with circular depressions (~1-5 cm depth, ~2-3 mm wide); B. Detailed analysis of grooves and striations showing polymodal distribution related to the P-PDC interactions (An = 140 striations, *a/b* = 1.42).

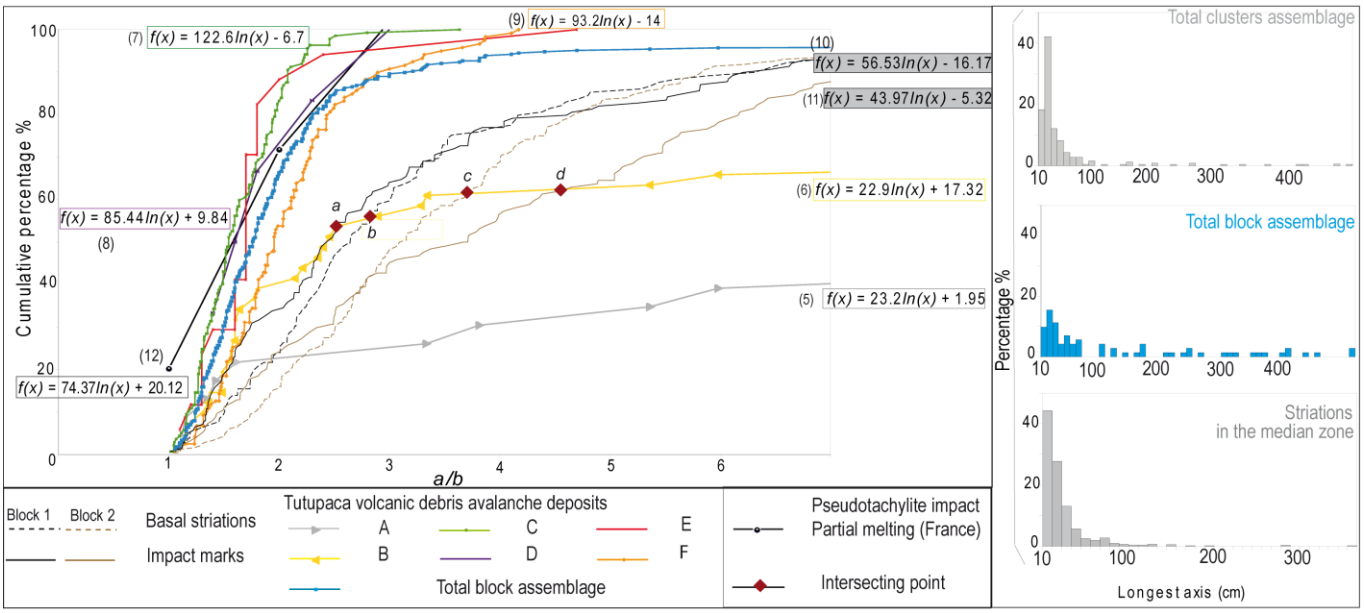

Revised Fig. 8. Sedimentological analysis of block lithofacies of the Paipatja avalanche deposits from proximal to distal zones. A. Cumulative curves of block lithofacies *vs.* *a/b* from SPO analysis (404 blocks, 635 striations and impact marks; Launeau and Robin, 2005); B. Histograms.

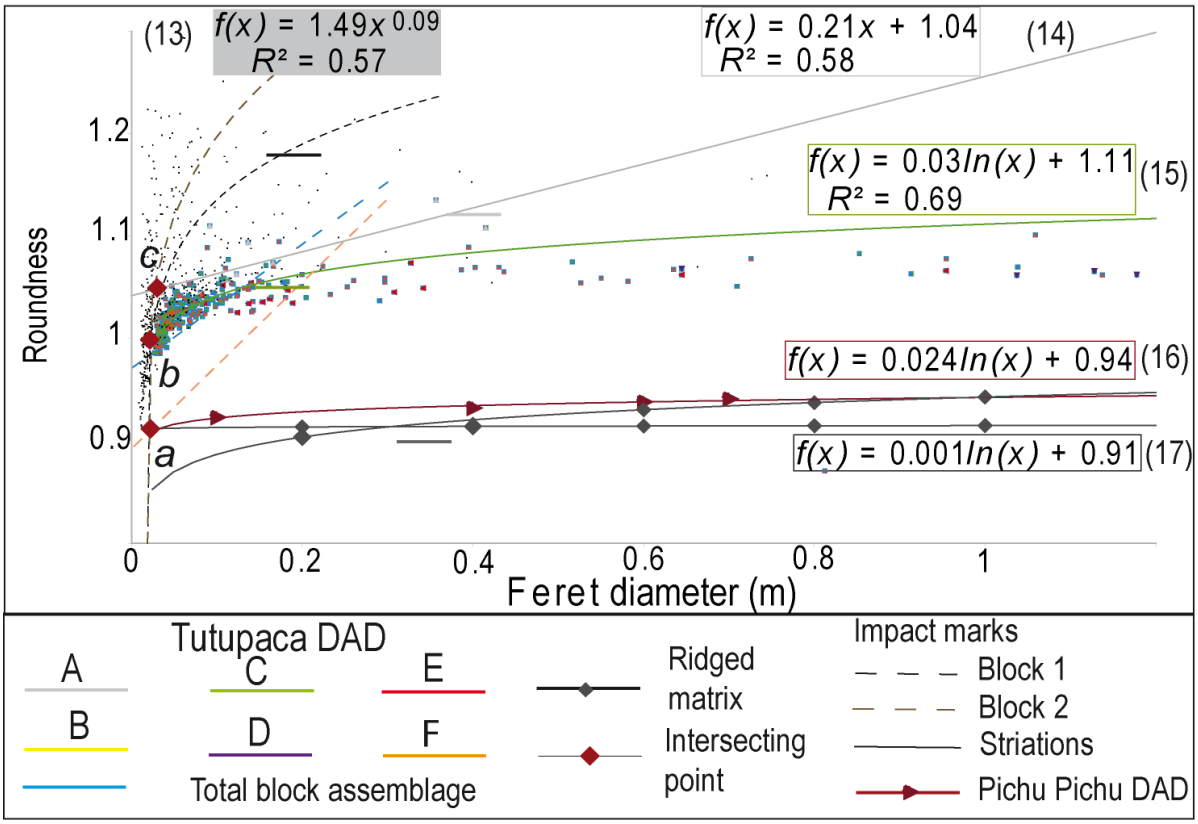

Revised Fig. 9. Roundness *vs.* Feret's diameter (m) of block lithofacies and striations in different zones from shape analysis using the software ImageJ (404 blocks, 635 striations and impact marks; Blott and Pye, 2008; Crawford and Mortensen, 2009). The *horizontal lines* indicate the Feret's diameter at which roundness stopped increasing. Error bars are smaller than the symbols.

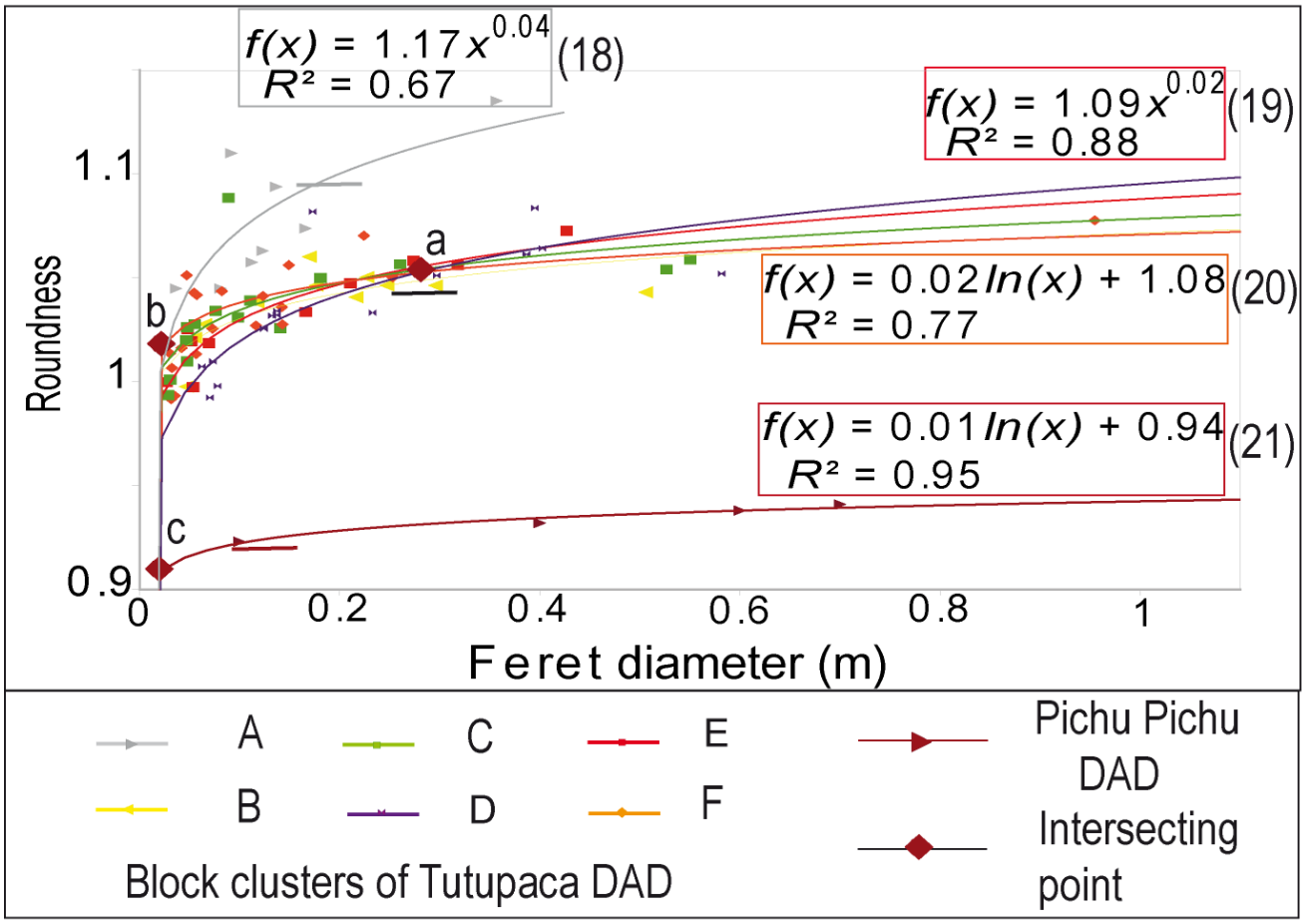

Revised Fig. 10. Roundness *vs.* Feret's diameter (m) of block clusters from shape analysis using the software ImageJ (Blott and Pye, 2008; Crawford and Mortensen, 2009). The *horizontal lines* indicate the Feret's diameter at which roundness stopped increasing. Error bars are smaller than the symbols (see Supplemental File 2).

Revised Table 1. List of acronyms and their definitions.

	Acronyms	Definitions
Quantitative parameters	*A*	Area
	a/b	the largest axis / minor axis
	D	Fractal dimension
	d	Depth
	E	Ellipse
	Ellipse/a/b	The ratio of the ellipse to the *a/b*
	FD	Feret's Diameter
	H	Height
	h	Exponent of the power regressions
	H/L	Apparent friction
	L	Length
	S	Surface
	T	Thickness
	v	Velocity
	V	Volume
	W	Width
Lithofacies	DR-DAD	Dome-rich debris-avalanche deposit
	HA-DAD	Hydrothermally-rich debris avalanche deposit
	P-PDC	Paipatja pyroclastic density current deposit

Revised Table 2. Methodology for block laboratory analysis.

Outcrop map and observations	Google Earth imagery, landforms, faults, orientations, lateral and vertical variations in block lithofacies and lithostratigraphy, textures.
Grain size analysis	Image analysis and Feret's diameter measurement. Clast size distribution: cumulative curves, fractal distributions, statistical parameters.
Shape analysis	Shape analysis with texture of blocks, preferred orientation of block largest axis and

shape parameters.

Revised Table 3. Clast shape parameters with Feret's Diameter (*FD*), Riley's circularity (*Rc*) and Roundness (*R*, Blott and Pye, 2008; Crawford and Mortensen, 2009; Bernard, 2015).

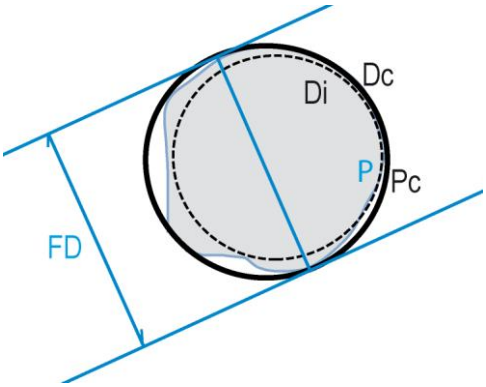	Feret's Diameter (*FD*) The longest distance between two parallel tangential lines
	Riley's circularity (*Rc*, Riley, 1941) $Rc = \sqrt{(Di / Dc)}$ *Di* the largest inscribed circle *Dc* the smallest circumscribed circle
	Roundness (*R*) $R = P / Pc$ *P* Perimeter *Pc* Convex perimeter

Revised Table 4. Fractal results of block lithofacies in different zones and striations compared to the surrounded matrix of the Paipatja avalanche deposits and P-PDC (see Supplemental File 1; Suzuki-Kamata et al., 2009).

	h	*D*	Correlation coefficient	Range of the clast size (cm)	Number of clasts
A	1,37	0,26	0,9	6.7-22.1	14
B	0,67	1,66	0,9	13.2-47.5	18
C	1,7	-	0,9	10.4-22.9	78
D	2,29	-	0.95	233.4-539.5	7
E	1,92	-	0.93	30.3-68.7	9
F	0,58	1,83	0,9	10.7-96.5	120
All zones	0,86	1,28	0,9	11.4-40.3	137
Surrounded matrix	0.07-1.16	0.67-2.84	0.91-0.98	0.001-6.4	-
Striations	1.18	0.6	0.9	5.94-44.68	265

Revised Table 5. Mean values of block shape parameters and striations from SPO and shape analysis using the software ImageJ (404 blocks, see Supplemental File 2; Launeau and Robin, 2005; Blott and Pye, 2008; Crawford and Mortensen, 2009; Bernard, 2015). These shape data have been associated with the correspondent standard errors.

	Roundness	Riley's circularity	*a/b*	Ellipse	Ellipse/*a/b*
A	1.07±0.01	0.73±0.03	1.68±0.14	3.61±0.74	2.29±0.54
B	1±0.02	0.69±0.02	1.88±0.38	3.2±0.65	1.7±0.24

C	1.02±0.001	0.68±0.006	1.63±0.3	3.34±0.25	2.04±0.15
D	1.13±0.07	0.64±0.05	1.91±0.26	5.15±2.18	2.7±0.59
E	1±0.02	0.64±0.02	1.8±0.2	5.01±1.25	2.78±0.33
F	1.05±0.03	0.63±0.01	2.1±0.06	3.95±0.24	1.88±0.35
Mean	1.23±0.009	0.66±0.005	1.7±0.03	3.5±0.15	2.05±0.1
Striations	0.9±0.01	0.3±0.007	3.69±0.1	21.9±1.57	5.82±0.5

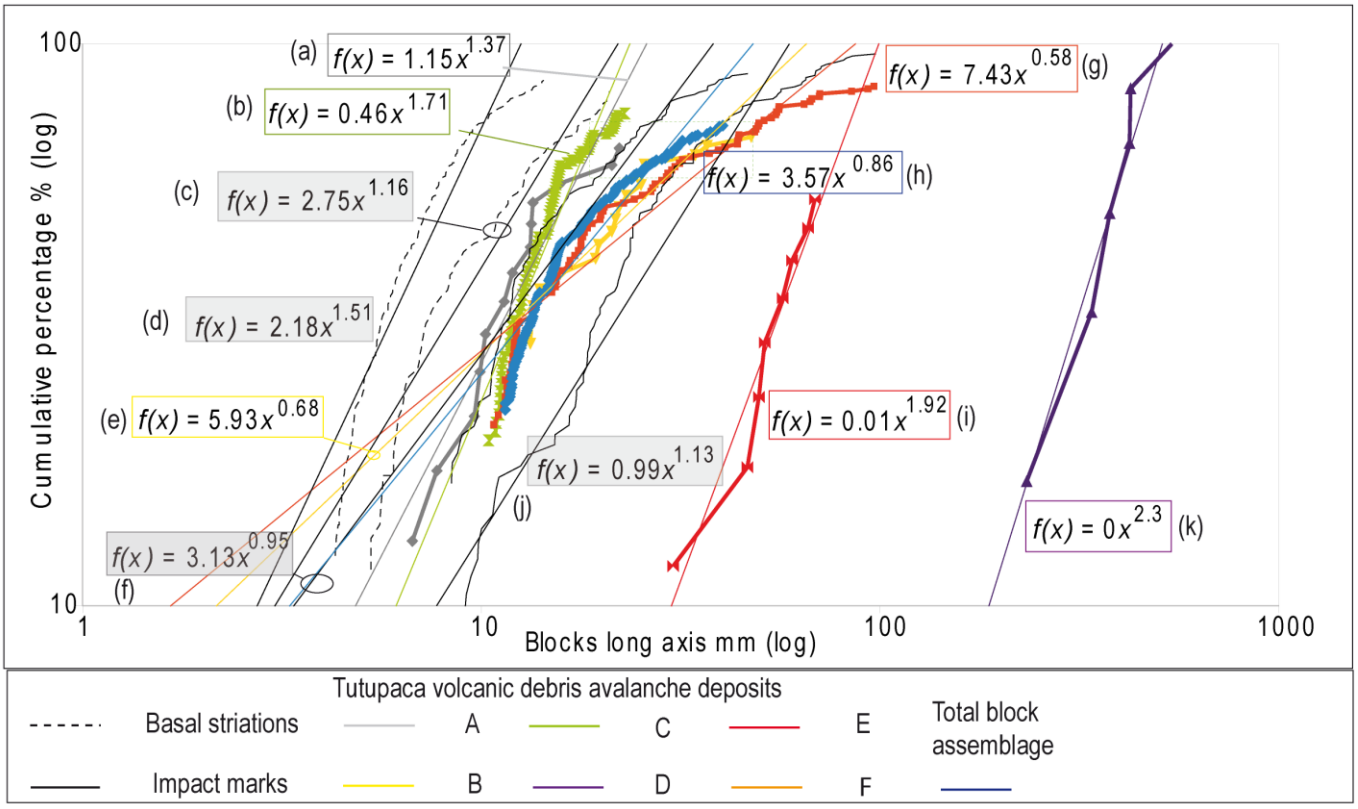

Supplemental File 1

Cumulative % *vs.* long clast-axis on double log graph. The exponent *h* of size distributions were estimated from the power regressions (*a*-*k*) by the methods of the least squares (R^2 >0.9 in Table 4, Eq. 6 in Suzuki-Kamata et al., 2009). The *h* values obtained for each structural unit ranged from 6.7 to 537.9 cm for block lithofacies and from 5.94 to 44.68 cm for striations. From following equation $2h + D = 3$ (Eq. 7 in Suzuki-Kamata et al., 2009), we translate the *h*-values into fractal *D* values in Table 4. The *h*-values for the block lithofacies and striations range from 0.58 to 2.29 (Table 4). Substitution of these values into the previous equation (Eq. 7 in Suzuki-Kamata et al., 2009), gives corresponding fractal *D*-values of 0.26 to 1.83. The negative values of fractal dimension have not been considered in Table 4.

Manuscript Number: VOLGEO-D-21-00343R2

Collisional interactions and the transition between lava dome sector collapse and pyroclastic density currents at Tutupaca volcano (Southern Peru).

Dear Karine Bernard,

Thank you for submitting your manuscript to Journal of Volcanology and Geothermal Research. I have received comments on your manuscript from two reviewers (accept and minor). Both reviewers found that you have significantly improved your manuscript. One of them asked for a minor revision and provided an edited file and some comments listed in the review. Both reviewers, though, mentioned some issues with figures 7 and 9. Therefore, I invite you to resubmit your manuscript after minor revision.

When revising your manuscript, please provide a 'response to the reviewers' that outlines every change made point-by-point in response to the reviewers' comments, stating clearly exactly what has been changed in the manuscript and providing line numbers wherever possible. Please also provide suitable rebuttals for any comments not addressed. Please note that your revised submission may need to be re-reviewed.

To submit your revised manuscript, please log in as an author at https://www.editorialmanager.com/volgeo/, and navigate to the "Submissions Needing Revision" folder.

NOTE: Upon submitting your revised manuscript, please upload the source files for your article. We cannot accommodate PDF manuscript files for production purposes. We also ask that when submitting your revision, you follow the journal formatting guidelines. For additional details regarding acceptable file formats, please refer to the Guide for Authors at: https://www.elsevier.com/journals/journal-of-volcanology-and-geothermal-research/0377-0273/guide-for-authors

Journal of Volcanology and Geothermal Research values your contribution and I look forward to receiving your revised manuscript.

Research Elements (optional)
This journal encourages you to share research objects - including your raw data, methods, protocols, software, hardware and more – which support your original research article in a Research Elements journal. Research Elements are open access, multidisciplinary, peer-reviewed journals which make the objects associated with your research more discoverable, trustworthy and promote replicability and reproducibility. As open access journals, there may be an Article Publishing Charge if your paper is accepted for publication. Find out more about the Research Elements journals at https://www.elsevier.com/authors/tools-and-resources/research-elements-journals?dgcid=ec_em_research_elements_email.

Kind regards,

Jose Luis Macias

Editor, Journal of Volcanology and Geothermal Research.
Editor and Reviewer comments:

Rebuttal letter

We thank the Chief Editor and all reviewers for their useful comments. The detailed and fair reviews, together with many insightful comments, have been greatly appreciated. We have taken account of the reviewer comments. Revised sentences, paragraphs, sections as well as changes in titles as recommended appear in blue. Below is a summary of our response to the comments of Editor-in-Chief Dr. Macias and

the two reviewers.

Comments of Chief Editor Dr. Macias:

Figures 9B and 10B with no clear correlations (with R^2 ≤0.5) that we attributed to the shape variations of block lithofacies and striations based on textural parameters have been removed according to reviewers 1 and 2. Supplementary files 1 and 2 focus on the original data used to calculate the fractal dimension, the mean values and standard errors of the shape parameters. We have checked the format of revised manuscript.

Reviewer #1: Dear Editor of JVGR,

After reading the new version of the manuscript "Collisional interactions and the transition between lava dome sector collapse and pyroclastic density currents at Tutupaca volcano (Southern Peru)" by Bernard et al., It is clear that the paper has been greatly improved. The comments made in previous reviews have been mostly solved. Nevertheless, It still seems that the correlations shown in Figures 9 and 10B are low to fully support all the inferences made from them. However, the detailed description of the Tutupaca debris avalanche and the deep textural analysis shown in this work is novel and of clear relevance to the scientific community and the study of debris avalanches. Based on this, I suggest approving the manuscript for its publication by JVGR.

Figures 9B and 10B with no clear correlations (with R^2 ≤0.5) with intersecting points that we attributed to the shape variations of block lithofacies and striations based on textural parameters have been removed according to reviewer 1. These paragraphs (lines 370-371, 527-529) related to Figs. 9B and 10B have been removed. The comments have been considered related to table 5 and supplemental file 2.

Lines 408-410. The Riley's circularity of block clusters shows decreasing values from the proximal to distal zones (Table 5, see Supplemental File 2) related to Feret's diameter, implying textural relationships between the block clusters with the run-out distance.

Lines 502-503. Textural relationships appear between proximal blocks and the striated blocks from the ridges (Table 5) with decreasing values of Riley's circularity.

Lines 540-543: The inherited shapes of the lava blocks and the co-genetic evolution between the blocks from the ridges and striations may be associated to secondary fracturing with partial decompression during run-out propagation (Bernard et al., 2019).

Lines 554-561. The Riley's circularity (Table 5, see Supplemental File 2) shows that the polyhedral blocks with conchoidal fractures and striations of the ridge structures differentiated from sub-rounded blocks in

the distal zone. These may be associated to an oriented abrasion and thermal shock generating tilted blocks with cracked surface. The clast breakage with striations due to collisional transport decreases the Riley's circularity (Table 5). These block lithofacies may be associated to crushing impact with frictional temperature during oscillatory stress (Bernard and van Wyk de Vries, 2017) related to decompression in rotational shearing, and matrix segregation.

Reviewer #2: Dear Authors:

In this new review, I have found the paper more complete and with a better readability. I consider that it contains relevant information and the methodology used offers interesting ideas for the reader who works with avalanches. The new paragraphs added in the introduction and in the methodology, as well as the various changes and attachments that have been made, have improved the work significantly. The majority of the suggested changes have been made; however, the text is still perfectible (see added file with annotations) and two non-negligible issues remain and must be solved.

The first is related to figures 9 and 10, the ultimate meaning of which is still difficult for the reader to understand and which, from my point of view, could hide a background error. In fact, in the original figure you submitted, on the abscissa there was a parameter called "Feret's Diameter" and it had a length in meters (m). With this grainsize parameter the graph made sense because it was a shape parameter (perimeter's roughness and Riley's Circularity) versus a grainsize. However, this parameter was poorly defined in the original text. In Table 2, where it appeared as the relationship between Feret max (a major diameter) and a Feret perpendicular to the former (an intermediate diameter), that is, a general form parameter. This error was pointed out in the first revision and the name was changed in Table 2 and in the figures. Anyhow, now the graph has a general form parameter on the ordinate (Max Feret diameter versus intermediate Feret diameter) and another general form parameter on the abscissa (Riley circularity). This being the case, it is autocorrelated data and does not provide useful information. This is a point that has to be unraveled.

The definitions and the figure of the shape parameters for the debris avalanche are described separately in Table 3. The Feret's diameter defined as the longest distance between two parallel tangential lines (Table 3) and roundness have been considered.

Lines 140-143. The shape analysis using the ImageJ Plugin “Gold morph” has been applied to 404 blocks and 635 striations of the avalanche units to compute minor and major axis length, Feret's diameter defined as the longest distance between two parallel tangential lines, perimeter and convex perimeter, radii of the smallest inscribed and largest circumscribed circles (Fig. 1B; Table 3; Crawford and Mortensen, 2009).

Lines 146-147. The values of Riley's circularity are less than 1 for the non-spherical volcanic clasts (Table 5).

Lines 156-157. The roundness, the Riley's circularity, the *a/b* ratio, ellipse, fractal *D*-values of each mesoscale structure have been calculated.

Figures 9B and 10B with no clear correlations (with $R^2 \leq 0.5$) that we attributed to the shape variations of block lithofacies and striations based on textural parameters have been removed according to reviewer 1. These paragraphs (lines 370-371, 527-529) related to Figs. 9B and 10B have been removed. The comments are considered related to table 5 and supplemental file 2.

Lines 408-410. Riley's circularity of block clusters shows decreasing values from the proximal to distal zones (Table 5, see Supplemental File 2) related to Feret's diameter, implying textural relationships between the block clusters with the run-out distance.

Lines 502-503. Textural relationships appear between proximal blocks and the striated blocks from the ridges (Table 5) with decreasing values of Riley's circularity.

Lines 554-561. The Riley's circularity (Table 5, see Supplemental File 2) shows that the polyhedral blocks with conchoidal fractures and striations of the ridge structures differentiated from sub-rounded blocks in the distal zone. These may be associated to an oriented abrasion and thermal shock generating tilted blocks with cracked surface. The clast breakage with striations due to collisional transport decreases the Riley's circularity (Table 5). These block lithofacies may be associated to crushing impact with frictional temperature during oscillatory stress (Bernard and van Wyk de Vries, 2017) related to decompression in rotational shearing, and matrix segregation.

Another important point to clarify and solve, is related to the fractal analysis of the granulometries, carried out using the method of Suzuki -Kamata et al., 2009. Table 4 shows values of negative fractal dimension (distributions C, D and E), which can be originated by two causes, 1) having plotted the granulometric curves in reverse or 2) having an unrealistic granulometric distribution due to insufficient data or having used a non-rigorous methodology (see annotations in the attached file).
Considering the great effort provided in improving the manuscript, the increased readability and the important and interesting data presented, I believe that the paper can be ready for publication in JVGR after having satisfactorily resolved the two indicated points and realized the minor changes suggested.
A cordial greeting
Damiano Sarocchi

The negative values of fractal dimension have been removed in Table 4 (See Supplemental file 1) and the standard errors ($<10^{-3}$) related to photographic shot geometries have been considered (lines 138-140).

Supplemental File 1

Cumulative % *vs.* long clast-axis on double log graph. The exponent *h* of size distributions were estimated from the power regressions (*a*-*k*) by the methods of the least squares ($R^2 >0.9$ in Table 4, Eq. 6 in Suzuki-Kamata et al., 2009). The *h* values obtained for each structural unit ranged from 6.7 to 537.9

cm for block lithofacies and from 5.94 to 44.68 cm for striations. From following equation $2h + D = 3$ (Eq. 7 in Suzuki-Kamata et al., 2009), we translate the *h*-values into fractal *D* values in Table 4. The *h*-values for the block lithofacies and striations range from 0.58 to 2.29 (Table 4). Substitution of these values into the previous equation (Eq. 7 in Suzuki-Kamata et al., 2009), gives corresponding fractal *D*-values of 0.26 to 1.83. The negative values of fractal dimension have not been considered in Table 4.

Lines 128-129

Where can these curves be found? are those the curves of figure 8? But they are only three curves. It is very important that all granulometries can be consulted, at least in supplementary material. The granulometries are those of figure 8? It should be noted that the curves are not complete, they have a bias towards the coarse clasts, completely missing the component of clasts below 10 cm for resolution limits. Explain somewhere how the granulometry was obtained. Are the percentages obtained by volumetric data (stereological method)? or are they just counts?

Lines 127-139. Fractal dimensions *h* and *D* of size distributions were estimated from the power regressions (Table 4, see Supplemental File 1, Suzuki-Kamata et al., 2009). The cumulative curves of the clast-size distributions *vs. a/b* (Fig. 8) were compared to distinguish the block avalanche units from proximal to distal zones. The calculated block-size distributions estimated from 41 outcrop photographs with the inertia and intercepts methods using the SPO analysis (from metric-size blocks to clasts >10 cm; Fig. 8B; Launeau and Robin, 2005). The longest axis of 404 block outlines were measured and counted per image area from the photographs. The normalized frequency histograms (Launeau and Robin, 2005) were produced by grouping the longest axis of blocks (cm) into 100-cm bins (number of size-intervals) and normalizing the number of occurrences in each bin to the total number of measurements from automatic image analysis. The sectional effects have been considered (Launeau and Robin, 2005). These data contribute to differentiate the effect of cataclasis between each fraction correlated with different structural units from proximal to distal zones. The subdued blocks and clasts below 10 cm are not considered related to resolution limits.

Line 136 : Are refering to Riley's value? This sentence is not clear

Line 146-147: The values of Riley's circularity are less than 1 for the non-spherical volcanic clasts (Table 5).

Lines 137-138. In this case, the resolution of the camera is not so important, what is rather important is how the photographs were taken, distance, geometry of the shot, objective used (the distortions in the image depend on this).

Lines 148-152. To characterize the two-dimensional shape of mesoscale structures, we took 5.9 megapixel photographs of abraded flat surfaces of two blocks with a digital camera. A digital camera (6.2-18.6 mm lens, 35-105 mm focal length) image at a camera distance of <20 cm had a standard error for mean distortion around ~10^{-3}. All the striations observed in the median zone have been quantified by using high-resolution images (3648 X 2736 pixels) of two block faces.

Lines 150-152

If the Feret ratio is a measure of the general form, as it appears in the definition given in table 2, and the Riley circularity is also a form factor related to the general form of the clasts, the graph does not make much sense, and data in this case would be autocorrelated.

The Feret's diameter (m), defined as the longest distance between two parallel tangential lines (Table 3, Figs. 9-10) have been considered.

Lines 162-164. Figure 9 shows the evolution of the roundness with Feret diameter for block lithofacies and striations. Figure 10 shows the evolution of the roundness with Feret diameter for block clusters.

Line 205. This symbol has already been used twice, for the depth of the grooves and to define one of the fractal dimensions. You have to change the symbols!

Lines 217-219. … characterized by torevas (H = 20-40 m, L = 1.5 km), long lateral levees (L = 1.5 km) and hummocky-structures (L = 200-800 m, H = 20-40 m) up to 4-6 km from the scar (Samaniego et al., 2015; Valderrama et al., 2016).

Lines 326-331. : It would be important to be able to consult the log-log graphs with "cumulative mass of fragments" vs "particle size" used to calculate the fractal dimension, as well as the original granulometries and known the number of clasts used to obtain the distributions. Maybe in the supplementary material. About the methodology used to obtain the granulometric distributions, see specific comment.

Supplementary file 1 focus on the original data used to calculate the fractal dimension. The number of clasts used to obtain the distributions have been considered in Table 4. The negative values of fractal dimension have been removed in table 3 (See Supplemental file 2) and the standard errors (<10^{-3}) related to photographic shot geometries have been considered (lines 138-140).

Lines 338-340. A specific clast-size fractal distribution is calculated in the range between 6.7 and 539 cm. The mean fractal D value, calculated from exponent h of power regressions, is around ~1.28 in the 11.4-40.3 cm clast-size range (Table 4; see Supplemental File 1; Suzuki-Kamata et al., 2009).

Lines 342-343. I think it is the sum of internal variability and measurement errors.

Lines 354-356. The calculated standard errors indicate the measurement errors and the sum of internal variability between the block shape parameters. These values imply distinct evolution between the avalanche block lithofacies and PDC.

Line 371. It is necessary to fully understand which is the parameter on the abscissa. Is it a coarse-shape parameter, or the clast's diameter? You need to clarify this better, if it is a scatter-plot with two parameters describing a coarse shape in both axes. It makes no sense, it doesn't provide useful information.

Lines 376-382. The mean values increase for roundness from 1 to 1.7 and ellipse/*a/b* from 0.2 to 2.7 (Table 5), while the values of Riley's circularity decrease. A regression characterizes the roundness *vs.* maximum Feret's diameter (Eq. 13 in Fig. 9) for the striations. The intersecting point *c* (Eqs. 13-14 in Fig. 9) with Feret's diameter <0.05 m and roundness around ~1.05 characterizes the inherited clast shape of the proximal block lithofacies generating striations and impact marks in the ridged debris-avalanche unit. We observed decreasing values of Riley's circularity related to Feret's diameter (Table 5).

revised Fig. 1. Eliminate Fourier Shape Analysis from the figure! This term has been removed.

Revised Fig. 3. These metric references, highlighted in pink, are not clear. Is it about blocks of 7-8 meters?? Based on this reference it would seem that they are 7-8 meters large. Anyway, if I'm not mistaken, in the foreground there is a 1.5 liter bottle of water, near a block. So the block would be no more than 2 m in diameter. These metric references have been considered in Figure 3.

revised Fig. 10: If the Feret ratio is a measure of the general form as it appears in table 2, and the Riley circularity is also a factor of the general form, the graph does not make much sense and the data in this case would be autocorrelated. The graph would make more sense if it was actually the Feret diameter. Or also the relationship between the Feret diameter of each particle and the Feret diameter i.e. of the largest particle present in the whole set (normalization), indicators of grain size. Revise this point or delete the figure. The Feret's diameter (m) have been considered. Figures 9B and 10B with no clear correlations (with $R^2 \leq 0.5$) that we attributed to the shape variations of block lithofacies and striations based on textural parameters have been removed according to reviewers 1 and 2.

It would be interesting to be able to consult the original data used to calculate the mean values and standard errors in supplementary material. See Supplemental file 2

revised Table 1. It seems to me that the same symbol has also been used for the depth of the grooves and also the height of the blocks! . In this case change symbols. These acronyms have been defined. The depth (*d*) of the grooves and striations are differentiated from the Height (*H*) of the blocks in Table 1.

revised Table 2. According to the definition of Feret Ratio in Tab.2, it is not a granulometry measurement, but rather a shape factor similar to elongation. The Feret diameter has been considered.

Revised Table 3. : The definition of Feret or Feret ratio, is one of the most important problems remaining in the paper. Observing the original figure, it is clear that it was a measurement of length in meters (m). Which makes much more sense than using a parameter in the x similar to the one in the y. See other comments and clarify this very important doubt. Fm. From the figure, it appears that Fm is half the Feret diameter at 90° of the Feret max.

The Feret's Diameter (*FD*), defined as the longest distance between two parallel tangential lines, has been considered in the figure of table 3.

Perimeter roughness. This measure, determined by the relationship between the real perimeter and the convex hull perimeter, is not so sensitive to roughness and rather reflects irregularities in the order of roundness. The Feret's Diameter (*FD*), defined as the longest distance between two parallel tangential lines, has been considered in the figure of table 3. The roundness parameter has been considered.

Revised Table 4 D. IMPORTANT!

Based on the methodology of Suzuki-Kamata et al. 2009, analyzing realistic granulometries, negative values of fractal dimension cannot come out. One possibility is that the distribution is inverted by mistake. Very abnormal granulometries for methodological reasons could also determine this type of results. Please check this very important point! It would be recommendable that at some point in the paper or in complementary material, details about the methodology used to construct the granulometric curves, would be given. Realistic and rigouros grain size, cannot be obtained from a photograph simply by measuring the apparent length of the major axis. It is necessary to use correct photographic shot geometries and a stereological method, such as Rosiwall intersection analysis, point

Supplementary file 1 focus on the original data used to calculate the fractal dimension. The number of clasts used to obtain the distributions have been considered in Table 4. The negative values of fractal dimension have been removed in table 3 (See Supplemental file 1) and the standard errors ($<10^{-3}$) related to photographic shot geometries have been considered (lines 138-140).

revised Table 5. No Fourier analysis was performed in this work. Extraordinarily low values for being dimensionless shape parameters! Excellent! This term has been removed. The standard errors of the scale and shape parameters have been considered. Supplementary file 2 focus on the original data used to calculate the mean values and standard errors of the shape parameters.

My coauthors and I feel the revised manuscript is now ready for publication in JVGR.

K. Bernard, 21 August 2022

*****

More information and support

FAQ: How do I revise my submission in Editorial Manager?

https://service.elsevier.com/app/answers/detail/a_id/28463/supporthub/publishing/

You will find information relevant for you as an author on Elsevier's Author Hub: https://www.elsevier.com/authors

FAQ: How can I reset a forgotten password? https://service.elsevier.com/app/answers/detail/a_id/28452/supporthub/publishing/kw/editorial+manager/

For further assistance, please visit our customer service site: https://service.elsevier.com/app/home/supporthub/publishing/. Here you can search for solutions on a range of topics, find answers to frequently asked questions, and learn more about Editorial Manager via interactive tutorials. You can also talk 24/7 to our customer support team by phone and 24/7 by live chat and email.

#AU_VOLGEO#

To ensure this email reaches the intended recipient, please do not delete the above code

Highlights

A combined approach helps to correlate the block clusters of avalanche deposits.

Striations are associated with the subsequent pyroclastic density currents.

Abstract

We describe sedimentological variations of the block-rich debris avalanche deposits and associated pyroclastic density current deposits emplaced around AD 1802 from Tutupaca volcano in southern Peru. We use these exceptionally well-preserved features to document the collisional shearing contact between the avalanche and coeval pyroclastic density currents. Furthermore, we show how the first stages of the edifice collapse and *syn*-cataclastic emplacement process affect the block-size distributions.

With field observations, we describe imbricated block clusters, jigsaw cracks and striations related to elongated ridge structures on the deposit surface. Sedimentological and statistical methods (Fourier Shape analysis and Shape Preferred Orientation measured on 208 blocks and 566 mesoscale structures) help us to characterize the cataclastic gradient and establish the collisional relationships between different units. We determine that the proximal impacted deposits and block lithofacies from ridges may be related to distal block units around ~10 km run-out distance. Different block clusters indicate a kinematic transition between avalanche units to pyroclastic density currents. Block shape parameters help to differentiate rounded blocks resulting from matrix abrasion with and striated blocks from ridges related to proximal imbricated block clusters. From the statistical dataset, a few equations have been developed indicating a common cataclastic origin with a co-genetic evolution of block lithofacies during sequential *syn*-cataclastic emplacement.

The dome collapse is associated with a specific granular flow regime between avalanche and pyroclastic density currents with secondary reworking. Cyclic impact waves contribute to block cluster growth. Clusters are disaggregated during shock propagation. The inherited shapes of the block lithofacies with *a/b* = 1.2-2 and ellipse = 0.2-2.5 indicate the reworking by impact waves. A multidirectional switch to mass spreading in the median zone between 2 and 6 km may be considered with secondary flow and segregation waves. A basal frictional regime with striations is differentiated from collisional cataclastic flow, generating polymodal grooves during peak velocity at the flow front. Impact forces around ~15.7 X 10^{10} N are implied by suggested clast velocities around 8.86 $m.s^{-1}$ and the transitional regime between avalanche units and pyroclastic density currents between 15.5 and 39.6 $m.s^{-1}$. An extensional disaggregation with the fractal dimensions (D) of the surrounded matrix between 0.6 and 2.8 characterizes the granular transport. A collisional shearing contact probably operated between avalanche units and pyroclastic density currents, which contribute to co-genetic evolution of block clusters from median to frontal distal zones. In the distal zone, abraded block clusters and tilted blocks are related to frontal reworking by impact wave.

The cataclastic gradient of avalanche units is correlated with the pyroclastic flow regime. Semi-quantitative analysis of block clusters provides information about *syn*-emplacement processes during

Conflict of Interest and Authorship Conformation Form

Please check the following as appropriate:

- o All authors have participated in (a) conception and design, or analysis and interpretation of the data; (b) drafting the article or revising it critically for important intellectual content; and (c) approval of the final version.
- o This manuscript has not been submitted to, nor is under review at, another journal or other publishing venue.
- o The authors have no affiliation with any organization with a direct or indirect financial interest in the subject matter discussed in the manuscript
- o The following authors have affiliations with organizations with direct or indirect financial interest in the subject matter discussed in the manuscript:

Author's name	Affiliation
Karine Bernard	LMV UCA *OPGC, Campus Universitaire des Cézeaux, 6 avenue Blaise Pascal, 63178 Aubière, France.*
Benjamin van Wyk de Vries	LMV UCA *OPGC, Campus Universitaire des Cézeaux, 6 avenue Blaise Pascal, 63178 Aubière, France.*
Pablo Samaniego	*IRD, OPGC, Campus Universitaire des Cézeaux, 6 avenue Blaise Pascal, 63178 Aubière, France.*
Patricio Valderrama	*Departemento de Ingenieria, Pontificia Univesidad Catòlica del Perú, Lima, Perú.*
Jersy Mariño	*Instituto Geológico Minero y Metalúrgico (INGEMMET), Observatorio Vulcanológico del Ingemmet, Barrio Magisterial Nro. 2 B-16, Umacollo, Arequipa, Perú.*

AUTHORSHIP STATEMENT

Manuscript title: Collisional interactions and the transition between lava dome sector collapse and pyroclastic density currents at Tutupaca volcano (Southern Peru).

All persons who meet authorship criteria are listed as authors, and all authors certify that they have participated sufficiently in the work to take public responsibility for the content, including participation in the concept, design, analysis, writing, or revision of the manuscript. Furthermore, each author certifies that this material or similar material has not been and will not be submitted to or published in any other publication before its appearance in the *Hong Kong Journal of Occupational Therapy*.

Authorship contributions

Authorship contributions

Please indicate the specific contributions made by each author (list the authors' initials followed by their surnames, e.g., Y.L. Cheung). The name of each author must appear at least once in each of the three categories below.

Category 1

Conception and design of study: K. Bernard, B. van Wyk de Vries, P.Samaniego, P. Valderrama, J. Mariño;

acquisition of data: K. Bernard, B. van Wyk de Vries, P.Samaniego, P. Valderrama, J. Mariño

analysis and/or interpretation of data: K. Bernard, B. van Wyk de Vries, P.Samaniego, P. Valderrama, J. Mariño

Category 2

Drafting the manuscript: K. Bernard, B. van Wyk de Vries, P.Samaniego, P. Valderrama, J. Mariño;

Category 3
Approval of the version of the manuscript to be published (the names of all authors must be listed):

K. Bernard, B. van Wyk de Vries, P.Samaniego, P. Valderrama, J. Mariño

Acknowledgements
All persons who have made substantial contributions to the work reported in the manuscript (e.g., technical help, writing and editing assistance, general support), but who do not meet the criteria for authorship, are named in the Acknowledgements and have given us their written permission to be named. If we have not included an Acknowledgements, then that indicates that we have not received substantial contributions from non-authors.

This statement is signed by all the authors (*a photocopy of this form may be used if there are more than 10 authors*)**:**

Author's name (typed)	Author's signature	Date
K. Bernard	K. BERNARD	22/04/2022
B. van Wyk de Vries		
P.Samaniego		
P. Valderrama		
J. Mariño		

Click here to access/download
Supplementary Material
shape parameters block clusters supplemental file 2.xls

Revised Manuscript with No changes Marked (Clean copy of the revised paper)
Click here to view linked References

1. Introduction

Volcanic debris-avalanche deposits are often associated with pyroclastic density currents and lahar deposits (*i.e.* Mount Saint Helens in the USA, Glicken, 1986), suggesting interactions during flow propagation. The stratigraphic relationships between the associated *syn*-eruptive volcanic deposits are described, implying differential kinematic between the mass flow such as striations and grooves on clast faces related to dome-collapse generating avalanche deposits interstratified between pyroclastic units (Mono Craters, CA, Dennen et al., 2014); matrix transformations into lahar deposits (Misti in Peru, Bernard et al., 2017). Block lithofacies are rarely used to characterize the differential movements inside the mass flow during *syn*-eruptive collapse. A basal frictional regime with striations is differentiated from an upper collisional cataclastic flow for block lithofacies (*e.g.* Parinacota and Ollagüe in Chile, Clavero et al., 2002; Clavero et al., 2004; El Zaguan, Mexico, Caballero and Capra, 2011).

Lava dome extrusion produced block lithofacies may be mixed with matrix-rich debris-avalanche deposits (Mount Saint Helens, Glicken 1986; Parinacota in Chile, Clavero et al., 2002; Tutupaca in Peru, Samaniego et al., 2015; Valderrama et al., 2016). Different avalanche structures are identified with such block lithofacies: (1) torevas that are large blocks (L >100 m), which occur in the proximal zones and could constitute up to ~30% of the debris avalanche deposits (Socompa in Chile, Davies et al., 2010). (2) Type A hummocks that are large cataclased blocks (H <80 m, w <300 m, L <400 m, Mount Saint Helens, Voight et al., 1981; Glicken, 1998; Jocotitlán in Central Mexico, Siebe et al., 1992; Parinacota and Taapaca in Chile, Clavero et al., 2002; Clavero et al., 2004) with steep slopes. (3) Longitudinal or transverse ridges (H = 10-30 m, Shea and van Wyk de Vries, 2008; Dufresne and Davies, 2009; Andrade and van Wyk de Vries, 2010), that are attributed to deflection of the mass flow (Valderrama et al., 2018). The alignment of blocks or isolated blocks between 0.01 and 1000 m can be observed in some debris avalanche deposits (Socompa, van Wyk de Vries et al., 2001; Shea and van Wyk de Vries, 2008). The frontal lobes thrust the large blocks in distal zones (Jocotitlán, Siebe et al., 1992) showing fluidization with matrix transformations into lahars (Perrier in French Massif Central, Bernard and van Wyk de Vries, 2017). Different mesoscale structures have been described related to specific kinematic context such as gravitational flank collapse with an initial dilation of jigsaw-fit textures (Mount Saint Helens, Glicken, 1986), abrasion and striations along fault planes (Mehl and Schmincke, 1999), collisional textures during transport (El Zaguán in Mexico, Caballero and Capra, 2011), and impact waves with pseudotachylite and gouge along avalanche fault zones (Pichu Pichu in Peru, Legros et al., 2000; Mont Dore in French Massif Central, Bernard and van Wyk de Vries, 2017).

Syn-eruptive collapses of a volcanic edifice and volcano-sedimentary processes have been well documented at Las Derrumbadas Volcano, Mexico (Guilbaud et al., 2022), Panum Crater, (Mono Crater, CA, Dennen et al., 2014) and Tutupaca volcano in southern Peru (Samaniego et al., 2015; Valderrama et al., 2016; Mariño et al. 2021). This volcano hosts probably the well-preserved and displayed lava dome related debris avalanche

and pyroclastic density current features that are young and little altered by the climate or human interference. Two volcanic avalanche units exposed in the northeastern part of the Tutupaca collapsed edifice are interstratified with the pyroclastic density current deposits (Samaniego et al., 2015). Block-rich ridge structures have been attributed to granular segregation and differential block velocities in the flowing mass, suggesting the interactions between debris-avalanche units and the associated PDC deposits.

In this study, we show how semi-quantitative sedimentological analysis of the block lithofacies and mesoscale structures associated to these exceptionally well-preserved volcanic deposits provide information about *syn*-emplacement processes during a collapsing dome generating pyroclastic density currents. To facilitate the reading of this study, we provide a list of the acronyms in Table 1.

2. Collisional interactions between volcanic-debris avalanche and pyroclastic density currents: a State-of-the-Art

The volcanic debris avalanche deposits are commonly associated with PDC. Mount Saint Helens in the USA (Crandell et al., 1984; Glicken, 1986), Bezymianni in Kamchatka (Siebert et al., 1987), Soufrière in Guadeloupe (Boudon et al., 1984) show several sequences of lava dome collapses associated with decompression to the co-magmatic deposits in *syn*-eruptive sequences. The hot volcanic debris-avalanche deposits, gravitational mass spreading (v = 50-70 m.s^{-1}) of the collapsed edifice, interacted with the blast-generated the PDC, transport of the fluidized mixture of clasts and gas ($v \geq$100 m.s^{-1}, Soufrière, Boudon et al., 1984; Mount Saint Helens 1980, Glicken, 1986; Bezyamanni 1956, Saint Augustine, Siebert et al., 1987). The PDCs are interstratified between the debris avalanche units, related to cyclic volcanoclastic sedimentation. Cyclic phases can be differentiated: precursor stages with seismes and localized collapses with hydrothermal alteration, large collapse of alterated lava-dome edifice with explosion and the blast-generated the PDC including an open conduit, and different post-collapse eruption. Volcanic lateral blast is associated to the successive shock waves during collapse, with ballistic clasts and sliding blocks generating internal shock structures. Transformations of the debris-avalanche deposits into lahars (v = 30-40 m.s^{-1}) by dewatering have been observed during initiation of pyroclastic flow such as Mount Saint Helens (Glicken, 1986).

Deposit structures have been formed by interactions between the moving avalanche and the superposed PDC, implicating a strong frictional contact. We observed aggregation of lava block clusters (Taranaki, Zernack et al., 2009) with brechification and curviplanar surfaces related to blocky morphology interactions, pyroclastic slump blocks with progressive disaggregation of blocks, fingering segregation related to ridge structures (Tutupaca, Samaniego et al., 2015; Valderrama et al., 2016), striations and flow bands (Lastaria in Chile, Naranjo and Francis, 1987) with distal digitations related to weak pyroclastic material.

Different generations of striations have been described related to sliding mode transport during interactions

between no-cohesive avalanche lithofacies and PDC: striations of the bedrock in scar (Mount Saint Helens, Glicken, 1986); grooves and striations at the base and the underlying substratum; and parallel grooves and furrow at the base and the upper part of faulted megablocks (Gran Canaria, Spain, Mehl and Schmincke, 1999). We differentiate an upper collisional regime with impact marks at the surface of block lithofacies (Parinacota and Ollague in Chile, Clavero et al., 2002; Clavero et al., 2004). Impact marks and linear trends appear concentrated on one side of blocks, showing conchoidal fractures related to collisional interactions between the blocks.

We examine how block lithofacies of volcanic debris avalanche deposits interact with PDC to generate block clusters and grooves with striations related ridges structures. We show how semi-quantitative sedimentological analysis of the block lithofacies and mesoscale structures provide information about *syn*-emplacement processes such as the force F of impact of clasts onto block surfaces and the clast velocity for making impact marks (Clavero et al., 2002).

3. Analytical methods

From the field observations on the debris-avalanche units, we have described the textural variations of the block lithofacies assemblages and assessed their relationships to avalanche fault zones. A semi-quantitative sedimentological analysis was conducted to characterize block distributions (Table 2). From these data, we were able to differentiate the block lithofacies in each zone associated with cataclastic gradient between the avalanche units and pyroclastic density current deposits (Samaniego et al., 2015; Valderrama et al., 2016). To facilitate the reading of this study, we provide a list of the acronyms in Table 1.

3.1. Field observations and outcrop analysis

The lithology of different outcrops were identified from proximal to distal zones to characterize the discontinuous block-rich lithofacies, related to interactions between volcanic avalanche and pyroclastic density current deposits. From field observations and Google Earth imagery, the block-rich avalanche units were described and mapped according to stratigraphic and geomorphological context and avalanche structures (Samaniego et al., 2015; Valderrama et al., 2016).

Quantitative morphological data such as area (S), thickness (T) and volume ($V = ST$; Table 1) on the surface avalanche deposits are calculated from the mapped surfaces and georeferenced Google Earth images (Samaniego et al., 2015; Valderrama et al., 2016). These morphological data are compared to other avalanche deposits worldwide such as those emplaced around Mount Saint Helens and Mount Shasta in the USA (Crandell et al., 1984; Glicken, 1986), Bezymianni in Kamchatka (Siebert et al., 1987), Parinacota in Chile (Clavero et al., 2002), Soufrière in Guadeloupe (Boudon et al., 1984) and Mont Dore in French Massif

Central (Bernard and van Wyk de Vries, 2017). From these examples, we correlate the morphological data with the structural units of avalanche deposits, implying interactions between lava dome sector collapse and pyroclastic density currents. The contacts between the block lithofacies and matrix textures of volcanic debris-avalanche deposits with interstratified PDC were analyzed. Lithostratigraphic sections were established and correlated with textural variations.

The use of the Shape Preferred Orientation 2003 software (Fig. 1A, SPO, Launeau and Robin, 2005) provided a semi-quantitative description of block avalanche units, allowing us to estimate imbrication of 508 blocks and block axial distributions with the inertia and intercepts method. Image analysis of the block lithofacies and mesoscale structures provide relative information because photographs can be affected by perspective. Two-dimensional shape parameters of blocks, such as the *a/b* ratio (the largest axis / minor axis) and sectional ellipse values from system of linear equations (see Launeau and Robin, 2005 for mathematical definitions), have been calculated, to characterize block fabric related to *syn*-emplacement structures (Bernard, 2015; Bernard and van Wyk de Vries, 2017; Bernard et al., 2019), together with striations and grooves in blocks. Ellipse/*a/b* values contribute to establish textural classes of avalanche fault zones (~2.14 for the plane collapse, 1.75 to 2 for the crushing, *a* <1.7 for the thermal effect of fragmentation, Bernard et al., 2019). Mesostructures such as fractures and striations from 2 mm to 20 cm were also analyzed.

3.2. Sedimentary analysis

From SPO analysis (Launeau and Robin, 2005) of the blocks, the fractal distributions were used to compare transport and cataclastic process acting on each avalanche unit. Each cumulative frequency is plotted *versus* clast long-axis on double-logarithmic graphs. Fractal dimensions *h* and *D* of size distributions were estimated from the power regressions (Table 4; see Supplemental File 1; Suzuki-Kamata et al., 2009). The cumulative curves of the clast-size distributions *vs. a/b* (Fig. 8) were compared to distinguish the block avalanche units from proximal to distal zones. The calculated block-size distributions estimated from 41 outcrop photographs with the inertia and intercepts methods using the SPO analysis (from metric-size blocks to clasts >10 cm; Fig. 8B; Launeau and Robin, 2005). The longest axis of 404 block outlines were measured and counted per image area from the photographs. The normalized frequency histograms (Launeau and Robin, 2005) were produced by grouping the longest axis of blocks (cm) into 100-cm bins (number of size intervals) and normalizing the number of occurrences in each bin to the total number of measurements from automatic image analysis. The sectional effects have been considered (Launeau and Robin, 2005). These data contribute to differentiate the effect of cataclasis between each fraction correlated with different structural units from proximal to distal zones. The subdued blocks and clasts below 10 cm are not considered related to resolution limits.

The shape analysis using the ImageJ Plugin “Gold morph” has been applied to 404 blocks and 635 striations

of the avalanche units to compute minor and major axis length, Feret's diameter defined as the longest distance between two parallel tangential lines, perimeter and convex perimeter, radii of the smallest inscribed and largest circumscribed circles (Fig. 1B; Table 3; Crawford and Mortensen, 2009). From these data, we calculate the *a/b* ratio, the roundness defined as the ratio of the perimeter to convex perimeter, and the Riley's circularity, the square root of the ratio of the diameter of the largest inscribed circle to the diameter of the smallest circumscribed circle of the volcanic clast (Table 3, Blott and Pye, 2008; Bernard, 2015). The values of Riley's circularity are less than 1 for the non-spherical volcanic clasts (Table 5).

To characterize the two-dimensional shape of mesoscale structures, we took 5.9 megapixel photographs of abraded flat surfaces of two blocks with a digital camera. A digital camera (6.2-18.6 mm lens, 35-105 mm focal length) image at a camera distance of <20 cm had a standard error for mean distortion around ~10^{-3}. All the striations observed in the median zone have been quantified by using high-resolution images (3648 X 2736 pixels) of two block faces. Abraded flat surfaces of the two megablocks on these scales contribute to preserve geometries of these grooves and striations with circular depressions (~1-5 cm depth, 2-3 mm wide). These are enough to generate semi-quantitative analysis using the ImageJ Plugin “Gold morph” and SPO (566 mesoscale structures, Launeau and Robin, 2005; Blott and Pye, 2008; Crawford and Mortensen, 2009). The roundness, the Riley's circularity, the *a/b* ratio, ellipse, fractal *D*-values of each mesoscale structure have been calculated. The calculated standard errors characterize the shape variations between the blocks rather than the measurements' uncertainty. Moreover, the calculated standard errors for image analysis are between 0.03 and 0.3 for *a/b* ratio and around ± 0.9 for ellipse values (Launeau and Robin, 2005; Table 5).

Several statistical regressions (Eqs. 1-21 in Figs. 2 and 8-10) have been established to characterize the evolution of block shape and striations related to cataclastic processes between the volcanic debris-avalanche units and pyroclastic density current deposits. Figure 9 shows the evolution of the roundness with Feret's diameter for block lithofacies and striations. Figure 10 shows the evolution of the roundness with Feret's diameter for block clusters. The intersecting points between few regressions indicate similar values of shape parameters related to the inherited clast shape for lava blocks and co-genetic relationships between block lithofacies.

Statistical and shape parameters were compared with those from other avalanche units in the Andean Central Volcanic Zone such as the Pichu Pichu debris avalanche deposit, and the matrix of the ridges from the Tutupaca volcanic debris-avalanche deposits (Bernard, 2015; Valderrama et al., 2016; Bernard et al., 2019).

The impact of clasts onto block surfaces (Clavero et al., 2002) can be approximated as $r = 0.5a^2/h$ with r, radius of spherical portion of clasts; a, radius of hemispherical damage zone, and h, distance that penetrated into the block. The force F of impact is given by Clavero et al. (2002):

$F = \Pi a^2 \rho_0$

where ρ_0 is the hardness of the material. The clast velocity for making impact marks can be estimated by using $V = (0.5\ \Pi\rho_0/Mr)^{1/2}a^2$ with M, the mass of the rock (Clavero et al., 2002). The avalanche velocity in the

middle zone is considered by using $v = (2gH)^{1/2}$.

A combination of several semi-quantitative methods has been used to determine (Table 1): (1) the links between the different block-rich units related to the debris avalanche and the associated pyroclastic density currents; (2) the quantitative sedimentary comparisons of the block lithofacies to define the conditions generating these deposits; (3) the in-motion controls and the dynamic cataclasis during the differential sedimentary emplacement between the volcanic debris-avalanche units and the pyroclastic density current deposits.

4. Geological and geomorphological context of the study area

4.1. Tutupaca volcanic complex and the geomorphological context

The Tutupaca volcanic complex (~5815 m on above sea level, Fig. 3) is composed by three edifices: an eroded basal edifice (Lower to Middle Pleistocene, Marino et al., 2021) with strong hydrothermal alteration; the Western Tutupaca peak, which was eroded by the late Pleistocene glaciers, and the Holocene Eastern peak composed of seven coalescing lava domes (Holocene, domes I to VII, Fig. 3B, Samaniego et al., 2015; Valderrama et al., 2016; Marino et al., 2021), constructed on the older hydrothermally-altered basal edifice. The activity of the recent domes is historic (about 218±14 calBP), and little altered by the arid, stable, cold climate, or by human activity, apart from a few small tracks and limited mining exploration excavations. The area is mostly wild, and in its natural state. The lava domes of the Eastern Tutupaca peak are cut by a horseshoe-shaped amphitheater open to the northeast, with an orthogonal direction to the N140° regional faults. From this, debris avalanche and pyroclastic density current deposits extend, are preserved with very little modification from their initial state (there is some limited frost shattering, and ice related solifluxion).

Geomorphological parameters on the surface avalanche deposits associated with PDC are calculated and compared to other avalanche deposits worldwide such as those emplaced around Mount Saint Helens and Mount Shasta in the USA (Crandell et al., 1984; Glicken, 1986), Bezymianni in Kamchatka (Siebert et al., 1987), Soufrière in Guadeloupe (Boudon et al., 1984). Impact marks of Parinacota debris avalanche in Chile (Clavero et al., 2002) and pseudotachylite impact in French Massif Central (Bernard and van Wyk de Vries, 2017) are considered. A relationship between area (A) and volume (V) is calculated for the Tutupaca units with $A = 28.07\ V^{1.01}$ (Eq. 1 in Fig. 2). These are compared to the power regressions of other volcanic debris-avalanche deposits (Eqs. 2-4 in Fig. 2, Glicken, 1986; Clavero et al., 2002; Legros, 2002; Bernard and van Wyk de Vries, 2017). We differentiate an intersecting point A with area around ~140 and 180 km^2 and volume between 5 and 7 km^3.

4.2. The Paipatja debris-avalanche deposits

Samaniego et al. (2015) described the Paipatja debris avalanche, exposed in the northeastern part of the Tutupaca volcano between the amphitheater and the Paipatja plain (L = 6-8 km, S = 12-13 km^2, T = 25-40 m, Samaniego et al., 2015; Valderrama et al., 2016). Stratigraphic and textural variations are correlated to the syn-emplacement structures. The hydrothermally rich debris avalanche deposit (HA-DAD, L = 6-8 km, V <1 km^3; H/L = 0.17-0.23, Samaniego et al., 2015), that involved large quantities of the basal edifice, is characterized by torevas (H = 20-40 m, L = 1.5 km), long lateral levees (L = 1.5 km) and hummocky-structures (L = 200-800 m, H = 20-40 m) up to 4-6 km from the scar (Samaniego et al., 2015; Valderrama et al., 2016).

Block ridge structures and levees are observed between 2 and 6 km from the amphitheater (Valderrama et al., 2016). In the median zone, elongated and sub-parallel ridge structures (w = 5-10 m, H = 2-5 m, L = 150-400 m, Fig. 3A), regularly spaced, are related to interstratified pyroclastic density current deposits between two avalanche units, implying a *syn*-collapse explosive eruption at Tutupaca volcano (Samaniego et al., 2015). The hydrothermally rich debris avalanche deposit is covered by Paipatja pyroclastic density current deposits (P-PDC, ~218 aBP, sections B to E in Fig. 3A).

A dome-rich debris-avalanche deposit (DR-DAD of Samaniego et al., 2015) overlain the P-PDC unit in the median zone (section B in Fig. 3). Cross-sections within the ridge structures reveal the dipping and undulating contacts between the P-PDC units and the DR-DAD (section B in Fig. 3A). The P-PDC, on the upper part of HA-DAD, appears thickest between the ridge structures and around the largest blocks (Valderrama et al., 2016). We have observed dome fragments (from centimeters to several meters in size), such as metric-size dacitic blocks and prismatically jointed blocks showing inherited jigsaw-cracks, cataclastic and shearing structures. The abraded and sub-rounded blocks are subdued in the underlying avalanche deposit and PDC.

The Tutupaca volcanic debris-avalanche deposits show different units with specific granular assemblages (30% of HA-DAD and 70% of DR-DAD, Valderrama et al., 2016). Dense blocks (3-20 cm in diameter) and bombs from the P-PDC unit (20-40%) have highly similar chemical content (~65-68 wt.% SiO_2, Samaniego et al., 2015), similar to the brecciated lava domes. A progressive decrease in block-size is observed with distance. Large blocks (~0.5-1 m in diameter) are occasional. The few distal blocks (>1 m in length) surrounded by P-PDC unit are associated to the underlying avalanche deposit.

4.3. The syn-emplacement block lithofacies

Using the Google Earth imagery, we differentiate different block lithofacies from proximal to distal zones. The eastern flank collapse of the Tutupaca volcano shows at the summit two brecciated zones related to lava dome collapse (domes V to VII in Fig. 3B, Fig. 4A). We observe along the East crest (1 in Fig. 4A) angular

dome fragments adjacent to the PDC (in red in Figs. 3A and 4A) without preferential orientation, and on the west side (2 in Fig. 4A) an impacted and crushed zone showing imbricated block clusters with tabular planar surfaces. The long axis of 56 blocks are tilted N112E. In the median zone, block ridge structures show an isolated polyhedral block (white arrow in Fig. 4B), which exhibits planar surfaces with angular edges. We observe in downstream sigmoid fish of clasts, which appears disaggregated and truncated in N40E, related to the interactions between avalanche and the blast-generated the PDC (Fig. 4B). The isolated distal blocks (>1 m in length, Fig. 4C) surrounded by P-PDC unit are transverse with extensional lateral spreading (N176E, Fig. 4C).

The textural and sedimentological variations of the block avalanche lithofacies (HA-DAD and DR-DAD) are described with associated volcanic deposits to correlate *syn*-emplacement process between volcanic debris-avalanche units and pyroclastic density current deposits.

5. Results

The SPO analysis of the block lithofacies contribute to a semi-quantitative description of block deposits. The comparison of each block lithofacies with cumulative curves and fractal distributions helps to distinguish the deposits. The analysis of the block shapes has enabled us to identify the inherited structures and the relationships between the proximal and distal block clusters.

5.1. Block lithofacies

In the Paipatja DAD, we have observed block clusters and block avalanche lithofacies with a specific distribution on and between blocks. From proximal to distal zones, the block characteristics were quantified using the software ImageJ and SPO analysis (>400 blocks, Launeau and Robin, 2005). We characterized the localized mesoscale structures observed on few blocks associated with the ridged structures.

5.1.1. Block clusters lithofacies of DR-DAD

Imbricated block clusters are localized under the collapse scar (A in Figs. 3A and 4A). The dacitic dome fragments (from centimeters to several meters in size) present similar chemical characteristics (64.5-65.9 wt. % SiO_2, Samaniego et al., 2015). We observed impacted blocks with planar fractures and undulated borders (Fig. 5A), and tilted blocks in imbricated piles. Inherited clasts are observed with jigsaw-fractured breccias showing polymodal distribution of the clasts and ellipse/*a/b* = 5.1 (Fig. 5B). Block-rich ridge structures of the Paipatja DAD (B in Fig. 3A) contain abraded and sub-rounded blocks, which are also found in the underlying avalanche deposit and P-PDC (ellipse/*a/b* = 2.3-2.6 in Fig. 5C). There are also impacted blocks (Fig. 5D)

showing polymodal distribution of the clasts**.** In the Paipatja plain, abraded and sub-rounded blocks are found isolated at the front of P-PDC (Fig. 3). Along the lateral levee, in the proximal zone, we have observed large blocks with sigmoidal jigsaw-breccias (Fig. 5E) and a bimodal clast distribution. Angular lava blocks (~1 m in length) are impacted between aligned and subdued blocks (Fig. 5F), which exhibit planar surface with conchoidal fractures or abraded surface with striations. We differentiate block clusters and ridged avalanche units (ellipse/*a/b* = 2.3-2.5, DR-DAD, Fig. 5G) from imbricated block clusters (ellipse/*a/b* = 1.74) and subdued and tilted blocks in the distal zone (ellipse/*a/b* ~2.12, PDC, Fig. 5H).

5.1.2. Block avalanche lithofacies

Some transverse blocks appear isolated or aligned in N30° (DR-DAD, Figs. 3B and 6A), parallel to the elongated depressions. We observed sub-rounded faces with striations in upstream and planar faces with conchoidal fractures in downstream. Along the lateral levee, we described quenched and cracked surfaces in the upper part with jigsaw-fit texture and imbricated subangular clasts along basal contact of blocks (Fig. 6B). A large polyhedral block (~3 m high and ~5 m length, HA-DAD, Fig. 6C) on the ridge crest presents an oriented abrasion: sub-rounded face in the front and planar face in the downstream. In the PDC deposits, a bimodal distribution of the surrounded clasts is quantified. The sub-rounded lava block displays two distinct surfaces: a quenched and cracked surface in the upper part and an altered vitreous phase in the lower part. A distal sub-rounded block, surrounded by the P-PDC deposits, appears isolated (Fig. 6D) with bimodal distribution of the surrounded clasts related to the PDC deposits. Subdued blocks exhibit abraded surfaces with striations.

5.1.3. Grooves and striations

At 5.5 km from the collapse scar, a few blocks associated with the ridge structures (Fig. 7A; Valderrama et al., 2016) exhibit grooves and striations with roughly circular depressions on the upstream, abraded face. These localized mesoscale structures are often irregular and grouped in the lower part of the abraded and striated surfaces. The largest striations (>3 cm wide) are parallel to each other (at 3.19°, Fig. 7) and observed in the upper part of the block face. There are small striations perpendicular to the grooves (Fig. 7B). Grooves or furrows 1-5 cm depth ranged from roughly circular (<5 cm in diameter) to elliptic (~8-15 cm for longest axis) in shape. Fractal *D* values, calculated from exponent *h* of power regressions (100 striations, Table 4; Suzuki-Kamata et al., 2009), are 1.09 in the 8.4-46.4 cm mark-size range.

The macroscopic characteristics of grooves and striations with circular depressions were used for the shape analysis with the software ImageJ and SPO analysis (566 mesoscale structures, Launeau and Robin, 2005). Grooves and striations show polymodal distributions, with ellipse/*a/b* around ~5.1-5.9 (Fig. 7A-B). In the lower part of the block face, basal striations (~2-3 mm wide) with perpendicular diaclasis are differentiated. Fractal *D* values, calculated from exponent *h* of power regressions (90 striations, Table 4, Suzuki-Kamata et

al., 2009), are 0.67 in the 5.2-20.96 cm mark-size range.

5.2. Sedimentary characteristics of block lithofacies

Sedimentary characteristics of block lithofacies were compared with fractal *D* values to distinguish textures in the block avalanche units (HA-DAD, DR-DAD) and PDC deposits from proximal to distal zones. Block lithofacies of HA-DAD are hydrothermalized and cataclased with jigsaw-cracks. These are angular to subangular in PDC (20-30% of HA-DAD, Samaniego et al., 2015). We differentiate imbricated blocks with jigsaw structures in zones A and C (Fig. 3A), the abraded and subdued blocks observed in ridges structures and the distal zone (F in Fig. 3A), and the dacitic block lithofacies in zones D and E. The cumulative curves of block-size distributions *vs. a/b* are compared to distinguish block lithofacies in different zones, which are characterized by five logarithmic regressions (Eqs. 5-9 with R^2 >0.9 in Fig. 8A). These are compared to the logarithmic regressions of the impact breccias in French Massif Central (Eq. 12 in Fig. 8A; Mont Dore, Bernard and van Wyk de Vries, 2017). The intersecting points *a* to *d* with *a/b* between 2.5 and 4.7 imply a co-evolution between the grooves and striations (Eqs. 10-11 with R^2 >0.9 in Fig. 8A) and the ridged debris-avalanche unit (Eq. 6), in accordance with the field observations. We differentiated the hydrothermalized matrix (HA-DAD) from the breccia matrix (DR-DAD) showing sandy-gravel lithofacies of the red matrix with few angular clasts (< cm, Bernard, 2015; Valderrama et al., 2016).

The effect of cataclasis is shown by a decrease in the content of the smallest fractions (<100 cm, Fig. 8B) of block lithofacies (<18%), an increase in the striation ratio (25 to 45%), together with a concomitant high ratio in amount of block clusters (~20 to 40%). The variations of these data are correlated with different structural units from proximal to distal zones. The basal striations appear differentiated (Table 4). A specific clast-size fractal distribution is calculated in the range between 6.7 and 539 cm. The mean fractal *D* value, calculated from exponent *h* of power regressions, is around ~1.28 in the 11.4-40.3 cm clast-size range (Table 4; see Supplemental File 1; Suzuki-Kamata et al., 2009). The distal block lithofacies present the highest *D* values around ~1.83 compared to the proximal ridged deposits around ~1.64. These are differentiated from the surrounded matrix between 0.64 and 2.84 in the 0.0016-6.4 clast-size range. The mean fractal *D* value of striations is around ~0.62 in a range from 5.9 to 44.6 cm.

5.3. Block shape parameters

Shape analysis using the software ImageJ and SPO analysis (404 blocks from the HA-DAD and DR-DAD, 635 striations; Launeau and Robin, 2005; Blott and Pye, 2008; Crawford and Mortensen, 2009) has been applied to compare shape parameters of blocks from proximal to distal zones, together with striations and

grooves in blocks. This comparison is intended to characterize the cataclastic evolution with co-genetic relationships between volcanic debris-avalanche units and P-PDC, including the inherited clast shape for lava blocks. The mean values of *a/b* ratio and ellipse (~1.7±0.03 and 3.5±0.15, Table 5) are different from the clasts observed in the matrix of ridged units (DR-DAD, ~1.69±0.05 and 2.72±0.09, 1891 clasts from SPO analysis, Bernard, 2015). The calculated standard errors indicate the measurement errors and the sum of internal variability between the block shape parameters. These values imply distinct evolution between the avalanche block lithofacies and PDC.

5.3.1. Avalanche block lithofacies

We distinguish an inherited clast shape for lava blocks with *a/b* = 0.9 and ellipse = -3.5 implying textural relationships between the block lithofacies of HA-DAD and DR-DAD. Three regressions characterize the roundness *vs.* maximum Feret's diameter (Eqs. 13-17 in Fig. 9) for the block lithofacies. Two regressions (Eqs. 14-15 in Fig. 9) characterize the block lithofacies observed in the proximal and median zones. These values are compared to the breccias forming the ridged avalanche matrix (HA-DAD and DR-DAD) and the distal lobe of the Pichu Pichu debris-avalanche deposit (Eqs. 14-15 and 17 in Fig. 9; Bernard, 2015).

5.3.2. Distal block lithofacies

Three points of intersection indicate similar values of roundness for different zones of cataclasis (*a-c* in Fig. 9A). We distinguish an inherited clast shape with roundness around ~0.9 (*a*, Fig. 9), indicating textural relationships between the tilted distal blocks (PDC) and the blocks from the ridges, close to those of the sheared lava breccias in the distal lobe of the Pichu Pichu debris-avalanche deposit. The intersecting points *b* and *c* with roundness between 1.05 and 1.08 imply a co-evolution between the impacted blocks (Eq. 14) observed in the proximal and distal zones and the sheared sigmoid along the lateral levee (Eq. 15 in Fig. 9).

5.3.3. Grooves and striations

The values of *a/b* = 3.2 and ellipse = 15 are correlated to a co-genetic evolution between the grooves and striations, the blocks from ridges and the distal, impacted blocks (PDC). The mean values increase for roundness from 1 to 1.7 and ellipse/*a/b* from 0.2 to 2.7 (Table 5), while the values of Riley's circularity decrease. A regression characterizes the roundness *vs.* maximum Feret's diameter (Eq. 13 in Fig. 9) for the striations. The intersecting point *c* (Eqs. 13-14 in Fig. 9) with Feret's diameter <0.05 m and roundness around ~1.05 characterizes the inherited clast shape of the proximal block lithofacies generating striations and impact marks in the ridged debris-avalanche unit. We observed decreasing values of Riley's circularity related to Feret's diameter (Table 5).

5.4. Block clusters and shape variations

More than six cluster structures have been described with the shape analysis using the software ImageJ and SPO analysis from 312 blocks in the unconsolidated avalanche matrix from the HA-DAD (Fig. 10). Lava block clusters (~30-70 vol.%) from 40 cm to 5 m in diameter are impacted and thrust in unconsolidated avalanche matrix. The *a/b* ratio related to ellipse values show increasing values for the impacted jigsaw-clusters; and for the tilted block in the distal zone. Similar characteristics appear for the striated blocks from the ridges and the distal clusters. Similar ellipse values are calculated between proximal jigsaw breccias and the tilted and impacted blocks in the distal zone (ellipse = 0.7); between distal clusters (ellipse = 1-1.8) or between tilted blocks in the distal zone (ellipse = 2.7). *Syn*-cataclastic emplacement of block clusters with a co-genetic evolution of shape parameters may be envisaged.

The roundness is high (>1) for the block clusters, close to those of the experimental crushed stones (Janoo, 1998). Four regressions characterize the roundness *vs.* Feret's diameter (Eqs. 18-21 in Fig. 10) between 0.05 and 1 m. The increasing macro-roundness reflects the effects of clast crushing due to the collisional transport and cataclastic sorting between the proximal and distal zones. We have highlighted a power regression for the imbricated block clusters in the proximal zone with roundness >1 (Eq. 18 in Fig. 10). Two categories of regressions are identified for the impacted and tilted block clusters in the distal zone with roundness between 0.9 and 1.08 (Eqs. 19-20 in Fig. 10). Three points of intersection (*a-c* in Fig. 10) indicate similar values of block roundness for cluster structures characterized by different regressions: between impacted and tilted blocks in distal zone (*a* = 1.05, Eqs. 19-20); between distal clusters and the striated blocks from the ridges (*b* ~1, Eqs. 18-20) or proximal breccias with jigsaw features. We distinguish an inherited block shape for lava blocks with roundness around ~0.9 and Feret's diameter = 0.05 m (*c* in Fig. 10), implying textural relationships between these block clusters and sheared contact of the Pichu Pichu volcanic debris-avalanche deposit.

The Riley's circularity of block clusters shows decreasing values from the proximal to distal zones (Table 5, see Supplemental File 2) related to Feret's diameter, implying textural relationships between the block clusters with the run-out distance.

6. Discussion

From field observations, we used complementary methods to describe surface and internal structures of the Paipatja volcanic debris-avalanche deposits of the Tutupaca volcano and the associated pyroclastic density currents. The quantitative sedimentary analysis contributes to correlate the block clusters, the block avalanche lithofacies and mesoscale structures with different stages of cataclastic flow regime between the DR-DAD and the associated pyroclastic density currents from proximal to distal zones. Quantitative

morphological and sedimentological parameters are correlated and compared to other avalanche deposits worldwide, showing that the brecciation have recorded the collisional interactions between lava dome sector collapse and pyroclastic density currents.

6.1. Classification of volcanic debris-avalanche deposits

The volcanic debris avalanche deposits are commonly associated with PDC. The area and volume of the volcanic debris avalanche deposits associated with PDC are compared to Bezymianny eruptive sequence (Siebert et al., 1987) showing lava dome collapses with hydrothermally alteration interacted with the blast-generated the PDC (Fig. 2): Mount Saint Helens in the USA (Glicken, 1986), Bezymianni in Kamchatka (Siebert et al., 1987), Soufrière in Guadeloupe (Boudon et al., 1984). A relationship between the area (*A*) and volume (*V*) for the Tutupaca units is compared to the power regressions of other volcanic debris-avalanche deposits such as Mount Shasta and Mount Saint Helens in the USA (Fig. 2, Glicken, 1986; Siebert et al., 1987; Legros, 2002). The fault breccias have recorded the propagation of impact waves. The Tutupaca volcanic debris-avalanche deposits with *H/L* around ~0.15-0.2 (12-13 km^2, <1 km^3, *L* = 6-8 km, Samaniego et al., 2015; Valderrama et al., 2016) show different units characterized by granular segregation and fingering instabilities (Figs. 3-4, Valderrama et al., 2018). A power regression (Eq. 2 in Fig. 2) characterizes the Tutupaca units compared to the proximal scar of the Mount Saint Helens deposits showing striations of the bedrock and the impacted distal zone in French Massif Central. This co-evolution of geomorphological parameters may be related to digitate shape of the avalanche deposits (Samaniego et al., 2015). The largest volcanic avalanche deposits (Mount Shasta, Legros, 2002) appears different from other volcanic debris-avalanche deposits in accordance with field observations, on ridge structures, striations, and block clusters. The geomorphological parameters of the largest avalanche units tend toward similar values (Eqs. 1-4 in Fig. 2). We differentiate the intersecting point A (Fig. 2) with an area around ~140 and 180 km^2 and volume between 5 and 7 km^3, implying a convergent evolution between the largest structural units with run-out distance of over 22 km (Mount Saint Helens in the USA and Parinacota in Chili, Fig. 2; Siebert and Roverato, 2020) and the high velocity of volcanic debris avalanche associated with the blast lateral collapse and fluidization.

For the Tutupaca volcanic debris-avalanche deposits, the mean values of *a/b* ratio and ellipse, around ~1.7 and ~3.5 respectively (Table 5) are between the Rio Chili, tilted block-rich debris-avalanche deposits in Peru and the lateral levee from the Mont Dore in French Massif Central (Bernard, 2015; Bernard et al., 2017). The mean ellipse/*a/b* values around 1.88 characterize the crushing effects (Table 5, Bernard et al., 2019). We differentiate the thermal effect of fragmentation in proximal zone with ellipse/*a/b* between 0.23 and 1.7 and the transfer of the plane collapse in the median zone showing ridge structures (ellipse/*a/b* = 2.04-2.78). For the Tutupaca example, we have a dome collapse with a cataclastic gradient and a granular segregation during

a lateral spreading over ~1 km (Fig. 3). These statistical comparisons with other volcanic debris-avalanche units contribute to establish a geomorphological classification of the volcanic debris-avalanche deposits related to kinematic process. Secondary reworking of the Paipatja volcanic debris-avalanche deposits with impact waves and fingering instabilities during flow propagation of the pyroclastic density current must be considered. Successive collapses of the volcanic edifice contribute to the discontinuous units of the debris-avalanche deposits.

6.2. Granular flow regime between the debris avalanche and pyroclastic density currents

Field observations show a reverse grading of the lithofacies assemblage (Socompa, van Wyk de Vries et al., 2001; Davies et al., 2010): the HA-DAD is overlain by the DR-DAD interstratified with pyroclastic density current deposits (Samaniego et al., 2015). A similar block-size distribution of the avalanche deposits and the regressions (Eqs. 5-12 in Fig. 8) indicate a similar cataclastic origin with a co-genetic evolution of block lithofacies linked with a sequential *syn*-cataclastic emplacement (Samaniego et al., 2015; Valderrama et al., 2016).

The comparison of each block size-fractions with cumulative curves and histograms (Figs. 8-10) help to identify the block lithofacies from proximal impact and cataclastic gradient with granular segregation in flowing mass (Valderrama et al., 2016). Sedimentary parameters show a co-genetic brecciation of block lithofacies (Eqs. 5-12, Fig. 8), which are compared to the impact breccia in French Massif Central. The lava dome brecciations have recorded the propagation of impact waves. The roundness *vs*. Feret's diameter suggests a co-genetic evolution between the proximal clusters, the abraded and striated blocks in the ridges and the distal block clusters (Eqs. 19-22 in Fig. 10A) due to differentiated breakage during collisional transport.

6.2.1. Cyclic impact waves and block clusters

The dome collapse with explosion is associated with a specific granular flow regime between avalanche and pyroclastic density currents with secondary reworking. The succession of slide blocks is associated to frontal propagation of cyclic impact wave in an extensional context during primary shear propagation generating a clastic matrix (PDC, Mount Saint Helens, Glicken, 1986). Inherited jigsaw-fit textures have recorded the initial dilation of the collapsed edifice (Mount Saint Helens, Glicken, 1986). The inherited shapes of the block lithofacies (a/b = 1.2-2, ellipse = 0.2-2.5) indicate the reworking by impact waves. Imbricated block clusters with jigsaw-fit texture and planar fractures are impacted under the collapse scar (A in Figs. 3A and 4A). Proximal imbricated block clusters may be generated during impact waves (Cox et al., 2019). Cyclic impact waves and initial dilation contribute to block cluster growth with jigsaw-fit texture during the first stage of avalanche emplacement. Clusters are disaggregated during shock propagation (Fig. 4A). The rock

fragmentation during the proximal impact wave increases the roundness (>1, Fig. 10; Szabo et al., 2015). The propagation of the impact wave with granular oscillatory stress (Bernard and van Wyk de Vries, 2017; Cox et al., 2019) may contribute to produce the imbricated block clusters. Waves during cyclic impact may be considered to cause block cluster growth.

Blocks are split into clusters of smaller aggregates during transport (Palmer et al., 1991). Stick-slip oscillations (Sandnes et al., 2011) and an oscillatory relative speed may be considered during impact waves and dilation, which change the apparent coefficient of friction in the proximal zone. The isolated sub-rounded blocks and impacted blocks (D ~1.64-2.83 and ellipse/a/b =1.7-1.8, Tables 4 and 5) may be related to cluster disaggregation (Fig. 8B) during shock propagation generating the polymodal clast distributions with a thinner clastic matrix related to polymodal striations of the blocks from the ridges (ellipse/a/b =1.7-1.8, Eqs. 9-12, Fig. 8, Table 5). The cataclastic finer fractions increase the particle-to-particle interactions during flow propagation (Dennen et al., 2014) generating grooves and striations on the abraded surface of the impacted blocks. Textural relationships appear between proximal blocks and the striated blocks from the ridges (Table 5) with decreasing values of Riley's circularity.

6.2.2. An upper collisional regime

Differentiated velocities related to transitional regime must be considered between the matrix-rich facies and the block facies ($v_1 < v_2$; Glicken, 1998; Caballero and Capra, 2011). Formation of the elongated ridges is attributed to granular segregation and differential block velocities in the flowing mass (Dufresne and Davies, 2009). The bimodal clast distributions in the medial zone (ellipse/a/b ~1.7) differentiate the transverse blocks, the elongated ridges and lateral levee with sigmoidal jigsaw-breccias (Fig. 6B-D). The DR-DAD lithofacies contribute to decreasing run-out velocity with localized secondary flow (Socompa, Kelfoun et al., 2008; Mont Dore in French Massif Central, Bernard and van Wyk de Vries, 2017) and segregation waves to the flow front (Gray, 2013).

A multidirectional switch of mass spreading may be considered, with segregation waves to the flow front (Glicken, 1998). Transverse orientations of blocks in the medial zone implicate a quick stop attributed to a compressive context. The lack of propagation of the proximal conditions contribute to plug flow and granular segregation, generating lateral levees and ridges in the upper collisional flow regime for the median zone (Shea and van Wyk de Vries, 2008; Valderrama et al., 2016). Along lateral levee, rafted blocks with sigmoidal jigsaw-breccias are related to transport by traction in shearing context, generating secondary fractures.

We differentiate the parent dome volcanic processes from the breakage due to collisional transport, which increases the roundness from 1 to 1.7, related to the frontal reworking by impact wave (Table 5). An upper collisional regime for block lithofacies generating impact marks is differentiated from basal frictional regime with striations (*e.g.* Parinacota and Ollagüe in Chile, Clavero et al., 2002, Clavero et al., 2004; El Zaguan, Mexico, Caballero and Capra, 2011). Collisional abrasion may be associated with the dispersive pressure

generated by the subsequent pyroclastic density current. Shock and brecciation of blocks limit the mixture of lithofacies (*e.g.* Pichu Pichu in Peru, Legros et al., 2000; El Zaguan, Mexico, Caballero and Capra, 2011). Stick-slip motion at the front of lobe and high-speed of blocks may also be considered (Bartali et al., 2015). Each of the block avalanche deposits and striations present a specific regression for the roundness *vs.* Feret's diameter diagram (Eqs. 13-17 with R^2 >0.5 in Fig. 9), implying a differentiated evolution of the breakage during collisional transport and granular segregation. Inherited clast shapes with roundness between 0.9 and 1.2 are related to a same cataclastic origin. The impact of clasts onto block surfaces ($r = 0.5a^2/h$, Clavero et al., 2002) can be approximated with a <5 cm radius of hemispherical damage zone, and h ~1-5 cm distance that penetrated into the block. Calculated r values between 2.5 and 12.5 cm is in accordance with the surrounded clasts. The impact force F has a value of about 15.7 X 10^{10} N by using $F = \Pi a^2 \rho_0$ with a typical ρ_0 value around ~2.10^9 Pa (Clavero et al., 2002). The clast velocity for making impact marks can be estimated around ~8.86 m.s^{-1} by using $V = (0.5\ \Pi\rho_0/Mr)^{1/2}a^2$ with M ~10^3 kg, a <5 cm and r values between 2.5 and 12.5 cm (Clavero et al., 2002), in accordance with impact marks analysis on clast faces of Panum block lithofacies (Mono Craters, CA, Dennen et al., 2014). The avalanche velocity in the middle zone (around ~3 and 6 km from source, Clavero et al., 2002) is considered between 15.5 and 39.6 m.s^{-1} by using $v = (2gH)^{1/2}$. Localized striations and grooves can be attributed to the peak velocity at the flow front. The inherited shapes of the lava blocks and the co-genetic evolution between the blocks from the ridges and striations may be associated to secondary fracturing with partial decompression during run-out propagation (Bernard et al., 2019).

The dome collapse is associated with a specific granular flow regime between avalanche and pyroclastic density currents: cyclic impact waves with disaggregation during shock propagation, and secondary flow with segregation waves. Basal frictional regime with striations is differentiated from higher collisional and cataclastic flow regime generating clast breakage and impact marks (*e.g.* Parinacota and Ollagüe in Chile, Clavero et al., 2002, Clavero et al., 2004; El Zaguan, Mexico, Caballero and Capra, 2011).

6.3. The frontal reworking

Logarithmic regressions of the abraded and sub-rounded block lithofacies in the median and distal zones (d ~1.64-1.83; ellipse/a/b ~2.7, Eqs. 7-11 in Fig. 8A) are close to those of the impact breccias along avalanche fault zone in French Massif Central (Eq. 12 in Fig. 8A, Bernard and van Wyk de Vries, 2017). The Riley's circularity (Table 5, see Supplemental File 2) shows that the polyhedral blocks with conchoidal fractures and striations of the ridge structures differentiated from sub-rounded blocks in the distal zone. These may be associated to an oriented abrasion and thermal shock generating tilted blocks with cracked surface. The clast breakage with striations due to collisional transport decreases the Riley's circularity (Table 5). These block lithofacies may be associated to crushing impact with frictional temperature during oscillatory stress

(Bernard and van Wyk de Vries, 2017) related to decompression in rotational shearing, and matrix segregation.

The inherited shapes of the blocks (*a/b* = 1.2-2; ellipse = 0.2-2.5; Riley's circularity ~0.6 in Table 5; Eq. 14 and *a* ~0.9 in Fig. 9) implied the reworking by impact wave (Cox et al., 2019) and similar processes of abrasion between the imbricated block clusters in the proximal zone, the striated blocks from ridges and the tilted distal blocks. These are close to those of the sheared lava breccias observed along the Pichu Pichu debris-avalanche deposit. Flow traction may contribute to block piles (Cox et al., 2019) up to a point where flows are not competent. Fractal *D*-values of the surrounded matrix between 0.6 and 2.8 are associated to an extensional disaggregation and granular transport (Table 4, Blekinsop and Fernandes, 2000). A *syn*-cataclastic emplacement of the blocks with a co-genetic evolution is differentiated between the proximal and median zones and between the striated blocks from ridges and the distal, impacted blocks.

7. Conclusions

Field observations together with quantitative sedimentological analyses help to characterize textural variations of the Paipatja avalanche deposits and the associated pyroclastic density current deposits from Tutupaca volcano in southern Peru. A typical lithofacies assemblage with a reverse grading shows jigsaw breccias, impacted block clusters and striations associated with the interaction between the debris avalanche and the subsequent pyroclastic density currents.

Cyclic impact waves and initial dilation of the Tutupaca lava dome have contributed to produce jigsaw breccias and imbricated block clusters during the first stage of avalanche emplacement. Cluster disaggregation during shock propagation contribute to an upper collisional regime, generating isolated blocks with striations. Transverse blocks, lateral levee and ridges are associated to a switch of mass spreading with granular segregation. The frontal reworking by impact wave with extensional disaggregation contributes to generate impacted block clusters in distal zone. From the statistical dataset, a few regressions have been established indicating the same cataclastic origin with a co-genetic evolution of block lithofacies.

Sequential events of *syn*-emplacement processes during impact waves have been established related to volcanic debris-avalanche units and pyroclastic density current deposits. These observations help to constrain the collisional shearing contact between avalanche units and associated pyroclastic density currents, and help to explain the block cluster growth and the block disaggregation correlated to sequential *syn*-emplacement processes of debris avalanche units with associated pyroclastic deposits.

The deposits at Tutupaca are exceptional for their freshness and clarity, and lack of disturbance. This area is an important record of lava dome collapse and debris avalanche and pyroclastic flow interaction.

Acknowledgments

596 The fieldwork in Peru trip has been funded by the “Institut de la Recherche pour le Développement” support
597 (O. Roche and P. Samaniego, IRD) for Tutupaca volcano. The geoheritage context is provided through the
598 UNESCO International Geosciences Program project 692, Geoheritage for Resilience.
599
600 **References**
601
602 Andrade, S.D., van Wyk de Vries, B., 2010. Structural analysis of the early stages of catastrophic strato-
603 volcano flank-collapse using analogue models. Bull. Volcanol. 72, 771-789.
604 Bartali, R., Sarocchi, D., Nahmad-Molinari, Y., 2015. Stick-slip motion and high speed ejecta in
605 granular avalanches detected through a multi-sensors flume. Eng. Geol. 195, 248-257.
606 Bernard, K., 2015. Quelques aspects sédimentaires des avalanches de débris volcaniques. Ph.D.
607 Thesis, Univ. Clermont-Auvergne, France (Unpub., in French). Available at: <NNT :
608 2015CLF22624>.<tel-01330779>.
609 Bernard, K., van Wyk de Vries, B., 2017. Volcanic avalanche fault zone with pseudotachylite and gouge
610 in French Massif Central. J. Volcanol. Geotherm. Res. 347, 112-135.
611 Bernard, K., Thouret, J-C., van Wyk de Vries, B., 2017. Emplacement and transformations of volcanic debris
612 avalanches - A case study at El Misti volcano, Peru. J. Volcanol. Geotherm. Res. 340, 68-91.
613 Bernard, K., van Wyk de Vries, B., Thouret, J-C., 2019. Fault textures in volcanic debris-avalanche
614 deposits and transformations into lahars: The Pichu Pichu thrust lobes in south Peru compared to
615 worldwide avalanche deposits. J. Volcanol. Geotherm. Res. 371, 116-136.
616 Blekinsop, T.G., Fernandes, T.R.C., 2000. Fractal characterization of particle size distributions in
617 chromitites from the Great Dyke, Zimbabwe. Pure Appl. Geophys. 157, 505-521.
618 Blott, S.J., Pye, K., 2008. Particle shape: a review and new methods of characterization and classification.
619 Sedimentology 55, 31–63.
620 Boudon, G., Semet, M.P., Vincent, P.M., 1984. Flank-failure-directed blast eruption at Soufrière,
621 Guadeloupe, French West Indies: A 3000-yr-old Mt. St. Helens? Geology 12, 350-353.
622 Caballero, L., Capra, L., 2011. Textural analysis of particles from El Zaguán debris avalanche deposit,
623 Nevado de Toluca volcano, Mexico: Evidence of flow behavior during emplacement. J. Volcanol.
624 Geotherm. Res. 200, 75-82.
625 Clavero, J.E., Sparks, R.S.J., Huppert, H.E., 2002. Geological constraints on the emplacement mechanism
626 of the Parinacota avalanche, northern Chile. Bull. Volcanol. 64, 40–54.
627 Clavero, J.E., Polanco, E., Godoy, E., Aguilar, G., Sparks, R.S.J., van Wyk de Vries, B., Perez de Arce, C.,
628 Matthews, S., 2004. Substrata influence in the transport and emplacement mechanism of the Ollagüe
629 debris avalanche (northern Chile). Acta Vulc. 16, 59–76.
630 Cox, R., O'Boyle, L., Cytrynbaum, J., 2019. Imbricated coastal boulder deposits are formed by storm

631 waves, and can preserve a long-term storminess record. Sci. Rep. 9, 10784.
632 Crandell, D.R., Miller, C.D., Glicken, H.X., Christiansen, R.L., Newhall, C.G., 1984. Catastrophic debris
633 avalanche from ancestral Mount Shasta volcano, California. Geology 12, 143-146.
634 Crawford, E., Mortensen, K., 2009. An Image J plugin for the rapid morphological characterization of
635 separated particle sand an initial application to placergold analysis. Comput. Geosci. 35, 347–359.
636 Davies, T.R., McSaveney, M.M., Kelfoun, K., 2010. Runout of the Socompa volcanic debris avalanche,
637 Chile: a mechanical explanation for low basal shear resistance. Bull. Volcanol. 72, 933-944.
638 Dennen, R.L., Bursik, M.I., Roche, O., 2014. Dome collapse mechanisms and block-and-ash flow
639 emplacement dynamics inferred from deposit and impact mark analysis, Mono Craters, CA.
640 J. Volcanol. Geotherm. Res. 276, 1-9.
641 Dufresne, A., Davies, T., 2009. Longitudinal ridges in mass movement deposits. Geomorphology 105, 171-
642 181.DOI:10.1016/j.geomorph.2008.09.009.
643 Glicken, H., 1986. Rockslide-debris avalanche of May 18, 1980, Mount Saint Helens Volcano,
644 Washington. Ph.D. Thesis, Univ. Calif. Santa Barbara, p. 303.
645 Glicken, H., 1998. Rockslide-debris avalanche of May 18, 1980, Mount St. Helens Volcano, Washington
646 Bull. Geol. Surv. Jpn. 49, 55-106.
647 Gray, J.M.N.T., 2013. A hierarchy of particle-size segregation models: from polydisperse mixture
648 to depth-averaged theories. AIP Conf. Proc., 1542, 66-73.
649 Guilbaud, M-N., Chedeville, C., Molina-Guadarrama, A-N., Siebe, C., 2022. Volcano-sedimentary
650 processes at Las Derrumbadas rhyolitic twin domes, Serdan-Oriental Basin, Eastern Trans-
651 mexican Volcanic Belt. Geol. Soc. Spec. Publ., 520, 31.
652 Janoo, V., 1998. Quantification of Shape, Angularity, and Surface Texture of Base Course Materials.
653 U.S. Army Corps of Engineers, Cold Regions Research & Engineering Laboratory, Hanover NH,
654 pp. 1-22 (Special Report).
655 Kelfoun, K., Druitt, T., van Wyk de Vries, B., Guilbaud, M-N., 2008. Topographic reflection of the
656 Socompa debris avalanche, Chile. Bull. Volcanol. 70, 1169-1187.
657 Launeau, P., Robin, Y.F., 2005. Determination of fabric and strain ellipsoids from measured sectional
658 ellipses - Implementation and applications. J. Struct. Geol. 27, 2223-2233.
659 Legros, J.F., Cantagrel, J.M., Devouard, B., 2000. Pseudotachylite (Frictionite) at the base of
660 the Arequipa Volcanic landslide (Peru): Implications for emplacement mechanisms. J.
661 Geol. 108, 601-611.
662 Legros, J.F., 2002. The mobility of long-runout landslides. Eng. Geol. 63, 301–331.
663 Mariño, J., Samaniego, P., Manrique, N., Valderrama, P., Roche, O., van Wyk de Vries, B., Guillou, H.,
664 Zerathe, S., Arias, C., Liorzou, C., 2021. The Tutupaca volcanic complex (Southern Peru):
665 Eruptive chronology and successive destabilization of a dacitic dome complex. J. S. Am. Earth

Sci., 109, 103-227.

Mehl, K.W., Schmincke, H.U., 1999. Structure and emplacement of the Pliocene Roque Nublo debris avalanche deposit, Gran Canaria, Spain. J. Volcanol. Geotherm. Res. 94, 105-134.

Naranjo, J.A., Francis, P., 1987. High velocity debris avalanche at Lastaria volcano in the north Chilean Andes. Bull. Volcanol. 49, 509-514.

Palmer, B.A., Alloway, B.V., Neall, V.E., 1991. Volcanic-debris avalanche deposits in New Zealand: lithofacies organization in unconfined, wet-avalanche flows. In: Fisher, R.V., Smith G.A; (Eds.), Sedimentation in volcanic setting. SEPM Spec. Pub. vol. 45, pp. 89-98.

Samaniego, P., Valderrama, P., Mariño, J., van Wyk de Vries, B., Roche, O., Manrique, N., Chedeville, C., Fidel, L., Malnati, J., 2015. The historical (218 ± 14 aAP) explosive eruption of Tutupaca volcano (Southern Peru). Bull. Volcanol. 77, 51.

Sandnes, B., Flekkoy, E.G., Knudsen, H.A., Maloy, K.J., See, H., 2011. Patterns and flow in frictional fluid dynamic. Nat. Commun. 2, 288.

Shea, T., van Wyk de Vries, B., 2008. Structural analysis and analogue modeling of the kinematics and dynamics of rockslide avalanches. Geosphere 4, 657–686.

Siebe, C., Komorowski, J-C., Sheridan, M-F., 1992. Morphology and emplacement collapse of an unusual debris avalanche deposit at Jocotitlán Volcano, Central Mexico. Bull. Volcanol. 54, 573-589.

Siebert, L., Roverato, M., 2020. A Historical Perspective on Lateral Collapse and Volcanic Debris Avalanche. In: Roverato, M., Dufresne, A., Procter, J., (Eds.), Volcanic Debris Avalanches from Collapse to Hazards. Springer, pp. 11-50.

Siebert, L., Glicken, H., Ui, T., 1987. Volcanic hazards from Bezymianny- and Bandai-type eruptions. Bull. Volcanol. 49, 435-459.

Suzuki-Kamata, K., Kusano, T., Yamasaki, K., 2009. Fractal analysis of the fracture strength of lava dome material based on the grain size distribution of block-and-ash flow deposits at Unze volcano, Japan. Sedim. Geol. 220, 162-168.

Szabo, I., Domokos, G., Grotzinger, J.P., Douglas, J.J., 2015. Reconstructing the transport history of pebbles on Mars. Nat. Commun. 6: 8366.

Valderrama, P., 2016. Origin and dynamics of volcanic debris avalanches: surface structure analysis of Tutupaca volcano (Peru). Earth Sciences. Univ. Blaise Pascal-Clermont-Ferrand II.

Valderrama, P., Roche, O., Samaniego, P., van Wyk de Vries, B., Bernard, K., Marino J., 2016. Dynamic implications of ridges on a debris avalanche deposit at Tutupaca volcano (southern Peru). Bull. Volcanol. 78, 14.

Valderrama, P., Roche, O., Samaniego, P., Van Wyk de Vries, B., Araujo, G., 2018. Granular fingering as a mechanism for ridge formation in debris avalanche deposits: laboratory experiments and implications for Tutupaca volcano, Peru. J. Volcanol. Geotherm. Res. 349, 409-418.

701 Van Wyk de Vries, B., Self, S., Francis, P.W., Keszthelyi, L., 2001. A gravitational spreading origin for the
702 Socompa debris avalanche. J. Volcanol. Geotherm. Res. 105, 225-247.

703 Voight, B., Glicken, H., Janda, R.J., Douglass, P.M., 1981. Catastrophic rockslide-avalanche of May 18.
704 In: Lipman, P. W., Mullineaux, D.R. (Eds.), The 1980 eruptions of Mount St. Helens, Washington.
705 U.S. Geol. Surv. Prof. Pap. vol. 1250, pp. 347-371.

706 Zernack, A., Procter, J., Cronin S., 2009. Sedimentary signatures of cyclic growth and destruction of
707 stratovolcanoes: a case study from Mt Taranaki, New Zealand. Sediment. Geol. 220, 288-305.

Figures and Tables

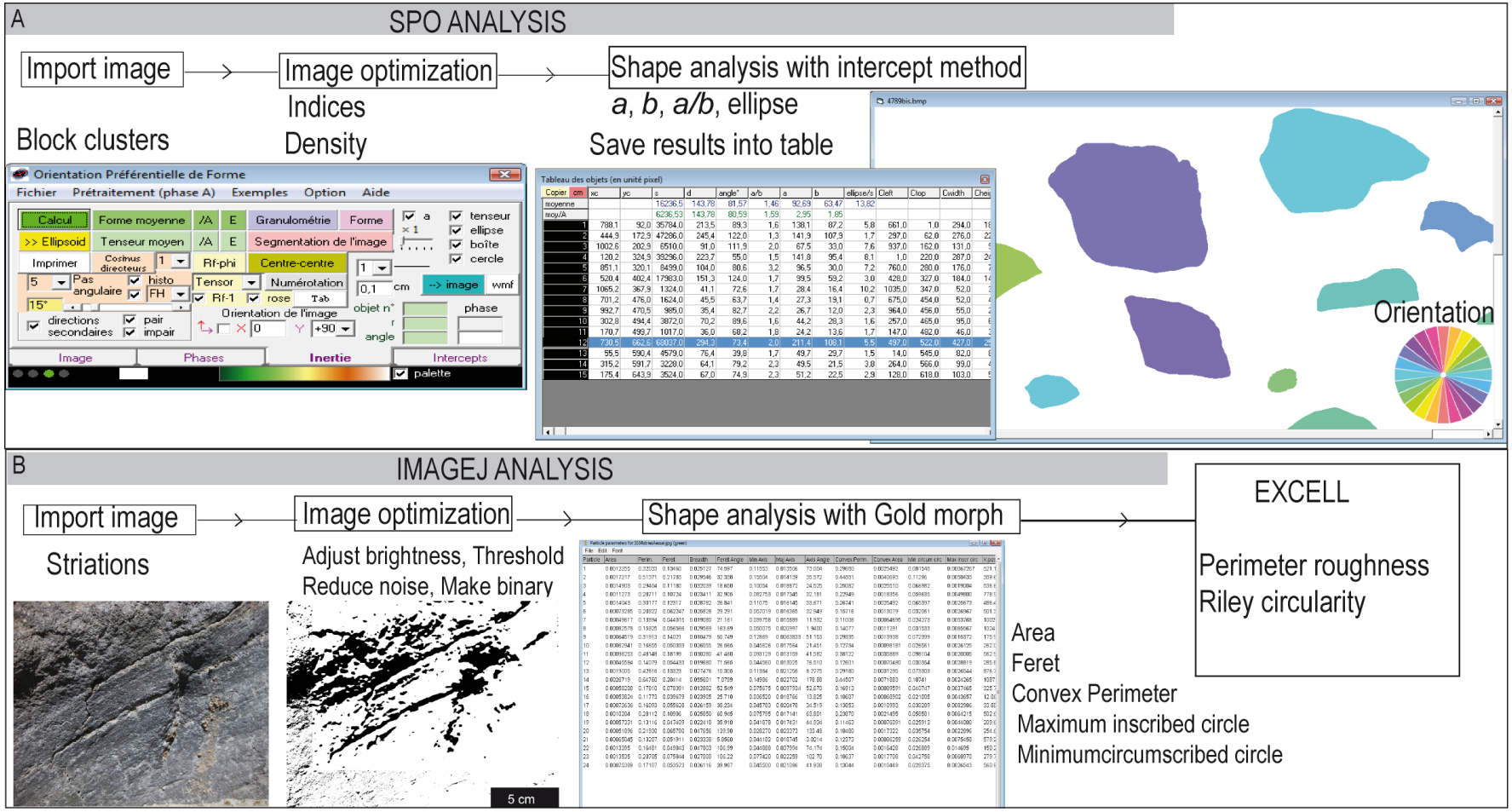

Fig. 1. The flow chart for image analysis. A. The SPO analysis (Launeau and Robin, 2005) of block clusters with the inertia and intercepts method; B. The shape analysis of striations using the ImageJ Plugin "Gold morph" (Crawford and Mortensen, 2009).

712

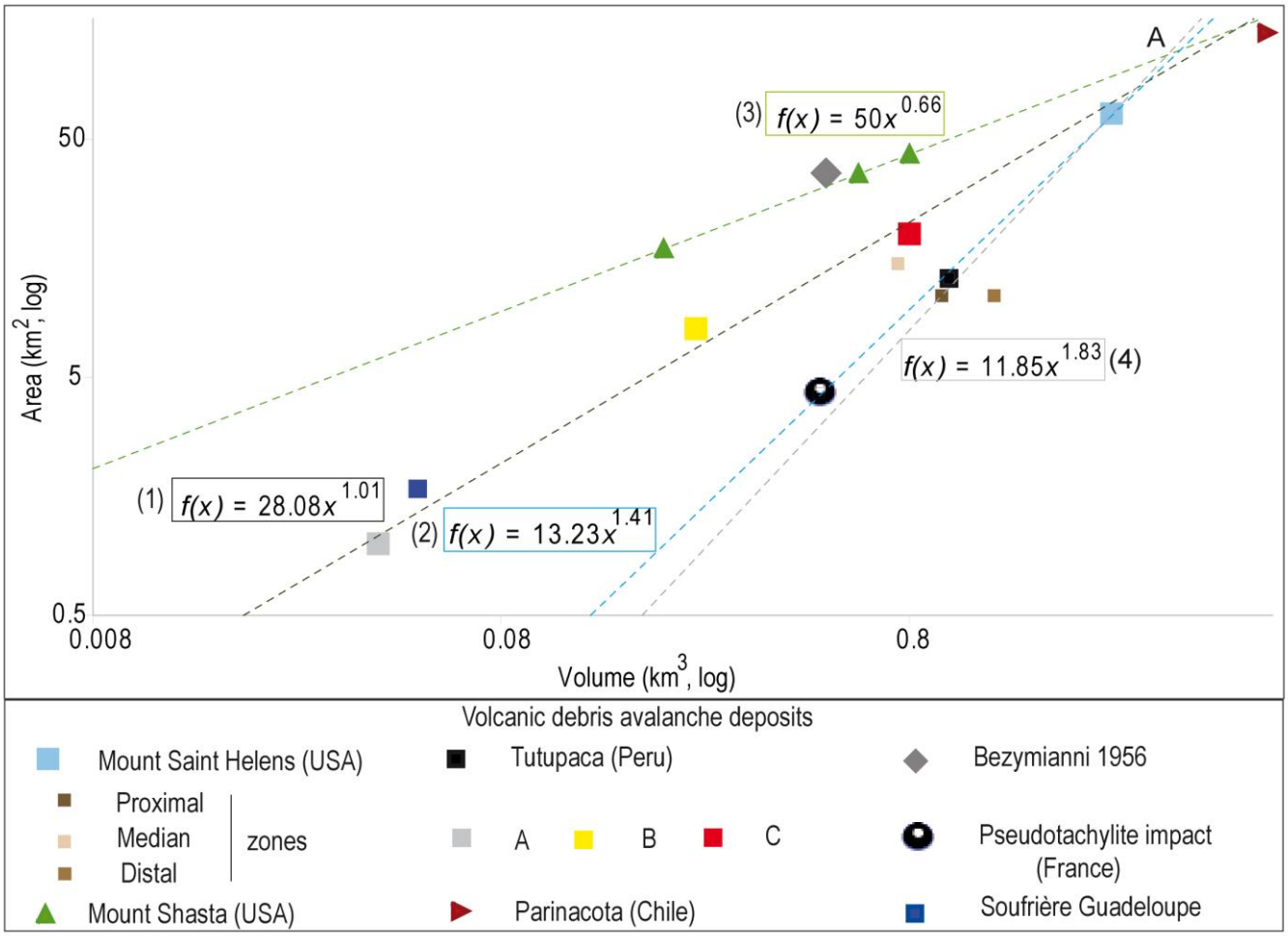

713

714 **Fig. 2.** Area (km^2) *vs.* volume (km^3) of volcanic debris avalanche deposits on double log graph: Mount
715 Shasta and Mount Saint Helens in the USA (Glicken, 1986; Siebert et al., 1987); Bezymianni in Kamchatka
716 (Siebert et al., 1987); Parinacota in Chile (Clavero et al., 2002; Legros, 2002); Tutupaca in Peru (Samaniego
717 et al., 2015; Valderrama et al., 2016); Soufrière in Guadeloupe (Boudon et al., 1984) and Mont Dore in
718 French Massif Central (Bernard and van Wyk de Vries, 2017). A. The proximal zone; B. The ridged unit; C.
719 The distal zone.

720

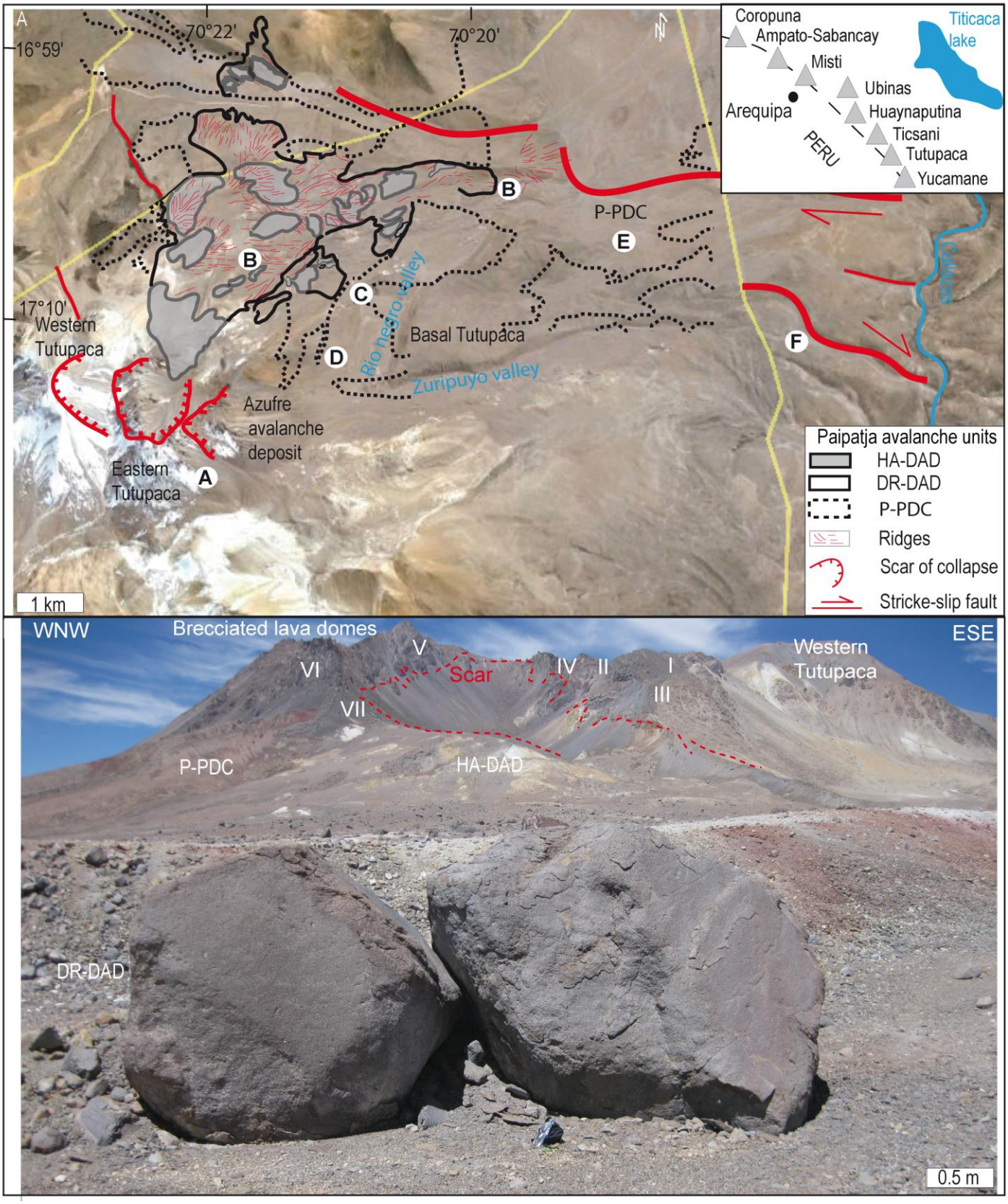

Fig. 3. Geological setting of the Paipatja avalanche deposits exposed in the northeastern part of Tutupaca volcanic complex (Southern Peru, modified from Samaniego et al., 2015; Valderrama et al., 2016). A. Landforms of the avalanche deposits and structures at the North East of the brecciated lava domes from Google Earth with stratigraphic sections. We differentiate the hydrothermal rich avalanche deposit (HA-

DAD, L = 6-8 km, V <1 km^3; H/L = 0.23-0.17, Samaniego et al., 2015); a dome rich debris-avalanche deposit (DR-DAD); the Paipatja pyroclastic density current deposits (P-PDC, ~218 ± 14 aBP). The right-top inset shows the location of Pleistocene volcanoes in the Andean Central Volcanic Zone. The white points indicate the outcrop locations of the clusters and the block lithofacies. A. Under the erosional amphitheater of collapse scar in proximal zone; B. Transverse alignment of blocks and ridge structures; C. Extensional fault zone with abrasion and jigsaw-fractured lithofacies; D. Shear zone along lateral levee; E. Impact and lava bombs; F. Buried blocks and abrasion. B. Panoramic view of the northeast of Tutupaca volcano, showing the horseshoe-shape amphitheater and lava domes (I to VI) and DR-DAD with transverse alignment of blocks. Most of the domes are constructed on the older hydrothermally altered basal edifice (Samaniego et al., 2015; Valderrama et al., 2016).

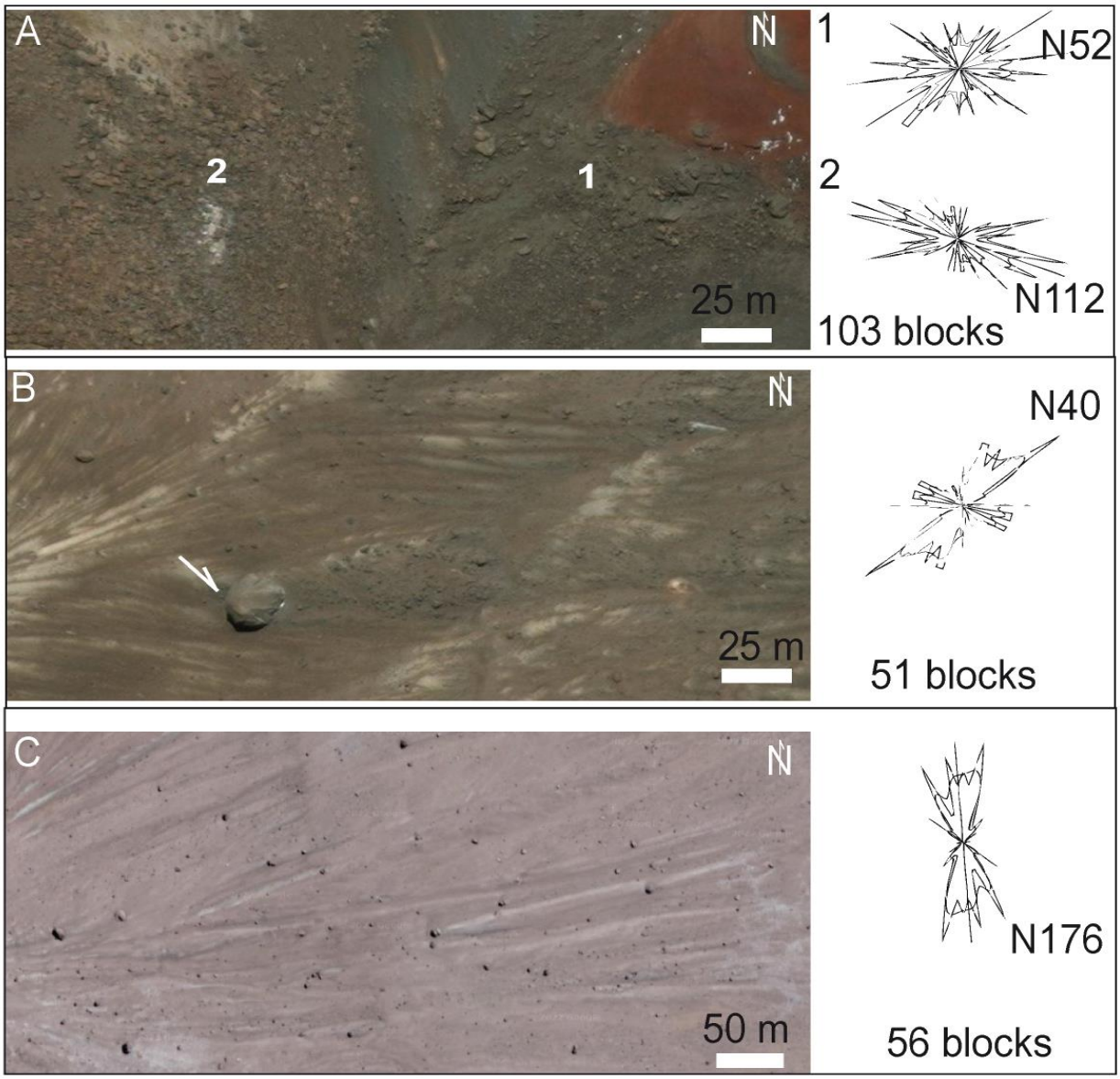

Fig. 4. The syn-emplacement block lithofacies and block orientations (SPO, Launeau and Robin, 2005) from proximal to distal zones using georeferenced Google Earth imagery. A. Proximal brecciated zones under the scar between domes V to VII: 1. An impacted and crushed zone showing imbricated block clusters without preferential orientation; 2. A tilted zone with N112E angular dome fragments adjacent to the PDC in red; B. Isolated polyhedral block (white arrow) of ridge structures in the median zone showing in downstream N40E disaggregated clasts; C. The transverse and isolated blocks (>1 m in length, N176E) surrounded by P-PDC unit in distal zone.

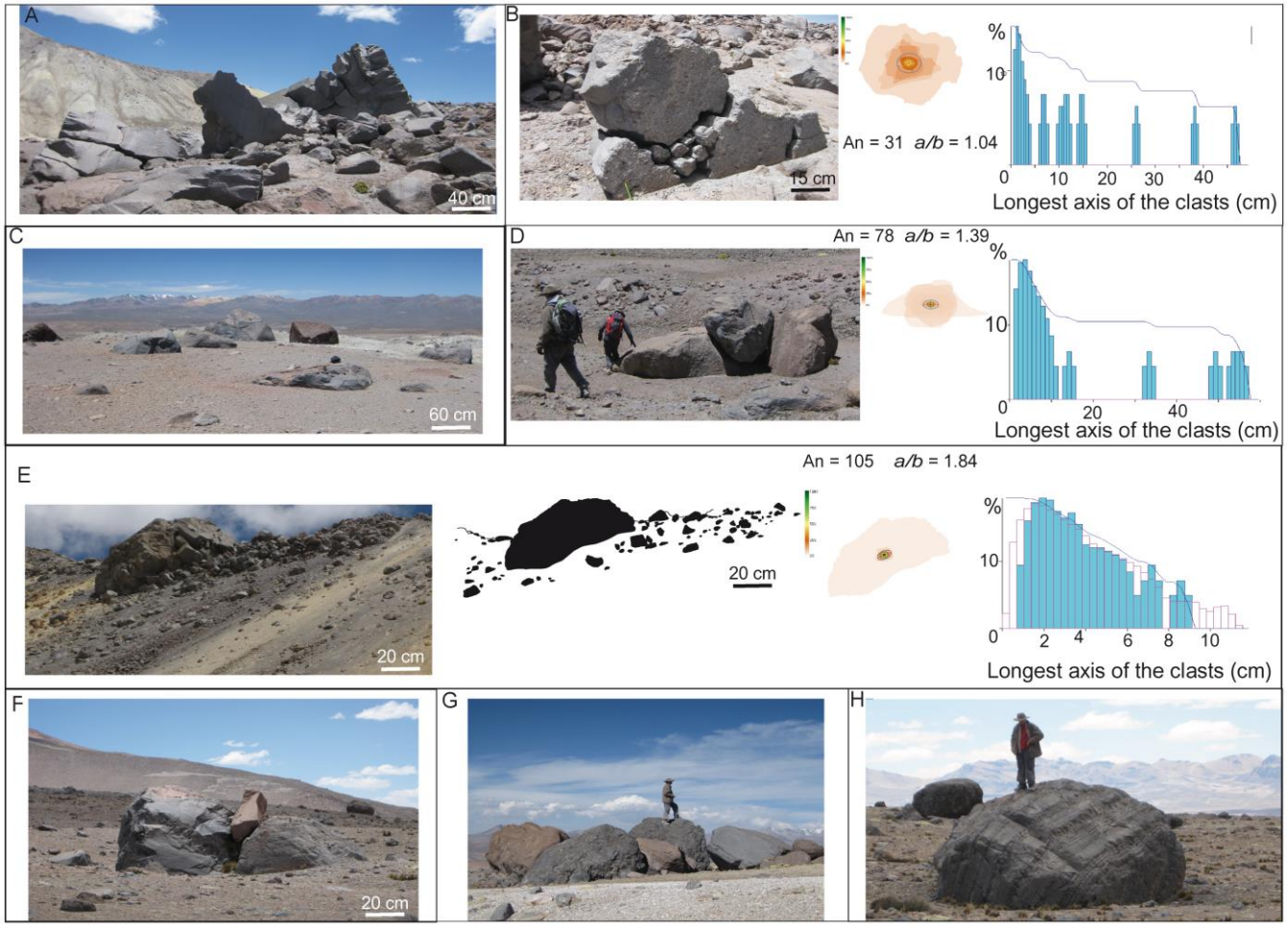

748

749 **Fig. 5.** Block clusters of DR-DAD from SPO analysis (Launeau and Robin, 2005). A. Vertical impact of blocks with abraded surface and undulated fractured
750 borders under the erosional amphitheater of collapse scar; B. Impacted jigsaw-clusters with polymodal clast distribution; C. Subdued blocks in transverse
751 ridges; D. Impacted blocks in distal zone with polymodal distribution of the clasts; E. Block along lateral levee with sigmoidal jigsaw-breccias showing a
752 bimodal clast distribution; F. Angular and impacted block between aligned and subdued blocks; G. Block cluster in distal zone; H. Subdued and tilted blocks.

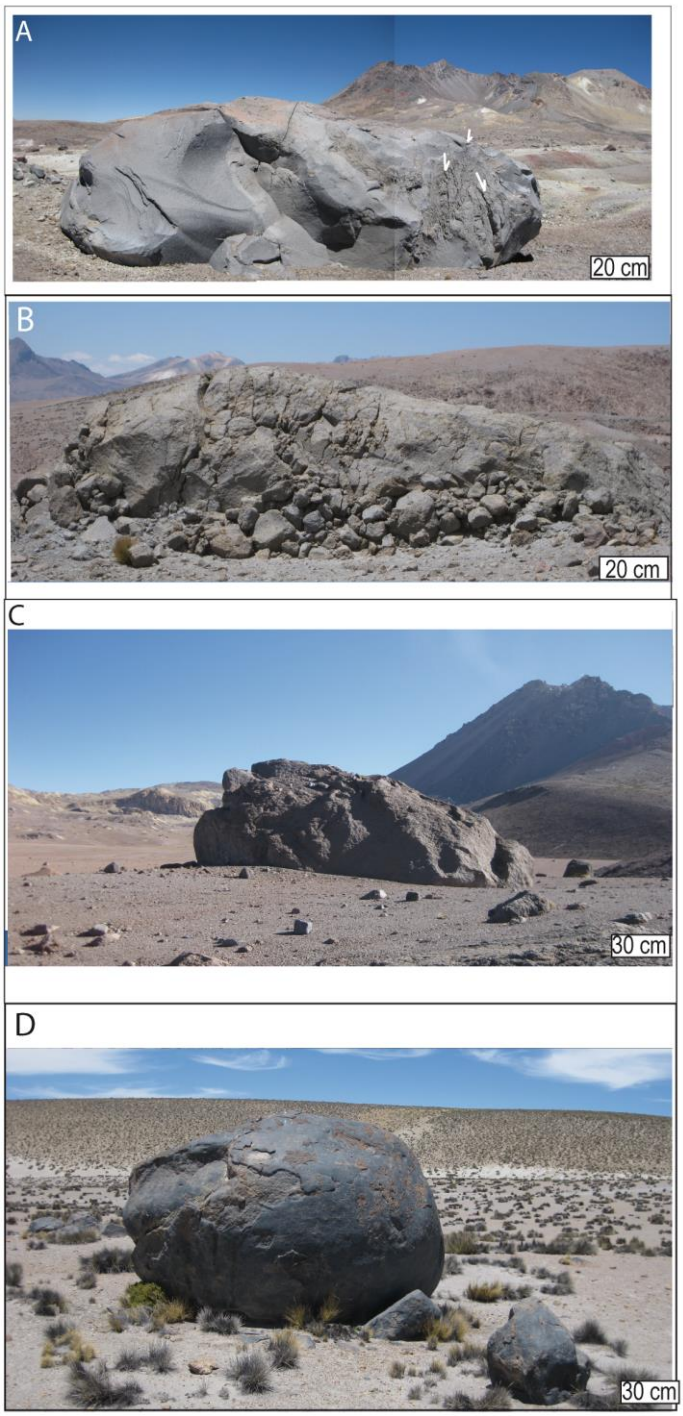

Fig. 6. Textural gradient of block lithofacies of the Paipatja avalanche deposits. A. Transverse blocks with an oriented abrasion: *white arrows* show striations on upstream sub-rounded faces and planar faces with conchoidal fractures in downstream; B. Large polyhedral block (~3 m high and ~5 m length) with an oriented abrasion, quenched and cracked surface in upper part and sub-rounded lava in altered vitreous phase in lower part; C. Transversal alignment of abraded blocks with bimodal clast distribution from SPO analysis (Launeau and Robin, 2005) related to pyroclastic density current deposits; D. Polymodal clast distribution (SPO analysis, Launeau and Robin, 2005) of pyroclastic density current deposits around a distal sub-rounded block.

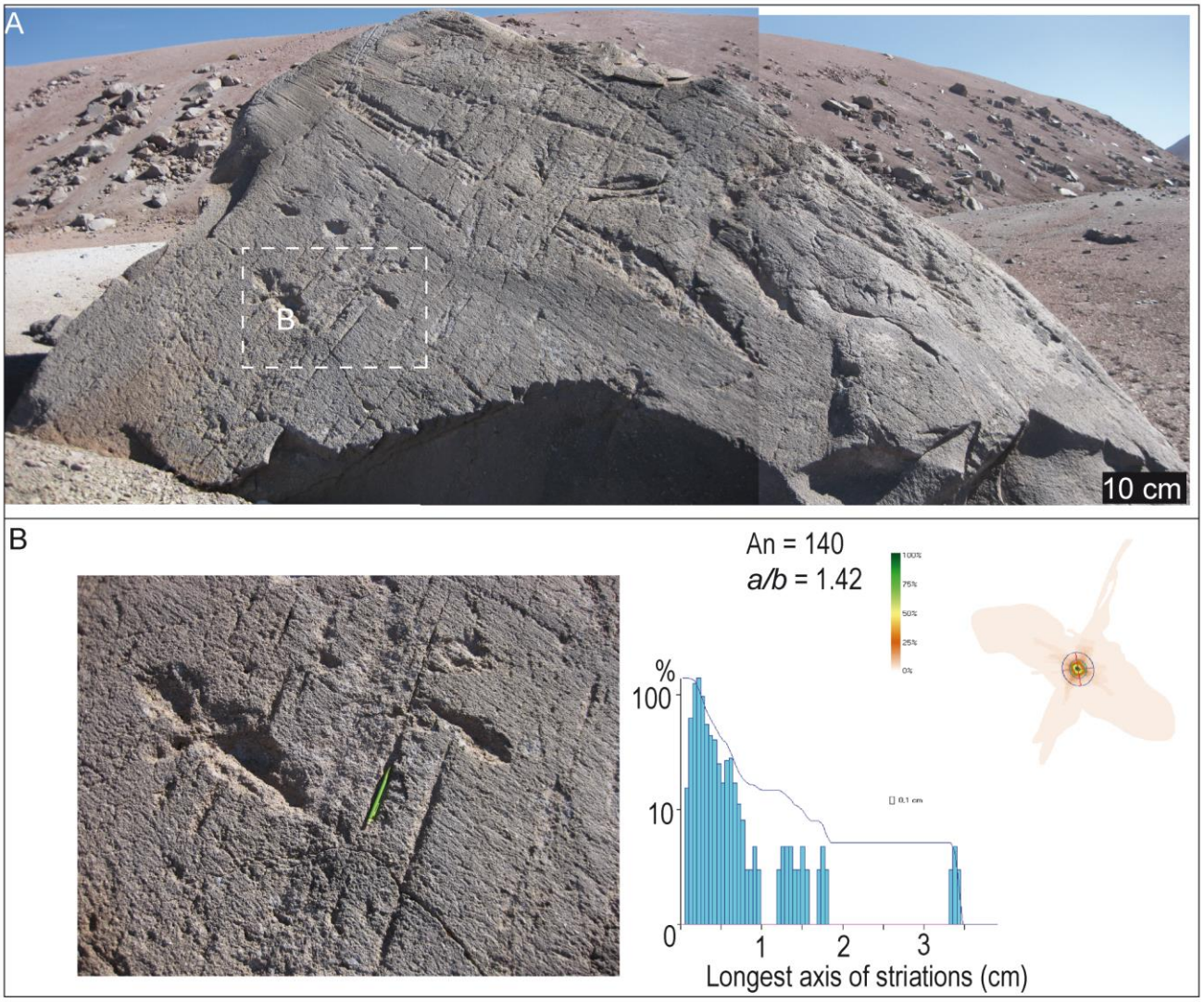

Fig. 7. Striations and grooves of ridged blocks from SPO analysis (635 striations, Launeau and Robin, 2005). A. Subdued block (~2 m high and 1.6 m length) with abraded planar surfaces, grooves and striations with circular depressions (~1-5 cm depth, ~2-3 mm wide); B. Detailed analysis of grooves and striations showing polymodal distribution related to the P-PDC interactions (An = 140 striations, *a/b* = 1.42).

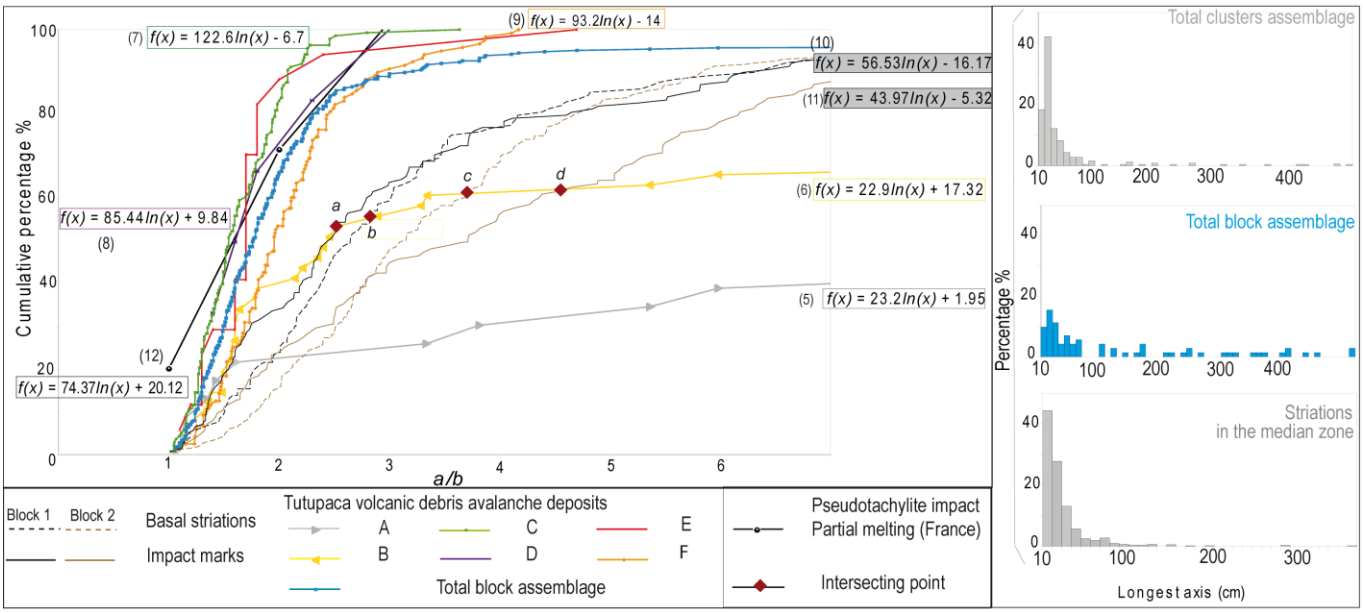

Fig. 8. Sedimentological analysis of block lithofacies of the Paipatja avalanche deposits from proximal to distal zones. A. Cumulative curves of block lithofacies *vs*. *a/b* from SPO analysis (404 blocks, 635 striations and impact marks; Launeau and Robin, 2005); B. Histograms.

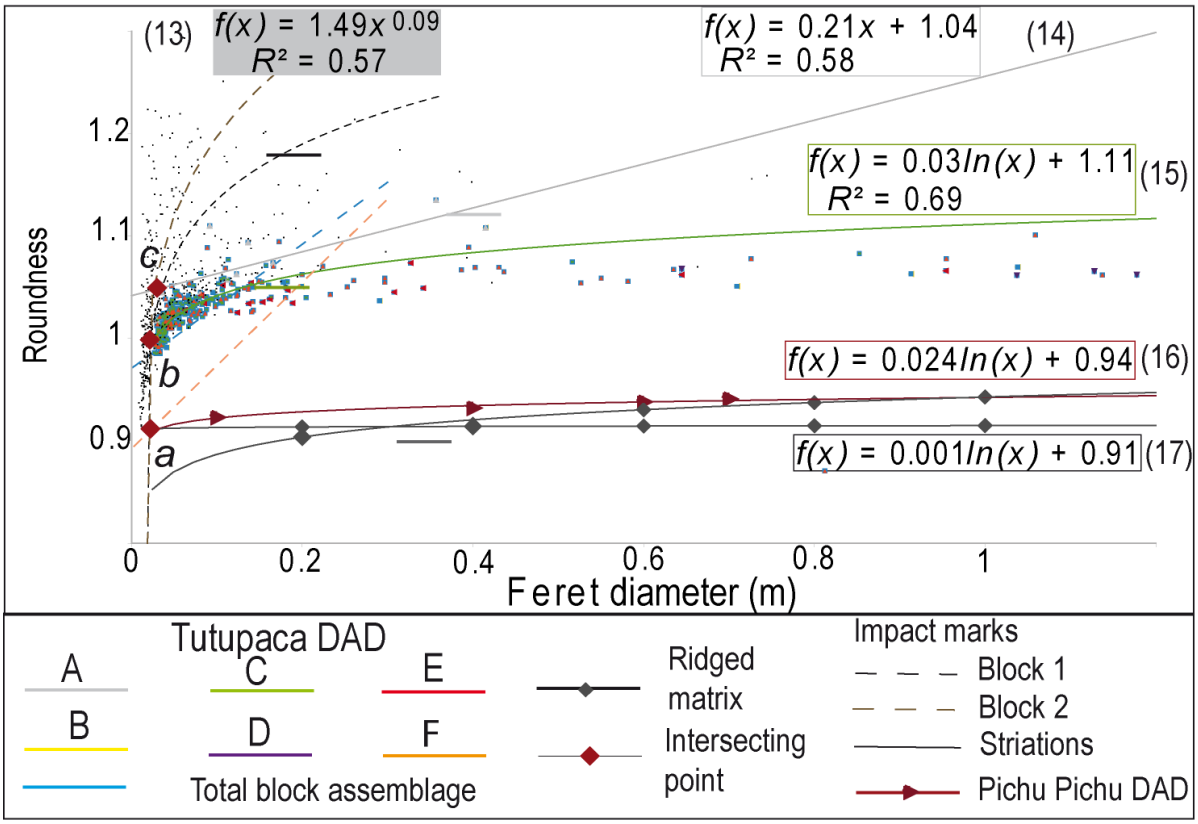

805

806

807

808 **Fig. 9.** Roundness *vs.* Feret's diameter (m) of block lithofacies and striations in different zones from
809 shape analysis using the software ImageJ (404 blocks, 635 striations and impact marks; Blott and Pye,
810 2008; Crawford and Mortensen, 2009). The *horizontal lines* indicate the Feret's diameter at which
811 roundness stopped increasing. Error bars are smaller than the symbols.

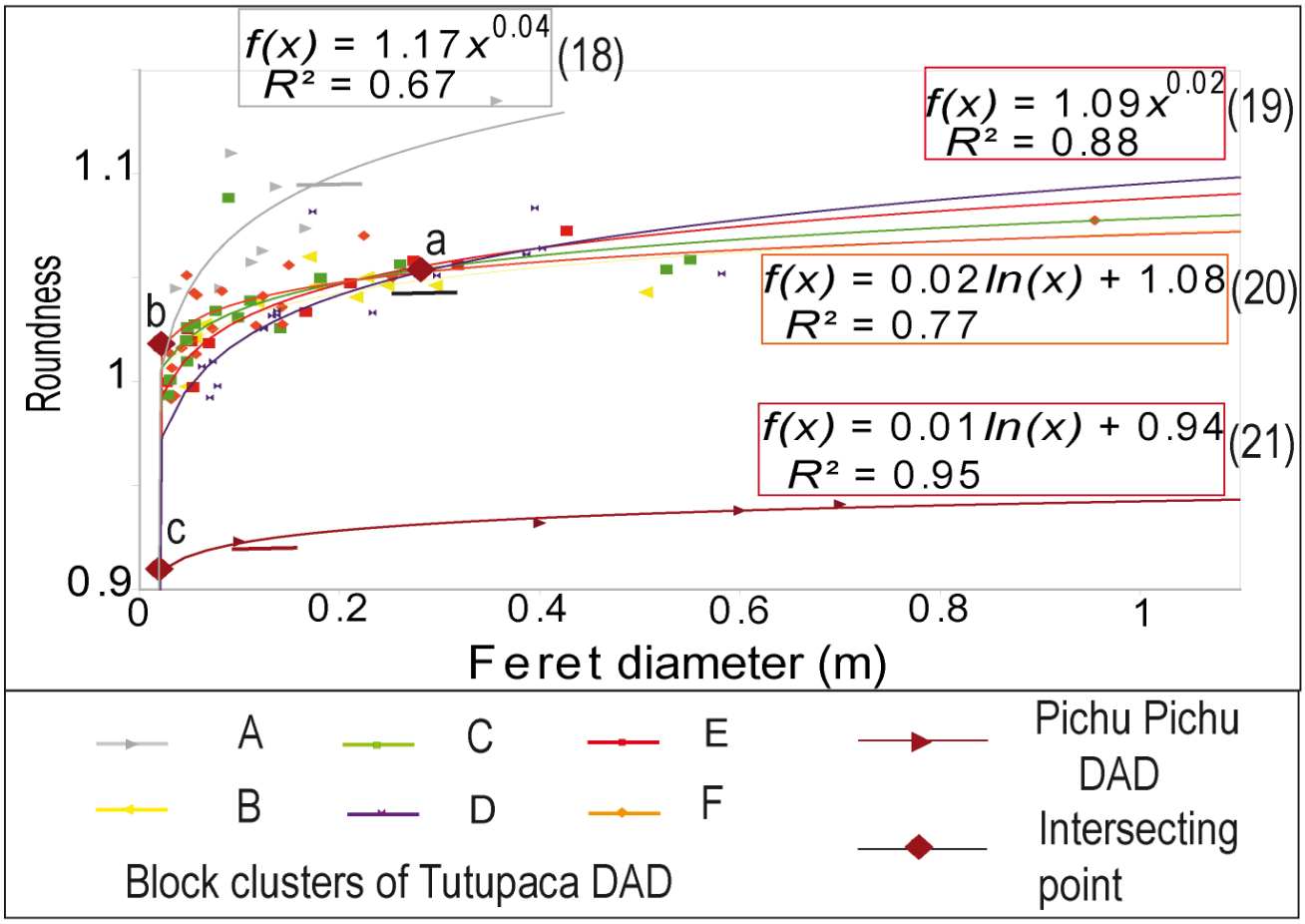

Fig. 10. Roundness *vs.* Feret's diameter (m) of block clusters from shape analysis using the software ImageJ (Blott and Pye, 2008; Crawford and Mortensen, 2009). The *horizontal lines* indicate the Feret's diameter at which roundness stopped increasing. Error bars are smaller than the symbols (see Supplemental File 2).

Table 1. List of acronyms and their definitions.

	Acronyms	Definitions
Quantitative parameters	*A*	Area
	a/b	the largest axis / minor axis
	D	Fractal dimension
	d	Depth
	E	Ellipse
	Ellipse/a/b	The ratio of the ellipse to the *a/b*
	FD	Feret's Diameter
	H	Height
	h	Exponent of the power regressions
	H/L	Apparent friction
	L	Length
	S	Surface
	T	Thickness
	v	Velocity
	V	Volume
	W	Width
Lithofacies	DR-DAD	Dome-rich debris-avalanche deposit
	HA-DAD	Hydrothermally-rich debris avalanche deposit
	P-PDC	Paipatja pyroclastic density current deposit

Table 2. Methodology for block laboratory analysis.

Outcrop map and observations	Google Earth imagery, landforms, faults, orientations, lateral and vertical variations in block lithofacies and lithostratigraphy, textures.
Grain size analysis	Image analysis and Feret's diameter measurement. Clast size distribution: cumulative curves, fractal distributions, statistical parameters.
Shape analysis	Shape analysis with texture of blocks, preferred orientation of block largest axis and

shape parameters.

Table 3. Clast shape parameters with Feret's Diameter (*FD*), Riley's circularity (*Rc*) and Roundness (*R*, Blott and Pye, 2008; Crawford and Mortensen, 2009; Bernard, 2015).

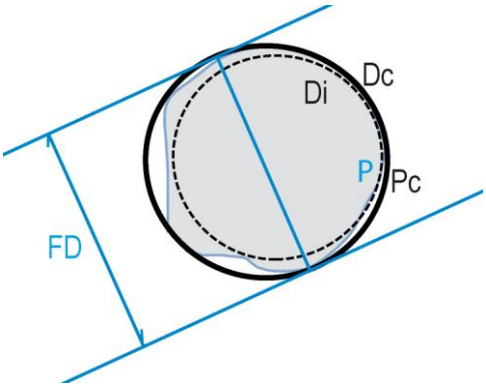	Feret's Diameter (*FD*) The longest distance between two parallel tangential lines
	Riley's circularity (*Rc*, Riley, 1941) $Rc = \sqrt{(Di / Dc)}$ *Di* the largest inscribed circle *Dc* the smallest circumscribed circle
	Roundness (*R*) $R = P / Pc$ *P* Perimeter *Pc* Convex perimeter

Table 4. Fractal results of block lithofacies in different zones and striations compared to the surrounded matrix of the Paipatja avalanche deposits and P-PDC (see Supplemental File 1; Suzuki-Kamata et al., 2009).

	h	*D*	Correlation coefficient	Range of the clast size (cm)	Number of clasts
A	1,37	0,26	0,9	6.7-22.1	14
B	0,67	1,66	0,9	13.2-47.5	18
C	1,7	-	0,9	10.4-22.9	78
D	2,29	-	0.95	233.4-539.5	7
E	1,92	-	0.93	30.3-68.7	9
F	0,58	1,83	0,9	10.7-96.5	120

All zones	0,86	1,28	0,9	11.4-40.3	137
Surrounded matrix	0.07-1.16	0.67-2.84	0.91-0.98	0.001-6.4	-
Striations	1.18	0.6	0.9	5.94-44.68	265

Table 5. Mean values of block shape parameters and striations from SPO and shape analysis using the software ImageJ (404 blocks, see Supplemental File 2; Launeau and Robin, 2005; Blott and Pye, 2008; Crawford and Mortensen, 2009; Bernard, 2015). These shape data have been associated with the correspondent standard errors.

	Roundness	Riley's circularity	*a/b*	Ellipse	Ellipse/*a/b*
A	1.07±0.01	0.73±0.03	1.68±0.14	3.61±0.74	2.29±0.54
B	1±0.02	0.69±0.02	1.88±0.38	3.2±0.65	1.7±0.24
C	1.02±0.001	0.68±0.006	1.63±0.3	3.34±0.25	2.04±0.15
D	1.13±0.07	0.64±0.05	1.91±0.26	5.15±2.18	2.7±0.59
E	1±0.02	0.64±0.02	1.8±0.2	5.01±1.25	2.78±0.33
F	1.05±0.03	0.63±0.01	2.1±0.06	3.95±0.24	1.88±0.35
Mean	1.23±0.009	0.66±0.005	1.7±0.03	3.5±0.15	2.05±0.1
Striations	0.9±0.01	0.3±0.007	3.69±0.1	21.9±1.57	5.82±0.5

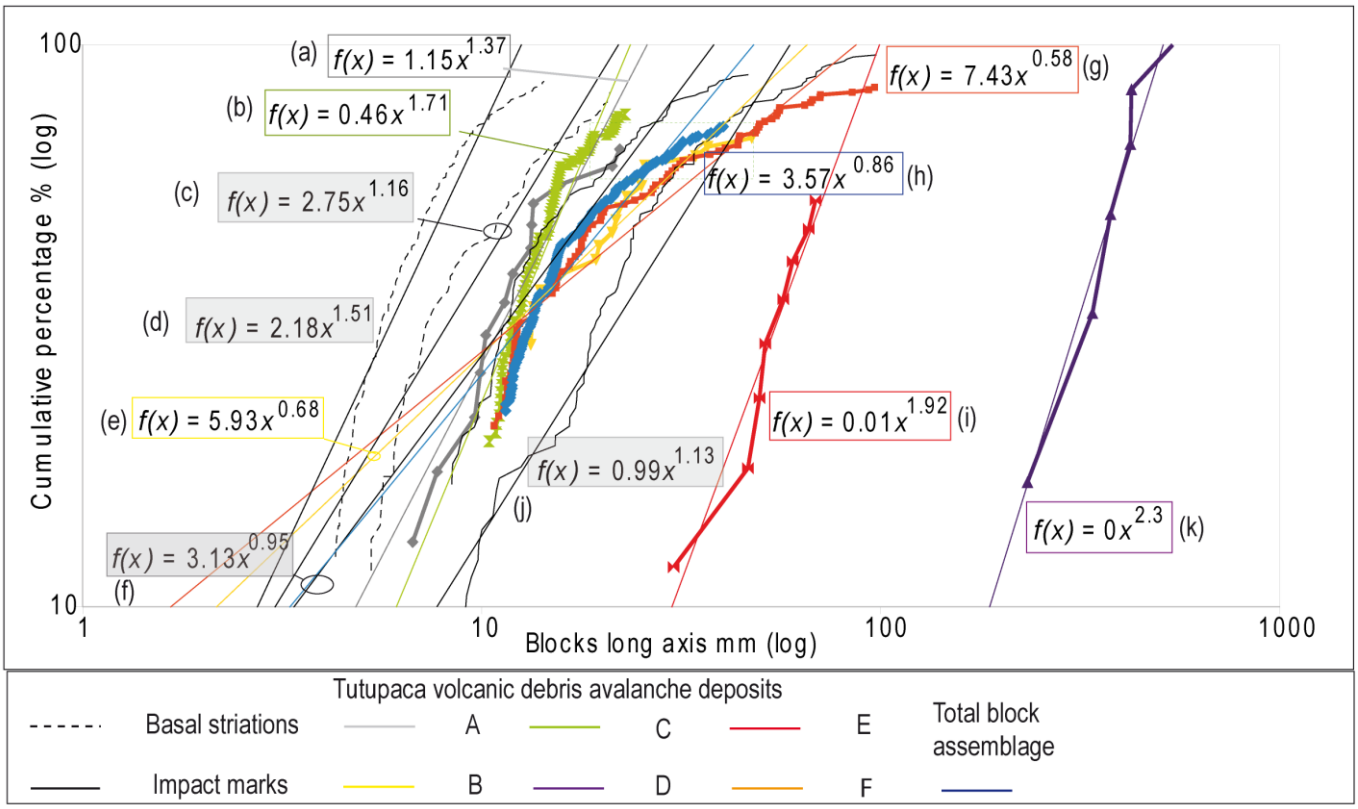

870
871 **Supplemental File 1**

872 Cumulative % *vs.* long clast-axis on double log graph. The exponent *h* of size distributions were
873 estimated from the power regressions (*a*-*k*) by the methods of the least squares (R^2 >0.9 in Table 4, Eq. 6
874 in Suzuki-Kamata et al., 2009). The *h* values obtained for each structural unit ranged from 6.7 to 537.9
875 cm for block lithofacies and from 5.94 to 44.68 cm for striations. From following equation $2h + D = 3$
876 (Eq. 7 in Suzuki-Kamata et al., 2009), we translate the *h*-values into fractal *D* values in Table 4. The *h*-
877 values for the block lithofacies and striations range from 0.58 to 2.29 (Table 4). Substitution of these
878 values into the previous equation (Eq. 7 in Suzuki-Kamata et al., 2009), gives corresponding fractal *D*-
879 values of 0.26 to 1.83. The negative values of fractal dimension have not been considered in Table 4.

880

881